

**MEASUREMENTS OF EMISSIONS FROM AGRICULTURAL
FIRES AND WILDFIRES IN THE U.S.**

A Dissertation
Presented to
The Academic Faculty

by

Xiaoxi Liu

In Partial Fulfillment
of the Requirements for the Degree
Doctor of Philosophy in the
School of Earth and Atmospheric Sciences

Georgia Institute of Technology
December 2016

COPYRIGHT © 2016 BY XIAOXI LIU

MEASUREMENTS OF EMISSIONS FROM AGRICULTURAL FIRES AND WILDFIRES IN THE U.S.

Approved by:

Dr. L. Gregory Huey, Advisor
School of Earth and Atmospheric Sciences
Georgia Institute of Technology

Dr. Rodney J. Weber
School of Earth and Atmospheric
Sciences
Georgia Institute of Technology

Dr. Yuhang Wang
School of Earth and Atmospheric Sciences
Georgia Institute of Technology

Dr. Robert J. Yokelson
Department of Chemistry
University of Montana

Dr. Nga Lee Ng
School of Chemical and Biochemical
Engineering and School of Earth and
Atmospheric Sciences
Georgia Institute of Technology

Date Approved: November 3, 2016

To my parents

ACKNOWLEDGEMENTS

I would like to sincerely and heartily express my gratitude to my advisor, Dr. Greg Huey, for the support he gave me throughout my doctoral studies. None of my research work would have been possible without his help. He inspires me with his knowledge in atmospheric chemistry and instrumentation. He provides me with accessible guidance, friendly working environment, and opportunities to participate in top scientific projects. I would like to thank our other group members: David Tanner, Bob Stickel, Dexian Chen, Jin Liao, and Maddi Frank. They were always around whenever I needed help. David and Dexian supported me greatly in acquiring CIMS-operating skills both in field and in laboratory.

Another mentor who has largely helped my research and introduced me to the field of biomass burning is Dr. Robert Yokelson. His prompt feedback and expertise in fires inspired me thoroughly in the development of this research. I would like to thank Dr. Yuhang Wang for his help during the field campaign in China and guidance in the modeling work involved in my research. Thanks to my two other committee members, Dr. Nga Lee Ng and Dr. Rodney Weber, for their insightful advice in aerosol chemistry.

I enjoyed working with all the colleagues who have provided me help throughout the course of graduate school: Mike Nicovich, Yuzhong Zhang, Hongyu Guo, Lu Xu, Hang Qu, Steve Sjostedt, Javier Sanchez, and Ting Fang. I owe thanks to my dearest friends with whom I had delightful times: Pengzi Yu, Yu Liu, Tao Yan, Jia He, and Yihai Fang.

Finally, I thank Tao Cheng for his love, patience, and help though the difficulties.

I would like to thank my parents for their continuous encouragement and support.

TABLE OF CONTENTS

ACKNOWLEDGEMENTS	iv
LIST OF TABLES	viii
LIST OF FIGURES	ix
LIST OF SYMBOLS AND ABBREVIATIONS	xiii
SUMMARY	xv
CHAPTER 1. Introduction	1
1.1 Biomass Burning Background	1
1.2 Motivation and Goals	2
1.3 Outline of the Thesis	3
CHAPTER 2. Instrumentation and Terminology	5
2.1 Aircraft Instrumentation	5
2.2 Emission Ratios, Emission Factors, and Modified Combustion Efficiency	10
CHAPTER 3. U.S. Agricultural Fire Emissions	13
3.1 Introduction	13
3.2 Methods	16
3.2.1 Airborne Sampling of Fires	16
3.2.2 Estimation of ERs, EFs, and MCE	20
3.2.3 Calculation of Brown Carbon (BrC) Absorption	24
3.3 Results	26
3.3.1 Initial Emissions	26
3.3.2 Annual Emissions of SO ₂ , NO _x , and CO from Crop Residue Burning in Southeastern U.S.	48
3.4 Conclusions	51
CHAPTER 4. Evolution of Ozone, Reactive Nitrogen, and Organic Aerosol in Agricultural Fire Plumes	53
4.1 Introduction	53
4.2 Methods	55
4.2.1 Characterizing Evolution with NEMRs	55
4.2.2 Lagrangian Plume Cross-Section Model	56
4.3 Results	60
4.3.1 Plume Evolution	61
4.3.2 Model Simulations	72
4.4 Conclusions	85
CHAPTER 5. Western U.S. Wildfires: Emissions and Air Quality Tradeoffs with Prescribed Burning	88
5.1 Introduction	88

5.2	Methods	91
5.2.1	Fire Descriptions	91
5.2.2	Calculation of ERs, EFs, and MCE	96
5.3	Results	98
5.3.1	Initial Emissions of Trace Gases	108
5.3.2	Initial Emissions of PM ₁	119
5.3.3	Relationship between EF and MCE	124
5.3.4	Emission Estimates from Western U.S. Wildfires	133
5.4	Conclusions	137
CHAPTER 6.	Conclusions	139
6.1	Summary of Findings	139
6.2	Future Research	141
REFERENCES		143

LIST OF TABLES

Table 1	– Aircraft measurements aboard the NASA DC-8 research aircraft during SEAC ⁴ RS.	7
Table 2	– G-1 aircraft measurements during BBOP used in this work.	9
Table 3	– Details of the agricultural fires sampled in the southeastern U.S.	20
Table 4	– Measured MCE and emission factors (g/kg) for all agricultural fires sampled during SEAC ⁴ RS in summer 2013. The study averages and the standard deviations are indicated in bold. Blank indicates no measurement available for the fire.	29
Table 5	– Statistics for the linear regression of fire-averaged EF as a function of fire-integrated MCE. Values in parentheses represent one standard deviation. Species are organized by the sign and significance of slopes and then by the magnitude of r^2 .	32
Table 6	– Comparison of EFs (g/kg) measured in field and lab for crop residue fuels. Values in parentheses represent one standard deviation.	33
Table 7	– Summary of the modeled evolution characteristics at an age of 1 h: ozone production efficiency (OPE), the ratio of NO _x oxidized to PAN to that oxidized to PAN plus HNO ₃ +nitrate ($P_{PAN}/(P_{HNO_3}+P_{PAN})$), and radical concentrations.	76
Table 8	– Details of the wildfires sampled in the western U.S.	93
Table 9	– Measured MCEs and emission factors (g kg ⁻¹) for the three wildfires in the western U.S. and comparison with aircraft-measured EFs from previous forest fire studies. Values in parenthesis are errors for single fire and standard deviations for all available EFs for study averages.	100
Table 10	– Comparison of aerosol EFs (g kg ⁻¹) and ERs to $\Delta(\text{CO}_2+\text{CO})$ for temperate fuels measured from aircraft.	120
Table 11	– Acres burned and estimated annual emissions (Gg yr ⁻¹) by western U.S. wildfires.	135

LIST OF FIGURES

Figure 1	– Locations of the 15 agricultural fires during the SEAC ⁴ RS campaign.	16
Figure 2	– Time series of CO, CO ₂ , HCl, chloride, SO ₂ , sulfate, particle light absorption coefficient at 532 nm, and radar altitude for two typical transects: (a) cross-plume transect of Fire 12 on 23 September 2013 and (b) source to downwind transect of Fire 4 on 11 September 2013.	18
Figure 3	– Fires sampled and DC-8 flight track with wind barbs on 23 September 2013. Flight track is colored by aircraft radar altitude. Red triangles represent the locations of the 5 agricultural fires sampled. Dashed black lines represent plume samples obtained.	19
Figure 4	– Emission ratio plots of (a) $\Delta\text{SO}_2/\Delta\text{CO}_2$ and (b) $\Delta\text{BC}/\Delta\text{CO}_2$ from Fire 4 on 11 September 2013.	22
Figure 5	– Excess PSAP light absorption coefficient at 365 nm normalized by excess CO and corresponding absorption Ångström exponent (AAE) in fresh smoke. BrC absorption was 2-5 times that of BC at 365 nm.	47
Figure 6	– Closure analysis of b_{ap} at 365 nm for agricultural fire plumes via scatter plot of the sum of BrC absorption determined from liquid extracts plus estimated BC absorption based on PSAP measurements and an AAE_{BC} of 1 versus total aerosol absorption based on PSAP data. Orthogonal distance regression fit result and the 1:1 line are shown. Measurement uncertainties of the various absorption coefficients are estimated to be ~19%-45%.	47
Figure 7	– Estimates of annual emissions of (a) SO ₂ , (b) NO _x , and (c) CO from crop residue burning in Arkansas, Louisiana, Mississippi, and Missouri. NO _x emission estimates are reported as NO ₂ . The green error bars of the estimates based on <i>Melvin</i> [2012] represent the ranges of the burned area reported and are smaller than the overall errors of the emission estimates.	50
Figure 8	– Evolution of ozone in the 7 aged plumes. Data were fit to a linear trend line. Vertical error bars are a result of measurement uncertainties. Only error bars of one fresh and one aged measurement are shown as examples for each fire. Horizontal error bars represent the 1σ uncertainty in the estimated age based on the variability of wind direction and wind speed. Note that the	62

downwind evolution of Fire 12 might reflect both source changes to some extent and plume aging.

- Figure 9 – Evolution of reactive nitrogen species in the 7 aged plumes. Data were fit to a linear or polynomial trend line. Vertical error bars are a result of measurement uncertainties. Only error bars of one fresh and one aged measurement are shown as examples for each fire. The 1σ uncertainty in the estimated age is same as that shown in Figure 8. NO_2 measurements are not available for Fire 13. Note that the downwind evolution of Fire 12 might reflect both source changes to some extent and plume aging. 64
- Figure 10 – Box-and-whisker plot of (a) $\Delta\text{OA}/\Delta\text{CO}$ change and (b) $\Delta b_{\text{ap,BrC}(365)}/\Delta\text{CO}$ change in the 7 aged plumes (boxes, 25th and 75th percentiles; whiskers, 10th and 90th percentiles; solid horizontal lines, medians; the two thick lines mean that only one data point is available for the corresponding age). Dashed horizontal lines represent a constant value of 1, i.e., no enhancement. 68
- Figure 11 – Evolution of elemental ratios in particulate matter as measured by the AMS in 6 aged plumes (not available for Fire 12). 71
- Figure 12 – CO mixing ratio vs. smoke age for the 5 selected cases. Green, red, and blue lines are for the slow, best fit, and fast plume dilution rates. Circles are the measured mixing ratios, with the horizontal error bars showing the uncertainty in the estimated age. Crosses are background CO concentrations outside the plumes. 74
- Figure 13 – Enhancement ratios of ΔO_3 to ΔCO vs. smoke age for the 5 selected cases. Green, red, and blue lines are for the slow, best fit, and fast plume dilution rates. Circles are the measured enhancement ratios, with the vertical error bars showing the uncertainty in the measurement. The uncertainty in the estimated age is not shown here but is same as in Figure 12. 75
- Figure 14 – Enhancement ratios of (a) ΔPAN to ΔCO , (b) ΔHNO_3 to ΔCO and $(\Delta\text{HNO}_3 + \Delta\text{nitrate})$ to ΔCO , and (c) $\Delta\text{nitrate}$ to ΔCO vs. smoke age for the 5 selected cases. Circles (solid circles for single NO_y species and open circles for HNO_3 by CIMS + nitrate by AMS) are the measured enhancement ratios, with the vertical error bars showing the uncertainty in the measurement. The uncertainty in the estimated age is not shown here but is same as in Figure 12. The red lines (solid and dashed) are base model results for the best-fit dilution rates. The blue (solid) and green (solid and dashed) lines are the results of the base model with estimated HONO (using FLAME-4 EF) and diacetyl (using FLAME-4 EF and one half of 78

FLAME-4 EF) initial emissions.

- Figure 15 – Additional sensitivity test results of $\Delta\text{PAN}/\Delta\text{CO}$ vs. smoke age for the 5 selected cases. Circles are the measured enhancement ratios, with the vertical error bars showing the uncertainty in the measurement. The uncertainty in the estimated age is not shown but is same as in Figure 12. The red, purple, blue, and green lines are the results of the base model, the base model with doubled acetaldehyde input, the base model with estimated methylglyoxal using EF(methylglyoxal) by [Stockwell *et al.*, 2015], and the base model with estimated diacetyl, HONO, and methylglyoxal using EFs by [Stockwell *et al.*, 2015]. 81
- Figure 16 – (a) Enhancement ratios of ΔOA to ΔCO vs. smoke age for the 5 selected cases. Circles are the measured enhancement ratios, with the vertical error bars showing the uncertainty in the measurement. The uncertainty in the estimated age is not shown but is same as in Figure 12. The red lines are parameterization results for the best-fit dilution rates assuming OA is non-volatile. (b) Elemental O/C ratios vs. smoke age for the 5 selected cases. Dots are the measured O/C ratios. The red and blue lines are model results of mixing effects only and of both mixing and oxidation effects, respectively. 85
- Figure 17 – Map of the three wildfires and flight tracks near the fire sources during BBOP and SEAC⁴RS. Flight tracks are colored by measured CO concentrations. The dates indicate the day each fire was sampled. 93
- Figure 18 – Examples of time series of CO₂, SO₂, methanol, O₃, and GPS altitude for: (a) Colockum Tarps; (b) Big Windy Complex; and (c) Rim Fire. Shaded area shows the duration of fresh plume used for analysis. 94
- Figure 19 – The average emission factors (boxes) and standard deviations (whiskers) for the 20 most abundant trace gases (excluding CO₂, CO, CH₄) measured from the three wildfires. 110
- Figure 20 – Emission factors (g kg⁻¹) of gaseous species as a function of MCE for the three wildfires of this study, the boreal forest fires of Simpson *et al.* [2011], and the prescribed fires of Burling *et al.* [2011] and Akagi *et al.* [2013]. Gases shown here are associated with slopes that are significantly different from zero. Correlation coefficients (r^2) were derived from bivariate linear regressions of all plotted data. 126
- Figure 21 – Emission factors (g kg⁻¹) of gaseous species as a function of MCE for the three wildfires of this study, the boreal forest fires of 129

Simpson et al. [2011], and the prescribed fires of *Burling et al.* [2011] and *Akagi et al.* [2013]. Gases shown here are associated with slopes that are not significantly different from zero. Correlation coefficients (r^2) were derived from bivariate linear regressions of all plotted data.

Figure 22 – Emission factors (g kg^{-1}) of all fine particle species as a function of MCE for the three wildfires of this study and the prescribed fire data of *May et al.* [2014]. Correlation coefficients (r^2) were derived from bivariate linear regressions of all plotted data. Only the slope of EF(OA) versus MCE is significantly different from zero. 132

LIST OF SYMBOLS AND ABBREVIATIONS

AAE	Absorption Ångström Exponent
AMS	Aerosol Mass Spectrometer
b_{ap}	Aerosol Absorption Coefficient
BB	Biomass Burning
BBOP	Biomass Burning Observation Project
BC	Black Carbon
BrC	Brown Carbon
CIMS	Chemical Ionization Mass Spectrometry
EF	Emission Factor
ER	Emission Ratio
FLAME-4	Fourth Fire Lab at Missoula Experiment
H/C	Hydrogen to Carbon Ratio
MCE	Modified Combustion Efficiency
NMHCs	Non-Methane Hydrocarbons
NMOCs	Non-Methane Organic Compounds
OA	Organic Aerosol
OVOCs	Oxygenated Volatile Organic Compounds
O/C	Oxygen to Carbon Ratio
PAN	Peroxyacetyl Nitrate
PM ₁	Particulate Matter with Aerodynamic Diameter < 1 μm
PM _{2.5}	Particulate Matter with Aerodynamic Diameter < 2.5 μm
POA	Primary Organic Aerosol

PSAP	Particle Soot Absorption Photometer
PTR-MS	Proton-Transfer-Reaction Mass Spectrometer
SEAC ⁴ RS	Studies of Emissions, Atmospheric Composition, Clouds and Climate Coupling by Regional Surveys
SOA	Secondary Organic Aerosol
VOCs	Volatile Organic Compounds
WAS	Whole Air Sampling

SUMMARY

Open biomass burning (BB), including natural wildfires and prescribed agricultural and forest management fires, produces significant amounts of trace gases and aerosol, which play important roles in atmospheric chemistry and climate. However, some types of BB such as agricultural fires and temperate wildfires remain under-sampled, which limits the understanding of their impacts on regional air quality. This thesis presents detailed airborne measurements of primary emissions from agricultural fires and wildfires in the U.S. and the chemical transformations of primary emissions in the agricultural fire plumes.

Emissions from 15 agricultural fires in the southeastern U.S. were measured from the NASA DC-8 research aircraft during the summer 2013 Studies of Emissions and Atmospheric Composition, Clouds and Climate Coupling by Regional Surveys (SEAC⁴RS) campaign. A detailed set of emission factors (EFs) for 25 trace gases and 6 fine particle species was reported. Observed EFs are generally consistent with previous measurements of crop residue burning, but the fires studied here emitted high amounts of sulfur dioxide (SO₂) and fine particles, especially primary organic aerosol (POA) and chloride. Filter-based measurements of aerosol light absorption implied that brown carbon (BrC) was ubiquitous in the plumes. With the calculated EFs, total annual SO₂, nitrogen oxides (NO_x) and carbon monoxide (CO) emissions from agricultural fires in Arkansas, Louisiana, Mississippi, and Missouri were estimated (within a factor of ~2) to be equivalent to ~2% SO₂ from coal combustion and ~1% NO_x and ~9% CO from mobile sources.

The chemical evolution of the primary emissions in 7 out of 15 agricultural plumes was examined in detail for ~1.2 hr. A Lagrangian plume cross-section model was used to simulate the evolution of ozone (O_3), reactive nitrogen species, and organic aerosol (OA). In aged plumes, rapid production of O_3 , peroxyacetyl nitrate (PAN), and nitrate were observed with $\Delta O_3/\Delta CO$, $\Delta PAN/\Delta NO_y$, and $\Delta nitrate/\Delta NO_y$ reaching ~0.1, ~0.3, and ~0.3. For 5 selected cases, the model reasonably simulated O_3 formation but underestimated PAN formation. No significant evolution of OA mass or BrC absorption was observed. However, a consistent increase in oxygen-to-carbon (O/C) ratios of OA indicated that OA oxidation in the agricultural fire plumes was much faster than in urban and forest fire plumes.

To better understand wildfire emissions and inform fire management, plumes from three wildfires in the western U.S. were measured from aircraft during SEAC⁴RS and the Biomass Burning Observation Project (BBOP), both in summer 2013. An extensive set of EFs for over 80 gases and 5 components of submicron particulate matter (PM_{10}) from temperate wildfires were presented here. These include some rarely, or never before, measured oxygenated volatile organic compounds and multifunctional organic nitrates. The EFs from three wildfires are compared with those from previous airborne measurements of temperate wildfires, boreal forest fires, and temperate prescribed fires. The wildfires studied emitted high amounts of PM_{10} (with organic aerosol, OA, dominating the mass) with an average EF that is over two times than those of prescribed fires. The EFs were used to estimate the annual wildfire emissions of CO, NO_x , total non-methane organic compound (NMOC), and PM_{10} from 11 western U.S. states. The estimated gas emissions are generally comparable with the 2011 National Emissions

Inventory (NEI). However, our PM_{10} emission estimate ($1530 \pm 570 \text{ Gg yr}^{-1}$) is over three times that of the NEI $\text{PM}_{2.5}$ estimate mainly due to our high $\text{EF}(\text{PM}_{10})$ and is also higher than the $\text{PM}_{2.5}$ emitted from all other sources in these states in the NEI. This suggests that the practice of prescribed burning may be an effective method to reduce fine particle emissions.

CHAPTER 1. INTRODUCTION

This chapter discusses the importance of biomass burning. The motivation of this thesis is explained and an outline of the thesis is provided.

1.1 Biomass Burning Background

Biomass burning (BB) produces significant amounts of trace gases and aerosol, such as carbon dioxide (CO_2), carbon monoxide (CO), methane (CH_4), non-methane hydrocarbons (NMHCs), nitrogen oxides (NO_x), ammonia (NH_3), sulfur dioxide (SO_2), black carbon (BC), organic aerosol (OA), and inorganic particulate matter [*Andreae and Merlet, 2001; Dennis et al., 2002; Akagi et al., 2011; McCarty, 2011; Huang et al., 2012; Kudo et al., 2014*]. These emissions play important roles in atmospheric chemistry and climate [*Crutzen and Andreae, 1990*]. Trace gases emitted by BB can have a significant influence on the formation of ozone (O_3), a major air pollutant and also a greenhouse gas. In addition, trace gases can also contribute to the formation of secondary aerosol particles [*Alvarado and Prinn, 2009; Yokelson et al., 2009*]. Aerosol directly emitted and formed in BB plumes impacts climate directly, through scattering and absorption of solar radiation, and indirectly, by modifying cloud microphysics and precipitation processes [*Reid et al., 2005*]. Particulate matter (PM), O_3 , and many other primary emissions and secondary products have negative health effects, which can be exacerbated when the smoke impacts populated areas [*Künzli et al., 2006; Naeher et al., 2007; Delfino et al., 2009*].

In recent years, biomass burning has been closely studied through many forms including laboratory burns, field measurements, in situ experiments, remote sensing, and modeling [Reid *et al.*, 2005; Akagi *et al.*, 2011]. A wide range of emitted species has been quantified and the transformation of primary emissions is reasonably well understood. However, many important types of BB remain under-sampled or rarely sampled, such as agricultural fires, wildfires in temperate regions, and biofuel burning. There are also many uncertainties about the effects of plume chemistry on the composition of the smoke and downwind air quality. Measurements that characterize emissions and evolution from the under-sampled fires are thus essential to improve emission estimates and air quality predictions on local to global scales.

1.2 Motivation and Goals

This research aims to improve the understanding of under-sampled BB, including agricultural fires and wildfires in the U.S., by utilizing airborne measurements of a wide variety of chemical species and physical parameters. These airborne measurements sampled plumes in the complex, natural environment and thus are representative of real-world emissions and smoke aging. They also provided valuable information on some previously rarely measured species and evolution.

A main focus of this research is a detailed study of primary emissions of 25 trace gases and 6 fine particle species from 15 agricultural fires in the southeastern U.S. (chapter 3). In addition, the chemical evolution of the primary emissions in 7 agricultural plumes was examined for ~1.2 h and then compared with simulated results using a Lagrangian plume cross-section model (chapter 4). Finally, the initial emissions,

including over 80 gases and 5 components of submicron particulate matter (PM_{10}), from three wildfires in the western U.S. as well as their air quality implications are examined (chapter 5). These results will help inform future fire management and atmospheric chemistry studies.

1.3 Outline of the Thesis

Chapter 1 introduces biomass burning. Many important biomass combustion sources still remain under-sampled. Hence, the motivation for this research is to provide missing information about primary emissions and evolution in these fires based on airborne measurements.

Chapter 2 summarizes the aircraft measurements used and gives a brief introduction to BB terminology and calculations used in this thesis to quantify BB emissions and evolution, including emission ratios (ERs), emission factors (EFs), and modified combustion efficiency (MCE).

Chapter 3 characterizes primary emissions from 15 agricultural fires in the southeastern U.S. sampled during the summer 2013 Studies of Emissions and Atmospheric Composition, Clouds and Climate Coupling by Regional Surveys (SEAC⁴RS) airborne field campaign. Filter-based measurements of aerosol light absorption were used to imply brown carbon (BrC) emission in the plumes. Using the measured EFs, total annual SO_2 , NO_x , and CO emissions from agricultural fires in Arkansas, Louisiana, Mississippi, and Missouri were estimated.

Chapter 4 examines the chemical evolution of the primary emissions in 7 agricultural fire plumes up to ~1.2 hr. A Lagrangian plume cross-section (LPCS) model was used to simulate the evolution of O₃, reactive nitrogen species, and OA.

Chapter 5 presents an extensive set of EFs for over 80 gases and 5 components of PM₁ from three wildfires in the western U.S. These include some rarely, or never before, measured oxygenated volatile organic compounds (OVOCs) and multifunctional organic nitrates. The EFs were used to estimate the annual wildfire emissions of CO, NO_x, total non-methane organic compound (NMOC), and PM₁ from 11 western U.S. states.

Chapter 6 concludes the thesis and summarizes the findings. Also discussed are some of the unresolved issues and potential future research about BB.

CHAPTER 2. INSTRUMENTATION AND TERMINOLOGY

This chapter summarizes the aircraft measurements used in the thesis and gives a brief introduction to BB terminology and calculations used to quantify BB emissions and evolution, including emission ratios (ERs), emission factors (EFs), and modified combustion efficiency (MCE).

2.1 Aircraft Instrumentation

In situ measurements were conducted from the NASA DC-8 aircraft during SEAC⁴RS and the Department of Energy (DOE) Gulfstream-1 (G-1) aircraft during BBOP. A wide range of chemical, physical, and optical measurements onboard DC-8 aircraft were used to characterize 15 agricultural fires in the southeastern and 2 wildfires in the western U.S. These measurements are listed in Table 1 along with methodologies, sample intervals, accuracies, and references. The set of SEAC⁴RS measurements used to characterize wildfire and agricultural fire emissions were almost identical, except for that the wildfire study includes an additional set of volatile organic compounds (VOCs) measured by whole air sampling (WAS) [Simpson *et al.*, 2011] and several oxygenated volatile organic compounds (OVOCs) and organic nitrates measured by chemical ionization mass spectrometry (CIMS) [Crounse *et al.*, 2006; Paulot *et al.*, 2009a; St. Clair *et al.*, 2014; Teng *et al.*, 2015].

Table 2 summarizes the BBOP trace gas and particle measurements used in this thesis, along with methodologies, sample intervals, accuracies, and references. While full details of most instruments deployed for BBOP are available in the references cited in

Table 2, here we describe a few exceptions. CO was measured on the G-1 by a commercial instrument based on cavity enhanced absorption (Los Gatos Research, San Jose, CA). O₃ was measured by a commercial analyzer (Thermo Scientific Model 49i) that was modified for internal calibrations. A commercial SO₂ analyzer (Thermo Scientific 43i) was modified to provide an internal chemical zero. The NO/NO₂/NO_y instrument was custom built by Air Quality Design, Inc. (Golden, CO).

All the SEAC⁴RS and BBOP data used in this work can be accessed through the NASA data archive (<http://www-air.larc.nasa.gov/cgi-bin/ArcView/seac4rs>, doi: 10.5067/Aircraft/SEAC4RS/Aerosol-TraceGas-Cloud) and Atmospheric Radiation Measurement website (<http://www.arm.gov/campaigns/bbop>), respectively. All aircraft data used were synchronized to a common time scale with 1 Hz resolution, which ensured accurate peak alignment.

Table 1 – Aircraft measurements aboard the NASA DC-8 research aircraft during SEAC⁴RS.

Measurement	Method	Sample Interval	Calibration Accuracy	Reference
SO ₂ , HCl	SF ₆ ⁺ chemical ionization mass spectrometry (CIMS)	0.5 s, 0.1 s @ 1.2 s ^a	15-25%	<i>Huey et al.</i> [2004]
PAN	I ⁺ CIMS	0.5 s @ 2 s ^a	15%	<i>Slusher et al.</i> [2004]
NO, NO ₂ , NO _y , O ₃	Chemiluminescence	1 s	3-15%	<i>Ryerson et al.</i> [1999], <i>Ryerson et al.</i> [2000]
VOCs, OVOCs ^b	Proton-transfer-reaction mass spectrometry	0.1 s @ 10 s ^a	5-15%	<i>Wisthaler et al.</i> [2002]
NMHCs	Whole air sampling & gas chromatography	30-60 s	1-5%	<i>Blake et al.</i> [2003], <i>Simpson et al.</i> [2011]
CO	Differential absorption CO measurement	1 s	5%	<i>Sachse et al.</i> [1987], <i>Diskin et al.</i> [2002]
CO ₂	Non-dispersive infrared spectrometer	1 s	0.25 ppm	<i>Vay et al.</i> [2011]
HNO ₃ , HCN, H ₂ O ₂ , OVOCs, and organic nitrates	CF ₃ O ⁺ CIMS	1 s	30-50%	<i>Crounse et al.</i> [2006], <i>St. Clair et al.</i> [2014], <i>Paulot et al.</i> [2009a]
Formaldehyde	Laser-induced fluorescence ^c / Difference frequency generation absorption spectroscopy ^d	1 s	4-10%	<i>Cazorla et al.</i> [2015], <i>Weibring et al.</i> [2006], <i>Weibring et al.</i> [2007]

Table 1 (continued).

Measurement	Method	Sample Interval	Calibration Accuracy	Reference
Non-refractory Submicron Aerosol (Sulfate, Nitrate, Ammonium, Chloride, Organics) ^e	High resolution time of flight mass spectrometry	1 s	34-38%	<i>Canagaratna et al. [2007]</i> , <i>Canagaratna et al. [2015]</i>
Black carbon aerosol ^f	Laser-induced incandescence	1 s	30%	<i>Schwarz et al. [2013]</i>
Particle absorption coefficients	Radiance Research particle soot absorption photometer	1 s	5%	<i>Virkkula et al. [2005]</i>
Photolysis frequencies	Spectral Radiometry	3 s	~12-25%	<i>Shetter and Müller [1999]</i>

^a Disjunct sampling.

^b In the case of multiple neutral precursors for a specific m/z signal, we consider only species with a relative contribution > 10% to the total signal [*Yokelson et al., 2013*; *Stockwell et al., 2015*; *Müller et al., 2016*].

^c Used to derive CH₂O emissions for the flights on 6, 9, 11, and 16 September, 2013.

^d Used to derive CH₂O emissions for the flight on 23 September 2013 when laser-induced fluorescence measurement was not available.

^e Particle diameter less than 1 µm.

^f Particle diameter range is ~90-550 nm.

Table 2 – G-1 aircraft measurements during BBOP used in this work.

Measurement	Method	Sample Interval	Calibration Accuracy	Reference/ Instrument
CO ₂ and CH ₄	Cavity ring down spectroscopy	~ 1 s	<70 ppb for CO ₂ , <0.5 ppb for CH ₄	<i>Crosson</i> [2008]/Picarro Inc.
CO	Cavity enhanced absorption	1 s	2%	Los Gatos Research
NO, NO ₂ , NO _y	Chemiluminescence	1 s	10%	Air Quality Design, Inc.
VOCs and OVOCs	Proton-transfer-reaction mass spectrometry	0.1 s @ ~3.4 s ^a	5-15%	<i>Wisthaler et al.</i> [2002]
SO ₂	Pulsed fluorescence	1 s	~5-10%	Thermo Scientific 43i
O ₃	UV optical absorption	1 s	5%	Thermo Scientific 49i
Non-refractory Submicron Aerosol (Sulfate, Nitrate, Ammonium, Chloride, Organics) ^b	Soot particle aerosol mass spectrometry	1 s	10%	<i>Canagaratna et al.</i> [2007]

^a Disjunct sampling.

^b Particle diameter less than 1 μm . A collection efficiency of 0.5 was used, though this may overestimate the non-refractory PM for dual vaporizer modes (refer to *Onasch et al.* [2012] Table 1 and discussions in *Lee et al.* [2015]).

2.2 Emission Ratios, Emission Factors, and Modified Combustion Efficiency

For all the identified BB plumes, the following quantities were derived: excess mixing ratio; normalized excess mixing ratio (NEMR); emission ratio (ER); emission factor (EF); and modified combustion efficiency (MCE). These parameters were then used to characterize initial emissions and plume evolution. The excess mixing ratio of a species X (ΔX) was calculated by subtracting the mixing ratio of X in the background air from that in the fire plume. The background concentrations were based on measurements made ~30 s before or after the plume encounter, at a similar location and altitude as the sampled plume. For this time period, both continuous and discrete instruments (Table 1 and Table 2) acquired sufficient data in background air. The NEMR was derived by dividing ΔX by the excess mixing ratio of a simultaneously measured species Y, where Y was usually a relatively long-lived tracer such as CO or CO₂ that enabled the NEMR to account for the influence of dilution. A special case of the NEMR is the ER, which is $\Delta X/\Delta Y$ specifically in fresh smoke up to a few minutes old sampled at or near the fire source. The ER has two important uses: (1) it can be used to calculate EFs; and (2) differences between the ERs measured at the source and the NEMRs measured downwind allow us to quantify post-emission gas and particulate phase chemistry and gas-particle partitioning. Fire-averaged ERs were used to compute EFs.

EFs, in units of grams of compound X emitted per kilogram of dry biomass burned, were derived for all the individual fires using the carbon mass balance method, which assumes that all the volatilized carbon is detected [Yokelson *et al.*, 1999]:

$$EF_X = F_C \times MW_X / MW_C \times C_X / C_T \quad (1)$$

where F_C is the carbon mass fraction and normally ranges between 45 and 55% except for organic soils and dung [Susott *et al.*, 1996; Yokelson *et al.*, 1997; McMeeking *et al.*, 2009]; MW_X and MW_C are the molecular weight of compound X and the atomic weight of carbon, respectively; and C_X/C_T is the number of emitted moles of compound X divided by the total number of moles of carbon emitted. C_X/C_T was calculated using

$$\frac{C_X}{C_T} = \frac{\frac{\Delta C_X}{\Delta CO_2}}{\sum_{j=1}^n (nC_j \times \frac{\Delta C_j}{\Delta CO_2})} \quad (2)$$

where $\Delta C_X/\Delta CO_2$ and $\Delta C_j/\Delta CO_2$ are the fire-averaged ER of species X to CO_2 and that of carbon-containing species j to CO_2 , respectively; and nC_j is the number of carbon atoms in compound j. The sum of the moles of carbon divided by the emitted moles of CO_2 , the denominator in Equation (2), was determined from the measured carbon-containing species such as CO_2 and CO.

BB emissions also vary with different combustion processes, e.g. flaming and smoldering. The MCE, which describes the relative amount of flaming or smoldering [Akagi *et al.*, 2011], was also calculated. MCE is defined as $\Delta CO_2/(\Delta CO_2 + \Delta CO)$. Higher MCE values indicate more flaming combustion and lower MCE more smoldering combustion. Pure flaming has an MCE near 0.99, while smoldering has an MCE over a larger range (~0.65-0.85) but is most often near 0.8. An overall fire-integrated MCE near

0.9 suggests roughly equal amounts of flaming and smoldering [*Akagi et al.*, 2011]. Fire-integrated MCEs are presented here for comparison to fire-averaged EFs.

CHAPTER 3. U.S. AGRICULTURAL FIRE EMISSIONS

This chapter characterizes primary emissions from 15 agricultural fires in the southeastern U.S. sampled during the summer 2013 SEAC⁴RS airborne field campaign.

3.1 Introduction

One important component of BB is agricultural field burning, a common practice worldwide. Emissions of global agricultural residue burning have been estimated as the fourth largest among all types of BB [*Andreae and Merlet, 2001*]. An estimated 500 Tg of crop residues were burned in fields annually in the developing world in the 1990s [*Yevich and Logan, 2003*]. Agricultural field burning is also extensive in the contiguous United States [*McCarty, 2011*], where wheat, rice, sugarcane, peanut, soybeans, barley, and corn croplands are thought to have the most significant burning activity [*Dennis et al., 2002*].

Agricultural fire emissions can have a large impact on atmospheric composition and air quality on regional scales. Previous studies demonstrated that the open burning of crop residues is a significant source of trace gases and aerosols such as CO₂, CO, CH₄, NMHCs, NO_x, NH₃, SO₂, BC, OA, and inorganic particulate matter [*Dennis et al., 2002; McCarty, 2011; Huang et al., 2012; Kudo et al., 2014*]. These emissions can lead to severe air quality problems. For example, *Zhang et al.* [2015] found that primary emissions from BB, mainly crop residue burning, contributed to $25 \pm 8\%$ of elemental carbon (EC) and 40-65% of non-fossil organic carbon (OC) in four major cities in China during an extreme haze episode in winter 2013. Despite the important impacts of the

emissions from agricultural burning, emission inventories are not well characterized. The uncertainty in agricultural burning emissions is primarily due to two factors: (1) many of the emitted species are rarely measured or even identified; and (2) the burn area and/or the fraction of crop residue burned is highly uncertain [McCarty *et al.*, 2009; Randerson *et al.*, 2012].

Field measurements from airborne and ground-based platforms are able to sample plumes in the complex, natural environment and are a valuable method to characterize fire emissions and evolution. However, field measurements of agricultural burning are scarce and have been mainly conducted in Mexico and China [Yokelson *et al.*, 2009; Yokelson *et al.*, 2011; Kudo *et al.*, 2014]. Although agricultural field burning is ubiquitous in the U.S., no field study to date has characterized the emissions and smoke chemistry of these fires. Laboratory studies are also an important method to characterize BB smoke. Recently, the fourth Fire Lab at Missoula Experiment (FLAME-4) conducted laboratory burning studies of trace gas and particle emissions and their subsequent evolution from several types of crop residues collected from various countries [Stockwell *et al.*, 2014]. These lab-burned crop residues include fuels that are important in the U.S., such as sugarcane, rice straw, and wheat straw.

The area of agricultural burning is usually estimated by surveys, conducted by state agencies, or by remote sensing [McCarty *et al.*, 2009; Melvin, 2012; Randerson *et al.*, 2012]. Both methods can underestimate the area burned and thus the magnitude of emissions. The survey method is limited as few states collect agricultural burning information and burning practices vary widely from state to state. Remote sensing methods have difficulty with detecting agricultural fires as they are often short-lived and

relatively small [Smith *et al.*, 2007; Hawbaker *et al.*, 2008; Chang and Song, 2010; van der Werf *et al.*, 2010].

A major goal of the recent Studies of Emissions and Atmospheric Composition, Clouds and Climate Coupling by Regional Surveys (SEAC⁴RS) airborne field campaign was to quantify the emissions and assess the atmospheric impacts of agricultural and forest fires. The heavily instrumented NASA DC-8 research aircraft was deployed during this mission, which enabled measurements of a wide variety of chemical species and physical parameters [Liu *et al.*, 2016; Toon *et al.*, 2016]. During SEAC⁴RS, five research flights targeted agricultural fire plumes during late summer of 2013.

This chapter presents the first detailed measurements of trace gas and fine particle emissions from 15 agricultural fires in the U.S., with locations shown in Figure 1. The vegetation burned is almost certainly rice straw because it is essentially the only crop residue burned in the Mississippi River Valley during the late summer and early fall [McCarty *et al.*, 2007]. With the measured EFs, we also estimate the annual agricultural fire emissions of SO₂, NO_x, and CO from the four states where the fires were sampled.

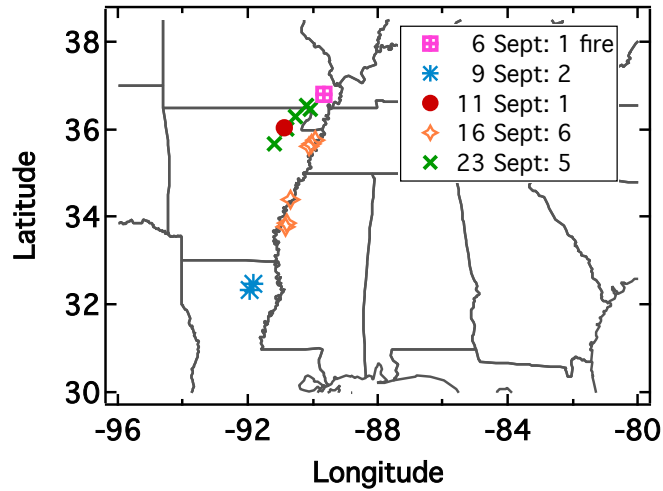


Figure 1 – Locations of the 15 agricultural fires during the SEAC⁴RS campaign.

3.2 Methods

3.2.1 Airborne Sampling of Fires

The aircraft sampled agricultural fires during the 5 research flights by either cross-plume or long-axis penetrations at its typical air speeds in the range $\sim 110\text{-}150 \text{ m s}^{-1}$. Figure 2 exemplifies two time series obtained following each strategy. The cross-plume transects were usually performed at or near the source at altitudes ranging from 0.3-1.3 km above the ground, which provided observations of fresh smoke younger than several minutes. However, since such sampling requires high time resolution measurements, some instruments could not get sufficient data, especially for small fires. Therefore the

long-axis sampling strategy, including source-to-downwind and downwind-to-source approaches, was also performed for some agricultural fires. The aircraft conducted the long-axis source-to-downwind sampling by entering the smoke column very close to the active flame front at an altitude between 0.2 and 1.3 km, mostly below 0.5 km. Maximum performance climbs were then attempted to match the rise of the smoke and to extend sampling in the smoke. As the plane flew down the long axis, it entered or exited both thicker and thinner plume regions, creating a series of peaks due to intermittent sampling of higher concentrations along the plume length. The sample age for each peak was calculated by dividing the downwind distance from the source by average wind speed, calculated using 3-D wind measurements [Chan *et al.*, 1998]. The source locations usually preceded the largest fresh peak by a few hundred meters since the smoke rose at an angle. The downwind-to-source sampling was performed as the reverse of the source-to-downwind sampling. With the long-axis strategy, the aircraft acquired samples of both fresh and aged plumes up to ~16 km downwind and ~1.2 h old. Figure 3 shows an example of a partial flight path over Arkansas on 23 September 2013 along with the locations of the 5 agricultural fires sampled. Table 3 summarizes the sampling times and locations of the 15 agricultural fires and the number of samples obtained by each of the two sampling strategies. Of the 15 fires, the sources of 12 fires were recorded by the aircraft cameras. The locations of these fires are defined as the centers of the burning fields with an accuracy of ~300 m for a typical sized field. For the 3 fires for which sources were not recorded, their source locations were defined as the point where the 1 s CO concentration was highest in each plume sample. The locations of the 15 fires are also displayed in Figure 1.

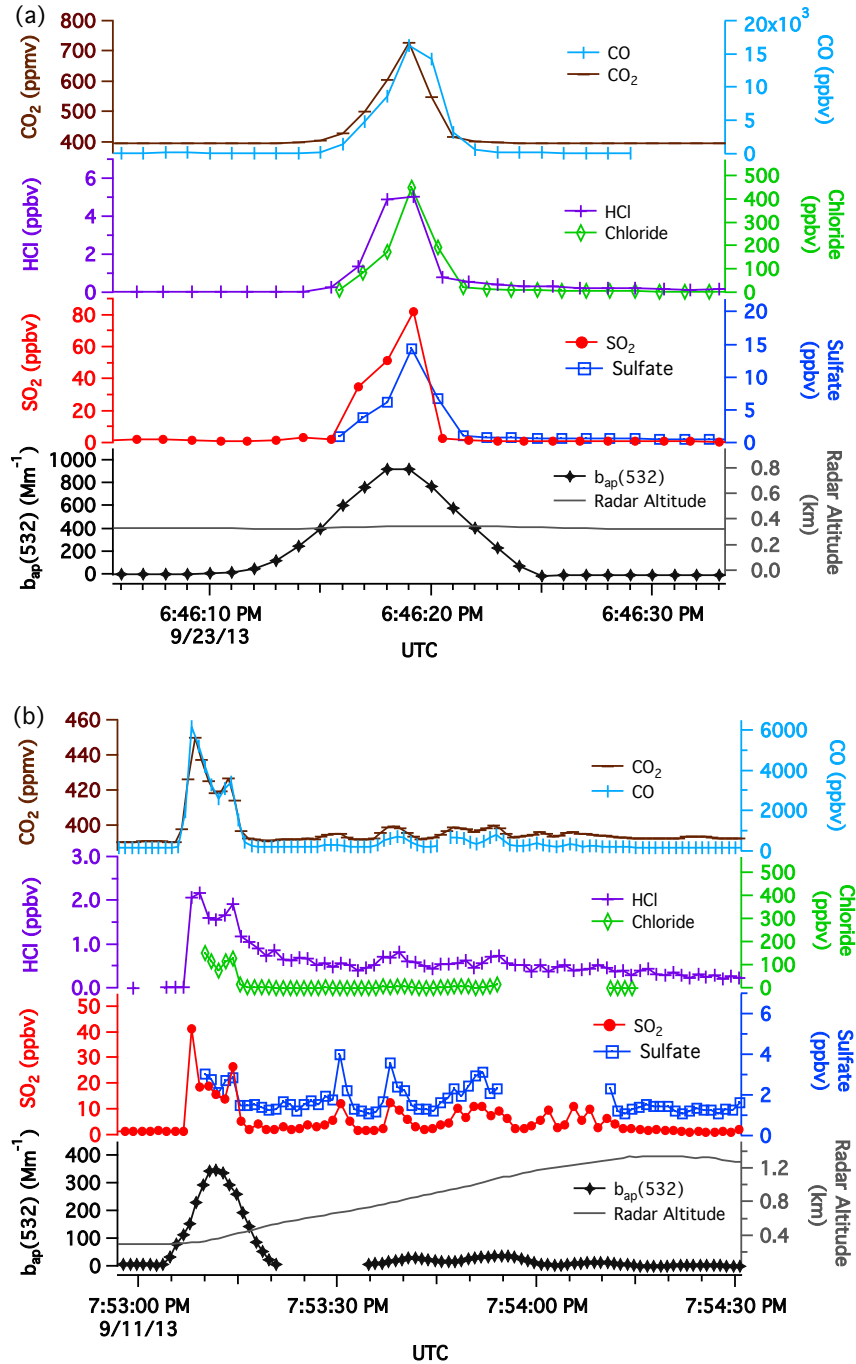


Figure 2 – Time series of CO, CO₂, HCl, chloride, SO₂, sulfate, particle light absorption coefficient at 532 nm, and radar altitude for two typical transects: (a) cross-plume transect of Fire 12 on 23 September 2013 and (b) source to downwind transect of Fire 4 on 11 September 2013.

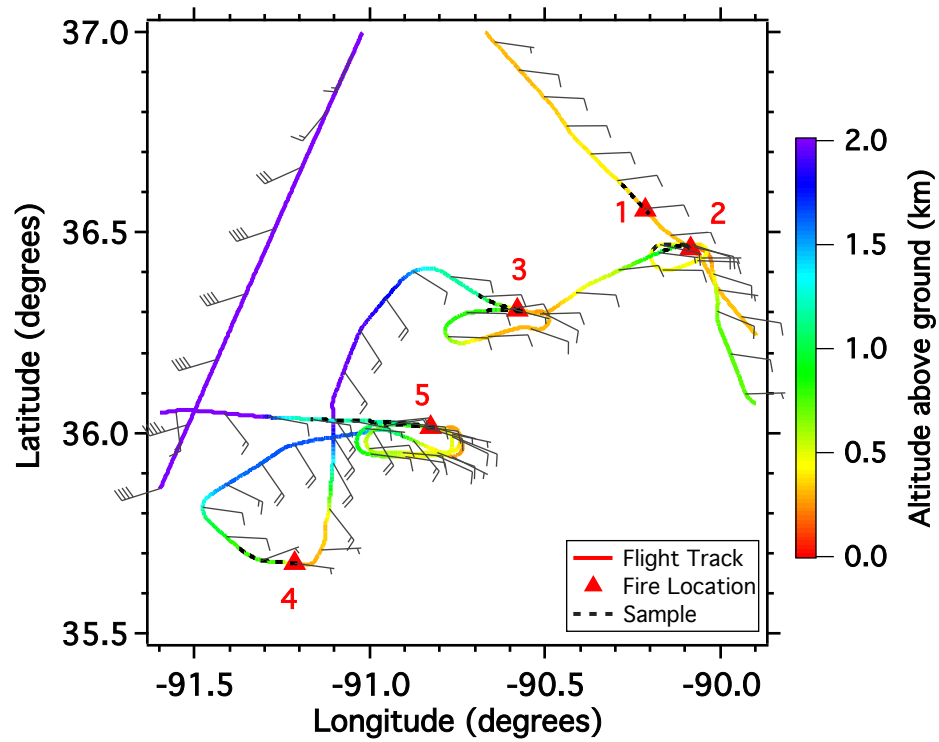


Figure 3 – Fires sampled and DC-8 flight track with wind barbs on 23 September 2013. Flight track is colored by aircraft radar altitude. Red triangles represent the locations of the 5 agricultural fires sampled. Dashed black lines represent plume samples obtained.

Table 3 – Details of the agricultural fires sampled in the southeastern U.S.

Date	Fire #	Local Time	Latitude	Longitude	Field Size ^a (ha)	State	No. of cross-plume samples	No. of long-axis samples
6 Sept	1 ^b	13:57-13:58	36.8143	-89.6778	22.27	MO	0	1
			36.8217	-89.6752	43.61			
9 Sept	2 ^c	18:22	32.4714	-91.8541	-	LA	1	0
	3	18:35-19:19	32.3365	-91.9755	37.24	LA	2	4
11 Sept	4	14:53-15:01	36.0497	-90.8913	127.59	AR	0	2
16 Sept	5	17:21-17:25	35.7742	-89.9388	30.39	AR	0	2
	6 ^c	17:27	35.6636	-90.0629	-	AR	0	1
	7	17:32-17:33	35.6278	-90.1471	26.94	AR	0	2
	8	17:49-17:50	34.4073	-90.7022	22.58	AR	0	1
	9	17:57	33.8702	-90.8243	17.15	MS	0	1
	10	17:58-17:59	33.7876	-90.8746	21.64	MS	0	1
23 Sept	11 ^c	13:43-13:44	36.5622	-90.2199	-	MO	1	0
	12	13:46-14:05	36.4647	-90.0898	30.97	MO	1	2
	13	14:09-14:21	36.3024	-90.5659	27.62	AR	1	2
	14	14:31-14:33	35.6727	-91.2077	18.15	AR	0	1
	15	14:46-15:07	36.0128	-90.8144	16.35	AR	0	3

^a Determined using Google Earth.

^b Two adjacent fields were burning at the same time and their plume columns merged into a single plume.

^c Fires for which the sources were not recorded by the aircraft cameras.

3.2.2 Estimation of ERs, EFs, and MCE

The enhancements of CO and CO₂ (the two main gaseous emissions from BB) were examined for all 5 flights to identify and delineate the edges of all agricultural burning plumes. BB tracers such as hydrogen cyanide (HCN) and acetonitrile (CH₃CN) were then

used to confirm that the CO and CO₂ enhancements were due to BB. For all the identified plumes, the following quantities were derived as described in chapter 2: excess mixing ratio, NEMR, ER, EF, and MCE. These parameters were then used to characterize initial emissions and plume evolution. As shown in Table 1, the data used in this study were generated from various continuous and discrete instruments with different time resolutions and response times. To allow comparison between different instruments, NEMRs (or ERs) were obtained by comparing the integrals of ΔX and ΔY of a series of peaks as the aircraft passed through an aged (or nascent) smoke plume (SO₂ and BC are shown as examples in Figure 4). Fire-averaged ERs were used to compute EFs. The fire-averaged molar ERs for gaseous species and mass ERs for particulate species relative to CO₂ or CO for each individual fire were computed as follows. First, if only one fresh plume transect was available for a fire, the ER for this fire was the ratio between the integral of ΔX over the entire fresh plume relative to that of ΔCO_2 or ΔCO over the entire fresh plume. Second, for multiple discrete samples of a fire, the fire-averaged ER was obtained from the slope of the least-squares line (with the intercept forced to zero) in a plot of one set of integrals of excess mixing ratios versus another [Yokelson *et al.*, 2009]. However, species measured by the PTR-MS were treated differently, because they were reported for 0.5-1 s measurements at a lower time resolution of every ~10 s. Potential errors due to different sampling frequencies limit deriving the ERs of these species directly from $\Delta X/\Delta \text{CO}$ in an environment with rapidly changing concentrations. For these species, we first obtained the ER relative to PTR-MS benzene averaged over each fire by comparing the integrated excess for an entire fire to the integrated excess amount for benzene. As benzene was also measured by the whole air sampling (WAS) system at

time resolutions of 30-60 s, this facilitated obtaining ERs of PTR-MS species relative to ΔCO . To be specific, these ERs can be obtained by multiplying the ER of $\Delta(\text{PTR-MS species})/\Delta(\text{PTR-MS benzene})$ by the fire-averaged ER of $\Delta(\text{WAS benzene})/\Delta\text{CO}$, with $\Delta(\text{WAS benzene})$ and ΔCO integrated over the same period within the plume. For the three fires where WAS benzene was not available (Fires 2, 7, and 11), the fire-averaged ERs of $\Delta(\text{PTR-MS benzene})/\Delta\text{CO}$ were used for obtaining ERs of PTR-MS species, in which $\Delta(\text{PTR-MS benzene})$ and ΔCO were averaged over the same sampling time.

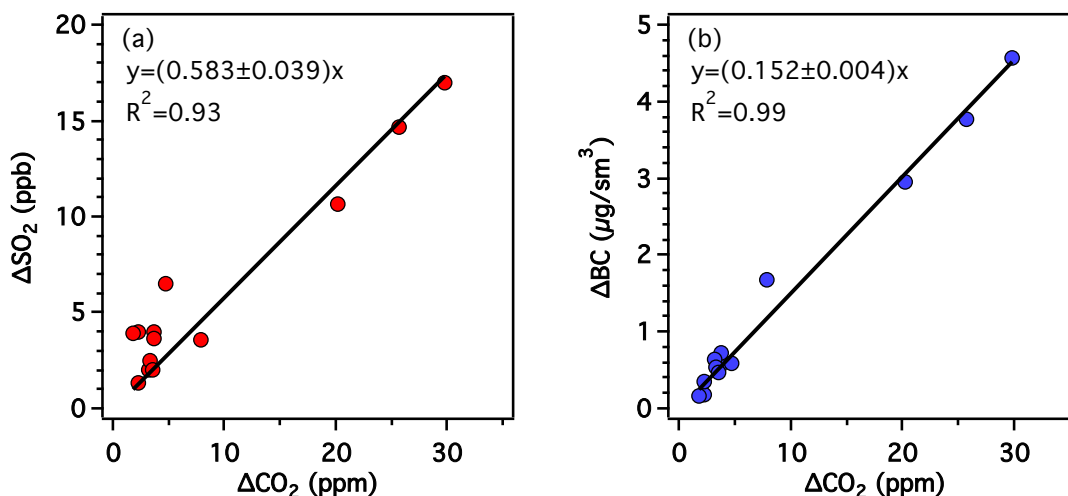


Figure 4 – Emission ratio plots of (a) $\Delta\text{SO}_2/\Delta\text{CO}_2$ and (b) $\Delta\text{ABC}/\Delta\text{CO}_2$ from Fire 4 on 11 September 2013.

Emissions undergo chemical and physical changes that can deplete or enhance their mixing ratios. In this study, short-lived compounds are defined as those with lifetimes less than ~ 1 day [Atkinson and Arey, 2003; Atkinson *et al.*, 2006; Simpson *et al.*, 2011]. To further identify any other reactive compounds, the NEMR of each species, which was obtained from long-axis samples, was plotted versus smoke age to identify possible evolution. For both the short-lived compounds and the longer-lived compounds that also exhibited evolution, the fire-averaged ERs were calculated only using the fresh samples that were less than ~ 10 min old and sampled within ~ 3 km of the sources where CO concentrations peaked. These reactive compounds include nitrogen monoxide (NO), nitrogen dioxide (NO₂), formaldehyde, acetaldehyde, isoprene/furan plus isomeric pentadienes and cyclopentene, monoterpenes, methyl vinyl ketone (MVK) plus its isomers methacrolein (MACR) and crotonaldehyde, nitrate, ammonium, and OA. The long-axis sampling strategy often gave inter-instrument NEMRs at a series of typically 5-10 downwind ages up to ~ 1.2 hr, which also enabled characterizing downwind plume evolution of reactive compounds (chapter 4).

EFs were derived using Equations (1) and (2), and a carbon mass fraction of $39.3 \pm 2.4\%$, which is an average of rice straw collected from California and Arkansas, US and from China based on elemental analysis (ALS Analytics, Tucson). The sum of the moles of carbon divided by the emitted moles of CO₂, the denominator in Equation (2), was determined from the measured carbon-containing species including CO₂ and CO. Sources of uncertainties that contribute to the overall uncertainty of individual EFs include (in order of significance): (1) the uncertainties in the integrated ΔX vary by species and fire, but are usually near instrumental uncertainties () given the significant enhancements in

fresh plumes; (2) the uncertainties in the slopes of ΔX versus ΔY are usually small ($<5\%$) while the ER-derivation method for PTR-MS species is likely associated with another $\sim 20\%$ uncertainty; (3) the $\sim 6\%$ uncertainty in the carbon mass fraction; and (4) the sum of the moles of carbon determined from CO_2 and CO could underestimate the total carbon by $2\sim 4\%$, which would lead to an overestimation of EFs by $2\sim 4\%$ [Akagi *et al.*, 2011]. In contrast to the individual EF uncertainty, fire-to-fire variability is the dominant uncertainty ($\geq 40\%$ except for CO_2 and CO) and is reported throughout.

Since BB emissions also vary with different combustion processes, e.g. flaming and smoldering, MCE was also calculated. Fire-integrated MCEs are presented here for comparison to fire-averaged EFs.

3.2.3 Calculation of Brown Carbon (BrC) Absorption

Particle absorption coefficients measured at two wavelengths (470 and 532 nm) by a particle soot absorption photometer (PSAP) were used to infer BrC absorption in fire plumes [Lack and Langridge, 2013]. PSAP data were corrected for a known scattering interference from particles deposited on the collection media based on Virkkula [2010]. The aerosol absorption Ångström exponent (AAE) was determined from a pair of observations at 470 and 532 nm and then used to estimate the aerosol absorption at 365 and 660 nm, using Equations (3)-(5).

$$AAE_{PSAP} = - \frac{\ln(b_{ap,PSAP}(532)) - \ln(b_{ap,PSAP}(470))}{\ln(532) - \ln(470)} \quad (3)$$

$$b_{ap,PSAP}(365) = b_{ap,PSAP}(532) \left(\frac{365}{532} \right)^{-AAE_{PSAP}} \quad (4)$$

$$b_{ap,PSAP}(660) = b_{ap,PSAP}(470) \left(\frac{660}{470} \right)^{-AAE_{PSAP}} \quad (5)$$

The light absorption by BC at 365 nm ($b_{ap,BC}(365)$) can then be derived by extrapolation using $b_{ap,PSAP}(660)$ and a BC AAE of 1 [Bergstrom *et al.*, 2002; Kirchstetter *et al.*, 2004; Schnaiter *et al.*, 2005], assuming that absorption at 660 nm is mainly due to BC and that the BrC contribution is minimal [Liu *et al.*, 2014].

$$b_{ap,BC}(365) = b_{ap,PSAP}(660) \left(\frac{365}{660} \right)^{-AAE_{BC}} \quad (6)$$

BrC absorption at 365 nm ($b_{ap,BrC}(365)$) was then determined as the difference between $b_{ap,PSAP}(365)$ and $b_{ap,BC}(365)$. For each fire, we calculated fresh ER and downwind NEMRs of $\Delta b_{ap,BrC}(365)/\Delta CO$, $\Delta b_{ap,BC}(365)/\Delta CO$, and $\Delta b_{ap,PSAP}(365)/\Delta CO$.

Using PSAP data to predict BrC absorption is an indirect method that has inherent uncertainties. AAE_{PSAP} , given in Equation (3), can be determined from different wavelength combinations (i.e., 470-532, 470-660, and 532-660 nm). For SEAC⁴RS data set, only one wavelength pair 470-532 nm is available. Measurement uncertainty of PSAP (5%) results in a 7% uncertainty in AAE_{PSAP} . Liu *et al.* [2015] and Liu *et al.* [2014] found that different pairs led to systematically different $b_{ap,PSAP}(365)$, predicted by Equations (3) and (4). They found that the 470-660 nm pair gave results for $b_{ap,PSAP}(365)$ in between the other pairs. The 470-532 nm pair and the 532-660 nm pair resulted in $b_{ap,PSAP}(365)$ that was ~20% higher and ~20% lower than the 470-660 nm pair,

respectively. Thus, our $b_{\text{ap,PSAP}}(365)$ estimated from the 470-532 nm pair likely has an uncertainty of 17%, when compared to the middle $b_{\text{ap,PSAP}}(365)$ predicted from the 470-660 nm pair. Another uncertainty comes from the attribution of BC. For example, since BC internally mixed with non-absorbing material would have an AAE_{BC} greater than 1, the attributed short-wavelength BC absorption was likely underestimated [Lack and Langridge, 2013]. Lack and Langridge [2013] proposed that the uncertainty in short-wavelength (404 nm) absorption by BC determined by extrapolation using an $\text{AAE}_{\text{BC}} = 1$ ranged from +7% to -22%. For this reason, we used 22% as an approximate uncertainty for the predicted $b_{\text{ap,BC}}(365)$. The uncertainties of the AAE attribution method and the PSAP measurement (5%) were then treated independently and propagated in quadrature yielding uncertainties in $b_{\text{ap,PSAP}}(365)$ and $b_{\text{ap,BC}}(365)$ of 19% and 23%, respectively. By combining these two uncertainties, the uncertainty in $b_{\text{ap,BrC}}(365)$ is estimated to be 20%-43%. Due to uncertainties associated with these various calculations, definitively attributing the difference to be due to BrC is highly uncertain. However, for BB plumes sampled in an airborne study, Liu *et al.* [2015] derived a reasonable closure (a slope within 22% of 1) between BC+filter-based BrC vs. absorption coefficients derived from the PSAP wavelength pair 470-660 nm, which suggests that PSAP AAEs greater than 1 were mainly due to the presence of BrC. Analogous to individual EFs, individual $\Delta b_{\text{ap,BrC}}(365)/\Delta \text{CO}$ in fresh plumes likely have an uncertainty of 21%-43% by combining the uncertainties in $b_{\text{ap,BrC}}(365)$ and CO measurements. The accuracy of downwind $\Delta b_{\text{ap,BrC}}(365)/\Delta \text{CO}$ may be slightly reduced by the diluted concentrations.

3.3 Results

3.3.1 Initial Emissions

The average MCEs and EFs for the 15 agricultural fires are shown in Table 4 along with the study-averaged MCE and EF. Among the species that were quantified by the fast measurements from the NASA DC-8 platform, at least 25 trace gases and 6 particle species exhibited elevated concentrations within the agricultural fire plumes. This represents the most comprehensive suite of species measured in the field in the U.S. for agricultural fires to date. The fire-integrated MCEs derived in this work range from 0.895 to 0.958, with an average of 0.930. Hence, most of these fires can be regarded as primarily flaming. EFs for most species depend on the MCE. For this reason, we examined the calculated MCE and its correlation with EFs. Table 5 shows the linear regression results of EFs as a function of MCE for all species, including slopes, y-intercepts, and r^2 . No species had a good correlation ($r^2 > 0.1$) and a positive slope significantly different from zero, which would signify production mainly by flaming combustion. Compounds with negative slopes are likely associated with smoldering combustion since the emissions increase as the MCE decreases (e.g., toluene, benzene). However, numerous factors besides flaming and smoldering could dominate the variability in EFs. For species containing elements other than carbon, hydrogen, or oxygen, the emissions can depend strongly on the fuel composition (e.g., SO_2 and NO_x) [Burling *et al.*, 2010]. In general the EFs of organic gases correlated better with MCE than the EFs of inorganic gases and particles. The SEAC⁴RS EFs were also compared to the limited crop residue burning EFs available from the literature, including both field and laboratory studies. Table 6 summarizes the average EFs, the crop residue fuels burned, and the measurement approach (i.e., field or lab study) for these studies. Note

that the EFs from *Stockwell et al.* [2015] are predicted EFs at the SEAC⁴RS-averaged MCE based on their linear regression between EF and MCE.

Table 4 – Measured MCE and emission factors (g/kg) for all agricultural fires sampled during SEAC⁴RS in summer 2013. The study averages and the standard deviations are indicated in bold. Blank indicates no measurement available for the fire.

Fire #	1	2	3	4	5	6	7	8
Date	6 Sep	9 Sep	9 Sep	11 Sep	16 Sep	16 Sep	16 Sep	16 Sep
MCE	0.895	0.919	0.914	0.906	0.920	0.944	0.930	0.939
Compound	Formula							
<i>Gases</i>								
Carbon dioxide	1289	1323	1316	1305	1325	1360	1340	1353
Carbon monoxide	96.2	74.3	79.2	86.1	73.2	51.2	63.8	55.5
Nitrogen monoxide	0.327	0.0613	0.0456	0.169	0.266	0.0904	0.118	0.125
Nitrogen dioxide	1.79	1.38	1.84	2.09	1.37	0.718	1.73	2.23
Hydrochloric acid	0.0207	0.00497	0.0253	0.0619	0.00792		0.0143	0.00545
Sulfur dioxide	0.807	0.334	0.698	1.11	0.228		0.792	0.863
Hydrogen cyanide	0.350		0.789	2.02	0.414	0.316	0.826	0.186
Formaldehyde	4.14	2.14	3.19	4.81	4.11	1.85	3.08	1.68
Methanol	4.10	3.83	1.36	0.725	0.785	0.865	0.545	0.0566
Hydroxyacetone	2.59		3.56	3.93	2.35	1.61	1.70	1.06
Acetonitrile	0.300	0.456	0.221	0.179	0.0535	0.0627	0.210	0.0638
Acetaldehyde	1.46	2.66	2.02	1.43	1.19	0.812	3.00	0.948
Acetone/propanal	0.555	1.697	1.12	0.329	0.436	0.439	0.893	0.0787
MVK/MACR/crotonaldehyde	0.773	0.612	0.661	1.17	0.285	0.252	0.528	0.234
Isoprene/pentadienes/cyclopentene/furan	0.651	0.910	0.820	0.0501	0.279	0.238	0.648	0.0661
Isoprene	0.975		0.684	0.710	0.330	0.243	0.263	0.235
hydroperoxyaldehydes								
Benzene	0.320	0.360	0.313	0.657	0.177	0.160	0.373	0.207
Monoterpenes ^a	0.530	0.197	0.546	0.357	0.155	0.160	0.404	0.159
Toluene ^b	0.355	0.224	0.211	0.284	0.0986	0.0871	0.250	0.0919
<i>Particles</i>								
Ammonium	0.509	0.0745	0.813	0.995	0.151	0.133	0.364	
Nitrate	0.441	0.283	0.326	0.419	0.398	0.316	0.425	
Chloride	1.30	0.323	2.37	3.23	0.132	0.138	0.715	
Sulfate	0.420	-0.026	0.139	0.199	0.361	0.111	0.146	
Organic aerosol	13.4	8.20	18.5	20.9	27.6	4.15	9.10	
Black carbon	0.270	0.209	0.059	0.106	0.024	0.027	0.192	0.316
Submicron aerosol ^c	16.3	9.06	22.2	25.8	28.6	4.88	10.9	

Table 4 (continued).

Fire #	9	10	11	12	13	14	15	Average	Standard Deviation
Date	16 Sep	16 Sep	23 Sep	23 Sep	23 Sep	23 Sep	23 Sep		
MCE	0.926	0.947	0.957	0.958	0.922	0.942	0.926	0.930	0.018
Compound	Formula								
<i>Gases</i>									
Carbon dioxide	1334	1364	1378	1379	1328	1356	1334	1339	26
Carbon monoxide	67.4	48.4	39.7	38.8	71.5	53.6	67.9	64.5	16.6
Nitrogen monoxide	0.179	0.285	0.111	0.444	0.244	0.435	0.863	0.251	0.211
Nitrogen dioxide	3.41	3.37		1.32		2.22	2.85	2.02	0.80
Hydrochloric acid		0.0131	0.0206	0.0162	0.0167	0.0158	0.0129	0.0181	0.0144
Sulfur dioxide		1.70	1.08	0.407	0.730	0.818	0.767	0.795	0.377
Hydrogen cyanide	0.823	0.308	0.334	0.308	0.532	0.339	0.990	0.610	0.479
Formaldehyde	2.26	1.64	1.90	1.49	3.09	2.02	1.97	2.63	1.05
Methanol		3.55	1.01	1.54	0.952	0.118	0.335	1.41	1.38
Hydroxyacetone	1.60	0.838	1.46	2.61	2.21	1.32	1.95	2.06	0.89
Acetonitrile		0.324	0.0955	0.0978	0.170	0.0281	0.105	0.169	0.123
Acetaldehyde		0.749	0.998	0.456	2.11	0.408	0.921	1.37	0.80
Acetone/propanal		0.923	0.433	0.375	0.806	0.296	0.551	0.638	0.417
MVK/MACR/crotonaldehyde		0.0266	0.256	0.201	0.618	0.162	0.501	0.449	0.305
Isoprene/pentadienes/cyclopentene/furan		0.195	0.261	0.221	0.674	0.253	0.491	0.411	0.282
Isoprene									
hydroperoxyaldehydes	0.298	0.214	0.246	0.469	0.440	0.287	0.285	0.406	0.229
Benzene		0.132	0.202	0.121	0.327	0.199	0.295	0.275	0.139
Monoterpenes ^a		0.236	0.0636	0.114	0.398	0.0360	0.256	0.258	0.164
Toluene ^b		0.184	0.0714	0.0872	0.160	0.0487	0.184	0.167	0.091
<i>Particles</i>									
Ammonium	0.348	0.582	0.355	0.234	0.612	0.341	0.420	0.424	0.261
Nitrate	0.229	0.168	1.22	0.0792	1.16	0.414	0.228	0.436	0.337
Chloride	1.07	1.66	0.176	1.22	0.883	0.555	1.16	1.07	0.89
Sulfate	0.102	0.115	0.184	0.0932	0.210	0.0504	0.135	0.160	0.115
Organic aerosol	8.81	7.02	11.0	10.8	18.0	11.0	12.2	12.9	6.3
Black carbon	0.521	0.226	0.158	0.049	0.037		0.082	0.163	0.141
Submicron aerosol ^c	11.1	9.77	13.1	12.5	20.9		14.2	15.4	7.1

^a Measured by PTR-MS at m/z 137 and calibrated using α -pinene. By burning rice straw in a laboratory experiment, *Stockwell et al.* [2015] found up to two additional peaks at m/z 137 that were oxygenated compounds. However, *Müller et al.* [2016] did not find a significant contribution from oxygenated compounds to this signal from forest fuel.

^b Measured by PTR-MS at m/z 93. *Müller et al.* [2016] found a 20% interference from the $C_6H_5O^+$ signal.

^c Sum of AMS species and BC.

Table 5 – Statistics for the linear regression of fire-averaged EF as a function of fire-integrated MCE. Values in parentheses represent one standard deviation. Species are organized by the sign and significance of slopes and then by the magnitude of r^2 .

Species	Slope	Y Intercept	r^2
<i>Species with positive slopes not significantly different from 0</i>			
SO ₂	4.25 (5.83)	-3.16 (5.42)	0.05
NO _x as NO	2.6 (10.8)	-0.82 (9.99)	0.005
NO	0.69 (3.23)	-0.39 (3.00)	0.004
Nitrate	0.98 (5.23)	-0.48 (4.86)	0.003
NO ₂	1.1 (13.7)	1.0 (12.7)	0.0005
<i>Species with negative slopes significantly different from 0</i>			
MVK/MACR/crotonaldehyde	-13.4 (2.7)	12.9 (2.5)	0.68
HCHO	-47.7 (9.3)	47.0 (8.6)	0.67
Toluene	-3.88 (0.85)	3.78 (0.79)	0.64
Monoterpenes	-6.66 (1.64)	6.45 (1.53)	0.58
HPALDs	-9.33 (2.35)	9.09 (2.19)	0.57
$\Delta b_{ap,BrC}(365)/(\Delta CO + \Delta CO_2)^a$	-0.226 (0.059)	0.226 (0.055)	0.53
Benzene	-5.17 (1.54)	5.08 (1.43)	0.48
Hydroxyacetone	-30.5 (10.8)	30.5 (10.1)	0.40
<i>Species with negative slopes not significantly different from 0</i>			
HCN	-13.4 (6.4)	13.0 (6.0)	0.27
Acetaldehyde	-21.9 (10.6)	21.8 (9.8)	0.26
OA	-173 (84)	173 (78)	0.26
Sulfate	-3.06 (1.56)	3.01 (1.45)	0.24
Isoprene/furan/pentadienes/cyclopentene	-7.35 (3.79)	7.24 (3.52)	0.24
Ammonium	-6.06 (3.66)	6.05 (3.40)	0.19
CH ₃ CN	-2.81 (1.72)	2.79 (1.60)	0.18
Chloride	-20.4 (12.5)	20.0 (11.7)	0.18
HCl	-0.274 (0.213)	0.273 (0.198)	0.13
CH ₃ OH	-20.9 (20.3)	20.8 (18.9)	0.08
Acetone/propanal	-6.18 (6.17)	6.39 (5.74)	0.08
BC	-0.54 (2.19)	0.67 (2.04)	0.005

^a The unit of the ER of $\Delta b_{ap,BrC}(365)/(\Delta CO + \Delta CO_2)$ is $Mm^{-1} \text{ ppb}^{-1}$.

Table 6 – Comparison of EFs (g/kg) measured in field and lab for crop residue fuels. Values in parentheses represent one standard deviation.

Compound	SEAC ⁴ RS (This Work)	FLAME-4 at SEAC ⁴ RS-Average MCE [<i>Stockwell et al.</i> , 2015]	<i>Akagi et al.</i> [2011] ^a	<i>Kudo et al.</i> [2014] ^b	<i>Hayashi et al.</i> [2014]	
Crop type	SE U.S. rice straw	Asian rice straw	Unidentified crop residue in Mexico	Chinese wheat	Japanese rice straw	
Measurement approach	Airborne field study	Lab study	Airborne field study	Ground-based field study	Lab study	
Moisture content (%)	-	-	-	-	10.6	20.0
MCE	0.930	0.930	0.925	0.930	0.949	0.910
CO ₂	1339 (26)	-	1664 (66)	1598 (5)	803 (65)	946 (49)
CO	64.46 (16.57)	-	85.6 (34)	77.2 (6.9)	27.2 (1.7)	59.4 (0.7)
NO	0.251 (0.211)	1.86 (0.28)	2.06 (0.79)	-	-	-
NO ₂	2.02 (0.80)	1.70 (0.25)	3.48 (2.11)	-	-	-
NO _x as NO	1.58 (0.63)	2.97 (0.32)	3.64 (1.13)	-	-	-
NH ₃	-	1.12 (0.77)	1.76 (1.35)	-	0.059 (0.045)	0.025 (0.020)
HCl	0.0181 (0.0144)	0.458 (0.308)	-	-	0.062 (0.003)	0.022 (0.006)
SO ₂	0.795 (0.377)	1.22 (0.34)	-	-	-	-
HCN	0.610 (0.479)	0.399 (0.160)	0.16 (0.30)	-	-	-
HCHO	2.63 (1.05)	1.29 (0.61)	1.85 (0.92)	1.07	-	-
CH ₃ OH	1.41 (1.38)	1.48 (1.56)	2.67 (1.58)	2.94	-	-
Hydroxyacetone	2.06 (0.89)	1.33 (1.47)	-	-	-	-
CH ₃ CN	0.169 (0.123)	0.230 (0.092)	-	0.20 (0.03)	-	-
Acetaldehyde	1.37 (0.80)	2.09 (1.46)	-	1.02	-	-
Acetone	0.638 (0.417) ^c	0.989 (0.532)	-	0.83 ^d	-	-
Propanal		-	-		-	-
MVK	0.449 (0.305) ^e	0.489 (0.398) ^d	-	0.43 (0.02) ^d	-	-
MACR			-		-	-
Crotonaldehyde		-	-	-	-	-

Table 6 (continued).

Compound	SEAC ⁴ RS (This Work)	FLAME-4 at		<i>Akagi et al.</i> [2011] ^a	<i>Kudo et al.</i> [2014] ^b	<i>Hayashi et al.</i> [2014]
		SEAC ⁴ RS-Average MCE [<i>Stockwell et al.</i> , 2015]				
Isoprene		0.203 (0.104)	-			-
Furan		0.325 (0.496)	-		0.52 (0.01) ^f	-
Pentadienes	0.411 (0.282) ^g	-	-	-	-	-
Cyclopentene		-	-	-	-	-
HPALDs	0.406 (0.229)	-	-	-	-	-
Benzene	0.275 (0.139)	0.302 (0.123)	-	0.53 (0.07)	-	-
Monoterpenes	0.258 (0.164)	-	-	-	-	-
Toluene	0.167 (0.091)	0.271 (0.138)	-	0.32	-	-
Ammonium	0.424 (0.261)	-	-	-	0.083 (0.020)	0.245 (0.092)
Nitrate	0.436 (0.337)	-	-	-	0.006 (0.002)	0.008 (0.000)
Chloride	1.07 (0.89)	-	-	-	0.30 (0.02)	0.69 (0.14)
Sulfate	0.160 (0.115)	-	-	-	0.027 (0.000)	0.063 (0.003)
OA	12.9 (6.3)	-	3.67 ^h	-	1.6 ⁱ	7.4 ⁱ
BC	0.163 (0.141)	-	0.75	-	-	-

^a Supplement Table 13 in *Akagi et al.* [2011].

^b The EFs in *Kudo et al.* [2014] were derived from two plumes. The values in parentheses are the ranges of data.

^c EF for acetone/propanal.

^d EF for MVK/MACR.

^e EF for MVK/MACR/crotonaldehyde.

^f EF for isoprene/furan.

^g EF for isoprene/furan/pentadienes/cyclopentene.

^h The average OA from *Yokelson et al.* [2009] (Table 3) from Fires 1 and 3.

ⁱ Derived from EF(OC) times a factor of 1.64 [*Canagaratna et al.*, 2015].

3.3.1.1 Emissions of Sulfur Compounds

Sulfur in soil partly comes from atmospheric deposition and is then made available to plants by bacterial activity [*Wilhelm Scherer*, 2009]. Another source of soil sulfur is S fertilization, which helps increase rice yield [*Tsujimoto et al.*, 2013]. Significant amounts of SO₂ and sulfate were observed in the sampled fire plumes, up to 80 ppbv and 15 ppbv (Figure 2), respectively. As can be seen from Table 4, the excess mixing ratios of SO₂ are substantially higher than those of sulfate. This indicates that the emitted sulfur was mainly in the form of gaseous SO₂. The average EF(SO₂) for SEAC⁴RS is 0.795 ± 0.377 g/kg, which is nearly 2 times higher than the existing EF(SO₂) for several other types of BB including tropical forest, savanna, and pasture maintenance fires [*Akagi et al.*, 2011]. This implies high sulfur content in rice straw, possibly resulting from high sulfur input into soil such as S fertilization or high absorption of sulfur by rice. When compared to the lab-predicted EF(SO₂) for Asian rice straw [*Stockwell et al.*, 2015], 1.22 ± 0.34 g/kg, the field average EF for US rice straw is lower, statistically significant based on t-test at a 95% confidence level. The differences between the lab-predicted EF(SO₂) and the field EF(SO₂) could be due to the differences in fuel, burning conditions, and sampling

methods. SO₂ has been established previously as a product of flaming combustion [Yokelson *et al.*, 1996; Andreae and Merlet, 2001]. For the agricultural fires sampled during SEAC⁴RS, although the slope of the linear fit of EF(SO₂) as a function of MCE is positive, the low r² with a value of 0.05 indicates that the amount of emitted SO₂ was not primarily dependent on the ratio of flaming to smoldering. It is likely that SO₂ emissions are highly dependent on fuel sulfur content, as also found in laboratory studies [Burling *et al.*, 2010; Stockwell *et al.*, 2014]. For particulate sulfate emissions, the average EF is 0.160 ± 0.115 g/kg. Hayashi *et al.* [2014] measured lower EF(sulfate) from Japanese rice straw with values of 0.027 ± 0.000 and 0.063 ± 0.003 g/kg under different residue moisture contents of 10.6% and 20.0%, respectively. The average EF(sulfate) during SEAC⁴RS is over 2 times higher than those measured by Hayashi *et al.* [2014], probably due to fuel variability.

3.3.1.2 Emissions of Chlorine Compounds

Sea salt deposition and the use of agricultural chemicals such as herbicides and insecticides can increase the chlorine content in plants and therefore chlorine emissions from BB. The chlorine-containing species quantified in this study are gaseous HCl and particulate chloride. For the 15 fires we sampled, average EFs of chloride and HCl are 1.07 ± 0.89 and 0.0181 ± 0.0144 g/kg, respectively. If we calculate the average molar ratio of emitted chloride to HCl from their average EFs, a ratio of ~ 60 indicates that chlorine was mainly emitted as chloride. Since the samples were all from inland areas, the high chloride emission from rice straw burning are more likely to result from the use of agricultural chemicals rather than impacts from sea salt. During FLAME-4, Stockwell *et al.* [2014] observed high HCl emissions with an average EF of 0.458 ± 0.308 g/kg,

adjusted to the SEAC⁴RS-averaged MCE. They also observed that the concentration of HCl decayed rapidly in several minutes in fresh smoke that was stored in low-light conditions for rice straw and other fuels. *Christian et al.* [2010] observed high chloride and below-detection-limit HCl in the fresh emissions from two barley residue fires in Mexico. *Stockwell et al.* [2014] obtained fresher samples in the lab, which were seconds old, while this study and *Christian et al.* [2010] sampled smoke that was usually several minutes old in field. Thus the reason that the field studies observed much less HCl might be that HCl rapidly decreased after emission by partitioning to the aerosol phase. In the lab study conducted by *Hayashi et al.* [2014], fire-integrated samples of HCl and chloride were collected by cellulose filters and glass-fiber filters, respectively. Therefore the observed high chloride and low HCl EFs were averages from a complete burning process from the ignition to the end of the smoldering period.

Lab studies have shown that the emission of HCl correlates with flaming combustion [*Burling et al.*, 2010; *Stockwell et al.*, 2014], while that of particulate chloride does not depend strongly on the ratio of flaming to smoldering [*Christian et al.*, 2003]. However, for the U.S. rice straw, the linear fits of EFs versus MCE in Table 5 indicate that neither HCl nor chloride strongly correlates with MCE ($r^2 \leq 0.18$). Analogous to sulfur, EFs of chlorine species are likely highly dependent on the fuel composition. *Christian et al.* [2003] and *Hosseini et al.* [2013] found a strong relationship between fuel chlorine content and chloride-containing particulate emissions for a series of laboratory fires. *Stockwell et al.* [2014] also found in lab studies that for a wide variety of biomass fuels, the emissions of HCl were positively correlated with fuel Cl. In this airborne study, a large fraction of HCl may have already incorporated into the particles

before being sampled, which could also lead to a weak correlation between EF(HCl) and MCE.

3.3.1.3 Emissions of Nitrogen Compounds

BB is an important atmospheric source of nitrogen species, primarily NH_3 and NO_x [Crutzen and Andreae, 1990; McMeeking *et al.*, 2009; Burling *et al.*, 2010]. Freshly emitted nitrogen-containing compounds measured during SEAC⁴RS are: HCN, CH_3CN , NO_x , nitrate, and ammonium. Another important nitrogen species not measured during SEAC⁴RS could be HONO. Significant direct emissions of HONO were reported at ~5-33% of NO_x from BB of various fuel types [Yokelson *et al.*, 2007; Yokelson *et al.*, 2009; Burling *et al.*, 2011; Akagi *et al.*, 2012; Akagi *et al.*, 2013] and at ~9% of NO_x for Asian rice straw burned in lab [Stockwell *et al.*, 2015]. Thus, HONO emission could be an important source of OH radicals. HCN and CH_3CN are widely recognized as useful BB tracers [Li *et al.*, 2000; de Gouw *et al.*, 2003; Li *et al.*, 2003]. The variability in HCN emissions is significant over a broad range of fuel types [Akagi *et al.*, 2011]. HCN from crop residue fires has previously been measured in the laboratory and in field studies in Mexico [Christian *et al.*, 2003; Akagi *et al.*, 2011; Stockwell *et al.*, 2014]. These measurements show that the average EF(HCN) for SEAC⁴RS rice straw fires is the largest among these crop residue fires with a value of 0.610 ± 0.479 g/kg (Table 6). This EF(HCN) is also slightly larger than those for other types of BB except forest fires and peat as reviewed in Akagi *et al.* [2011]. In general, airborne and ground-based EF(HCN) for pine/conifer fuels show a strong negative correlation with MCE over a wide range of 0.85-0.96, suggesting that HCN is primarily released from smoldering combustion [Akagi *et al.*, 2013]. By contrast, no statistically significant linear dependence of airborne

EF(HCN) on MCE was detected in this work (Table 5). Airborne HCN EFs measured in some other studies of “non-pine” ecosystems, e.g. African savanna fires [Yokelson *et al.*, 2003], are also effectively independent of MCE. The emission of CH₃CN is lowest among all the nitrogen-containing species (Table 4). The average EF(CH₃CN) reported here is smaller than those reported in the literature for crop residues (Table 6), although not statistically significant. The EF(CH₃CN) for individual fires ranges from 0.0281 to 0.456 g/kg and is weakly correlated with MCE (Table 5). The study-averaged ER of $\Delta\text{CH}_3\text{CN}/\Delta\text{HCN}$ is 0.22 ± 0.20 , smaller than previous laboratory and field measurements of 0.30-0.56 for a wide range of non-boreal [Christian *et al.*, 2003; Yokelson *et al.*, 2008; Crounse *et al.*, 2009; Yokelson *et al.*, 2009] and boreal [Simpson *et al.*, 2011] fuel types.

In this study, the average EF(NO₂), 2.02 ± 0.80 g/kg, is approximately 8 times the average EF(NO), 0.251 ± 0.211 g/kg. This NO₂/NO ratio, largely controlled by photostationary state, is the largest among the crop residue studies listed in Table 6. Since NO and NO₂ are rapidly interconverted, it is also useful to report an EF for “NO_x as NO”. The EF(NO_x) of this study is 1.58 ± 0.63 g/kg, the smallest among the studies listed in Table 6. As for the EF(NO_x) versus MCE plots, although some laboratory and field measurements have shown that NO_x is emitted primarily via flaming combustion [Lobert *et al.*, 1991; Yokelson *et al.*, 1996; Goode *et al.*, 2000], neither EF(NO), EF(NO₂), nor EF(NO_x) from SEAC⁴RS correlates with MCE (Table 5). Instead, NO_x emissions might have been driven more by fuel nitrogen content than MCE, as found in Burling *et al.* [2010], Andreae and Merlet [2001], and McMeeking *et al.* [2009]. However, since SEAC⁴RS agricultural fires emitted less NO_x and CH₃CN but more HCN, it is likely that the emissions of gaseous nitrogen compounds depend not only on the total fuel nitrogen,

but also the composition of N-containing precursors in fuel and burning conditions [Becidan *et al.*, 2007; Bai *et al.*, 2013]. Gaseous HNO_3 was not significantly elevated within most of the fire plumes. Other studies have reported that HNO_3 did not correlate with elevated CO within fresh or aged BB smoke [Yokelson *et al.*, 2009; Alvarado *et al.*, 2010]. The reason for this may be that HNO_3 is converted efficiently to nitrate due to the availability of NH_3 in the plumes, as indicated by high ammonium emissions. The evolution of nitrogen species will be discussed in detail in chapter 4.

Particulate nitrate and ammonium are often minor components of the emitted nitrogen species. Akagi *et al.* [2011] reviewed the emissions of these particles in various BB types. The observed nitrate EFs ranged from 0.016 to 0.14 g/kg and those of ammonium were smaller than 0.006 g/kg. McMeeking *et al.* [2009] also found particulate nitrate and ammonium to account for only a small fraction of the fuel nitrogen for 33 different US plant species and rice straw collected from Taiwan burned in a lab study. Their study-averaged values of EF(nitrate) and EF(ammonium) for rice straw were 0.04 ± 0.03 g/kg and 0.26 ± 0.16 g/kg, respectively. Hayashi *et al.* [2014] also observed very low emissions of nitrate and relatively higher emissions of ammonium under both dry and moist conditions (Table 6). During SEAC⁴RS, fresh nitrate and ammonium emissions with average EFs of 0.436 ± 0.337 g/kg and 0.424 ± 0.261 g/kg were measured, respectively, which are larger than the existing literature values. In addition, both nitrate and ammonium exhibited enhancement in aged smoke. If the initial emitted and subsequently produced nitrate and ammonium are summed, both nitrate and ammonium would have even higher emissions than the lab studies of McMeeking *et al.* [2009] and Hayashi *et al.* [2014].

3.3.1.4 Emissions of Gas-Phase Non-Methane Organic Compounds (NMOCs)

Among the reported gas-phase NMOCs, rice straw fires had the highest average EFs for formaldehyde, hydroxyacetone, methanol, and acetaldehyde. In previous studies, formaldehyde is consistently one of the most abundant OVOCs emitted by fires [Goode *et al.*, 2000; Yokelson *et al.*, 2003]. The field burning of US rice straw produced significant amounts of formaldehyde with an average EF of 2.63 ± 1.05 g/kg, which is the largest EF among all types of BB shown in Table 6 and in Akagi *et al.* [2011], except charcoal making.

Hydroxyacetone has both biogenic and BB sources. It is the precursor of other atmospherically important species, such as methyglyoxal, formic acid, and acetic acid [Grosjean *et al.*, 1993; Butkovskaya *et al.*, 2006]. Hydroxyacetone emissions have recently been reported for both field and laboratory fires from various fuels [Christian *et al.*, 2003; Akagi *et al.*, 2011; Yokelson *et al.*, 2013; St. Clair *et al.*, 2014]. Christian *et al.* [2003] reported very large quantities of hydroxyacetone, 21-34 g/kg, from burning Indonesian rice straw in piles under smoldering combustion (a common practice in Indonesia and East Asia) with a MCE of ~ 0.81 . Rice straw burned in FLAME-4 also had a relatively high average EF (1.33 ± 1.47 g/kg) for the SEAC⁴RS-averaged MCE value. The fires sampled during the SEAC⁴RS also produced high amounts of hydroxyacetone with an average EF of 2.06 ± 0.89 g/kg.

In SEAC⁴RS and previous studies, methanol was consistently one of the most abundant OVOCs emitted by crop residue fires and other types of BB [Christian *et al.*,

2003; Kudo *et al.*, 2014; Stockwell *et al.*, 2014; Stockwell *et al.*, 2015]. The SEAC⁴RS and the FLAME-4 lab-predicted EFs of methanol agree very well (Table 6).

Acetaldehyde plays an important role in the formation of PAN, O₃, and HO_x radicals and also has large effects on modeled smoke plume chemistry [Singh *et al.*, 1995; Trentmann and Andreae, 2003; Trentmann *et al.*, 2005]. The annual emission of acetaldehyde from BB has been estimated as 3 Tg [Millet *et al.*, 2010]. As the principal carbonyl precursor of PAN (44% of the global source) [Fischer *et al.*, 2014], acetaldehyde emitted from BB likely has an important impact on the regional and global PAN budget. Burning crop residues emits relatively large amounts of acetaldehyde relative to other types of fuel. Among the 5 types of crop residues burned in FLAME-4, sugar cane and rice straw had the largest acetaldehyde EFs [Stockwell *et al.*, 2015]. We report an average EF(acetaldehyde) of 1.37 ± 0.80 g/kg, which is smaller than that measured in FLAME-4 [Stockwell *et al.*, 2015], though the uncertainties are large (Table 6). The impact of acetaldehyde emissions on PAN formation in aged smoke is studied in detail by the LPCS model and is discussed in chapter 4.

Other quantified organic gases include (in order of abundance by mass): acetone/propanal, MVK/MACR/crotonaldehyde, isoprene/furan/pentadienes/cyclopentene, isoprene hydroperoxyaldehydes (HPALDs), benzene, monoterpenes, CH₃CN, and toluene. Among these species, the OVOCs are relatively abundant initial emissions from BB. HPALDs are autoxidation products of isoprene via 1,6-H-shift isomerizations of peroxy radicals produced from OH+isoprene [Crounse *et al.*, 2011; Crounse *et al.*, 2013]. Their production is expected to be important in low-temperature combustion chemistry as occurs in BB [Cox and Cole, 1985; Rogge *et*

al., 1991]. The first direct emissions of HPALDs from BB were measured during SEAC⁴RS, with an average EF of 0.406 ± 0.229 g/kg. For those overlapping species in Table 6, the average EFs of our field study and those predicted from the FLAME-4 EF vs. MCE plot are shown to agree well, considering the differences in fuel and burning conditions. There were larger discrepancies in the NMOC EFs derived in this work as compared to those in *Kudo et al.* [2014], although the average MCEs were similar. In general, *Kudo et al.* [2014] obtained higher EFs, perhaps because of the difference in the composition of wheat and rice straw.

The emissions of all the NMOCs are negatively correlated with MCE (Table 5), meaning they are primarily emitted from smoldering combustion. However, variability in the relationship between EFs and MCE does exist. MVK/MACR/crotonaldehyde, toluene, monoterpenes, and HPALDs correlate reasonably well with MCE (r^2 from 0.57 to 0.68). On the other hand, acetone/propanal and methanol are the NMOCs that were least dependent on MCE, both with $r^2 = 0.08$. The acetone/propanal and MCE correlation is reported the first time here. For methanol, unlike in this study, good correlation (r^2 from 0.68 to 0.90) between the EF(methanol) and MCE have been reported in previous lab and field studies focusing on the fuels burned in prescribed and savanna fires [*Christian et al.*, 2003; *Yokelson et al.*, 2003; *Burling et al.*, 2010; *Burling et al.*, 2011].

3.3.1.5 Emissions of Carbonaceous Aerosols

Open BB, as a primary source of carbonaceous aerosols, contributes one-third of the global BC and two-thirds of the global POA budget [*Bond et al.*, 2004]. BC is known to be the most absorbing aerosol in the visible wavelengths in the atmosphere [*Bond et*

et al., 2013]. Recent studies have shown that BB OA contains substantial amounts of light-absorbing BrC [Kirchstetter *et al.*, 2004; Chen and Bond, 2010; Lack *et al.*, 2012; Saleh *et al.*, 2013; Washenfelder *et al.*, 2015]. EFs and chemical properties of BC and OC from BB are quite variable and uncertain [Reid *et al.*, 2005]. Here we examine the first suite of field measurements of BC and OA emitted from agricultural fires. We also use the PSAP data to infer the existence and absorption properties of BrC.

The EFs of BC in this work vary between 0.024 and 0.521 g/kg, with an average of 0.160 ± 0.115 g/kg (Table 4). This average value is ~5 times smaller than that derived from field measurement of EC from Mexican crop residue burning (Table 6) and is also smaller than the EF(BC) reviewed in Akagi *et al.* [2011] for all types of BB except charcoal making. Previous studies have shown that BC is a flaming combustion product [Christian *et al.*, 2003; Reid *et al.*, 2005]. However, our BC EFs are essentially independent of MCE (Table 5). Therefore, given the complexity and variability of biomass combustion, the variance of EF(BC) was not attributable simply to the relative amount of flaming or smoldering for the SEAC⁴RS agricultural fire measurements.

OA comprised the largest chemical component of fine particles in smoke from the sampled agricultural fires, with an average EF of 12.9 ± 6.3 g/kg (Table 4). Yokelson *et al.* [2009] and Hayashi *et al.* [2014] observed significantly less OA emissions from crop residue fires (Table 6). Contrary to BC, OA is mainly produced by smoldering combustion [Reid *et al.*, 2005]. OA EFs are negatively correlated with MCE ($r^2 = 0.26$), as expected (Table 5). This correlation is weaker than some previously observed average EF(OC)-and-MCE correlations with $r^2 = 0.36$ for various plant species burned in lab [McMeeking *et al.*, 2009; Jolleys *et al.*, 2014]. It is possible that some of the variance in

these OA EFs could be due to fire variability. The strength of the relationship between EF(OA) and MCE can also be degraded by gas-particle partitioning effects. POA emitted from fires has been observed to be semi-volatile [Donahue *et al.*, 2006; May *et al.*, 2013]. Thus, although the samples used to calculate EF(OA) are relatively fresh, the POA may still have gone through variable gas-particle partitioning related to dilution and temperature changes as the smoke mixes with background air.

As shown in Figure 5, the calculated PSAP AAEs range from 2.2 to 4.2 near the 15 fire sources, higher than the average AAE of the background air just outside of the plumes (1.60 ± 0.40). The average AAE for the agricultural fires, 3.34 ± 0.62 , is similar to the AAEs of 3.5 to 4.0 for the fresh plumes of a large wildfire, the Rim fire, sampled during the same campaign [Forrister *et al.*, 2015]. Corresponding to the elevated AAEs, derived BrC absorption at 365 nm normalized by ΔCO was significantly elevated in all 15 fresh agricultural fire plumes, also shown in Figure 5. In contrast, the absorption at 365 nm contributed by freshly emitted BC was lower, or 15%-93% of that contributed by BrC. The average fresh $\Delta b_{\text{ap,BrC}}(365)/\Delta\text{CO}$ and $\Delta b_{\text{ap,BC}}(365)/\Delta\text{CO}$ of this study are $0.223 \pm 0.053 \text{ Mm}^{-1} \text{ ppbv}^{-1}$ and $0.078 \pm 0.036 \text{ Mm}^{-1} \text{ ppbv}^{-1}$, respectively. Direct measurements of light absorption spectra from liquid extracts of aerosols collected on 20 teflon filters were also available for these agricultural fires. After applying a factor of 2 for conversion of light absorption from liquid solution to particles [Liu *et al.*, 2013; Liu *et al.*, 2015; Washenfelder *et al.*, 2015], the average $\Delta b_{\text{ap,BrC}}(365)/\Delta\text{CO}$ determined from liquid extracts is $0.25 \pm 0.27 \text{ Mm}^{-1} \text{ ppbv}^{-1}$, which agrees with the average derived from PSAP measurements. The uncertainty of the extract-derived $\Delta b_{\text{ap,BrC}}(365)/\Delta\text{CO}$ by particles is estimated to be at least ~45% by combining the uncertainties in the conversion factor [Liu

et al., 2013] and the measurements. The real uncertainty is likely larger because the background absorption near the plume often cannot be obtained due to the low sampling frequency of 5-7 min. By performing orthogonal distance regression for the sum of $b_{ap,BrC}(365)$ determined from liquid extracts and $b_{ap,BC}(365)$ based on PSAP measurements and an AAE_{BC} of 1 versus total PSAP absorption at 365 nm, we obtained a slope of 0.81 ± 0.09 and an intercept of -0.74 ± 3.29 (Figure 6). A slope near 1 and a relatively good correlation ($r = 0.91$) indicate a reasonable closure between extract-derived BrC plus PSAP-derived BC and PSAP absorption for the agricultural fire plumes, although there are uncertainties associated with the assumptions made. *Forrister et al.* [2015] determined from liquid extracts a similar fresh $\Delta b_{ap,BrC}(365)/\Delta CO$ of $0.25 \text{ Mm}^{-1} \text{ ppbv}^{-1}$ in the very large plume of the Rim Fire. In this study, the relatively good correlation ($r^2 = 0.53$) between $\Delta b_{ap,BrC}(365)/(\Delta CO + \Delta CO_2)$, analogous to EFs but in a unit of $\text{Mm}^{-1} \text{ ppb}^{-1}$, and MCE indicates that BrC was mainly a product of smoldering combustion.

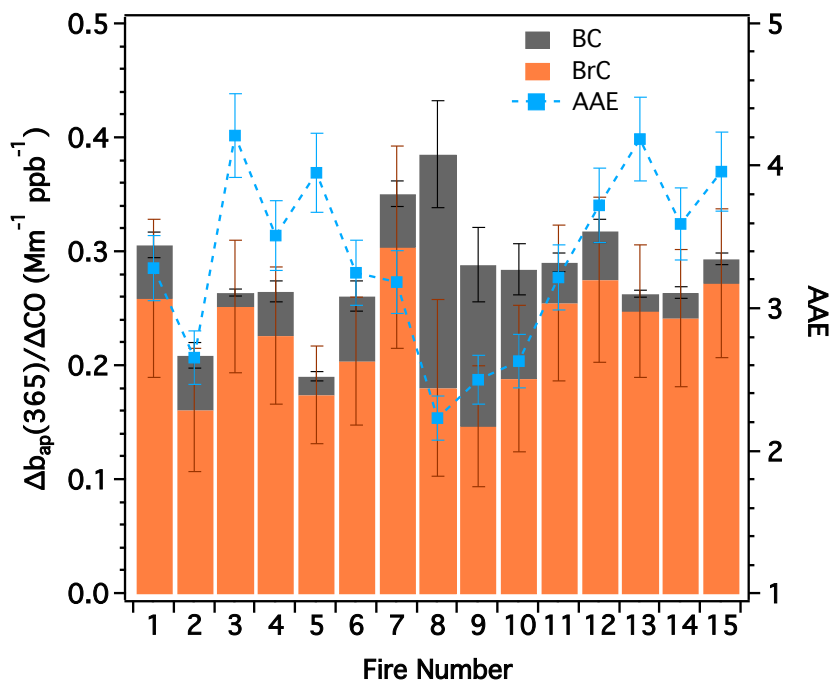


Figure 5 – Excess PSAP light absorption coefficient at 365 nm normalized by excess CO and corresponding absorption Ångström exponent (AAE) in fresh smoke. BrC absorption was 2-5 times that of BC at 365 nm.

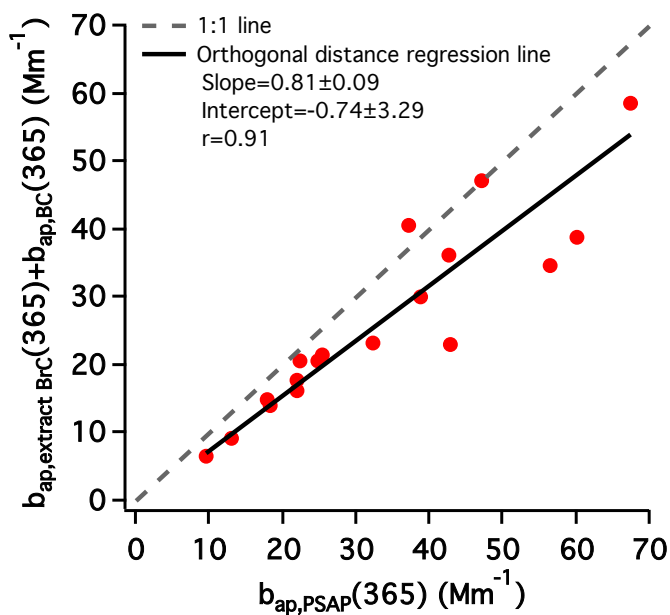


Figure 6 – Closure analysis of b_{ap} at 365 nm for agricultural fire plumes via scatter plot of the sum of BrC absorption determined from liquid extracts plus estimated BC absorption based on PSAP measurements and an AAE_{BC}

of 1 versus total aerosol absorption based on PSAP data. Orthogonal distance regression fit result and the 1:1 line are shown. Measurement uncertainties of the various absorption coefficients are estimated to be ~19%-45%.

3.3.2 Annual Emissions of SO₂, NO_x, and CO from Crop Residue Burning in Southeastern U.S.

The measured EFs were used to estimate the annual emissions of three trace gases, SO₂, NO_x, and CO, from agricultural field burning in the four states where the agricultural fires were sampled (Arkansas, Louisiana, Mississippi, and Missouri) and hence to compare with the 2011 National Emissions Inventory (NEI; <http://www.epa.gov/ttnchie1/net/2011inventory.html>; accessed data in June 2015). Although the lab study by *Stockwell et al.* [2014] found roughly similar emissions from various crop materials including rice straw (generally within a factor of 2-3), it is very likely that the emissions of some species can be more variable across crop type (e.g., Table 5). However, since the field EF data for other crops in the U.S. are not available, the same EFs are assumed for all crops to roughly estimate the annual emissions of trace gases from open burning in the four states. This non-crop-type specific EF assumption for SO₂, NO_x, and CO likely results in an uncertainty of about a factor of 2. Emissions were calculated using the *Seiler and Crutzen* [1980] method of multiplying EF, burned area, fuel loading (mass of biomass per unit area), and combustion completeness (fraction of biomass consumed by fire). The EFs obtained in SEAC⁴RS were coupled with fire

activity data from three studies based on different methods: *McCarty et al.* [2009] is based on remote sensing and *Melvin* [2012] and *Reid et al.* [2004] rely on government statistics. *McCarty et al.* [2009] estimated the area of crop residue burning using satellite data from 2003 to 2007. *Reid et al.* [2004] reported government statistics for agricultural burning for Arkansas, Louisiana, and Missouri collected in 2002. In Figure 10 of *Melvin* [2012], acre ranges of agricultural and forestry prescribed burning in 2011 were based on state records. We estimated the agricultural burning area for each state by multiplying the average prescribed burning area by 37%, which is the overall percentage of agricultural burning in the southeast region according to Figure 5 of *Melvin* [2012]. In addition, the dry mass of rice straw was taken as $0.58 \pm 0.14 \text{ kg m}^{-2}$ [*Oanh et al.*, 2011] and we assume that 100% of biomass was consumed in burning. Figure 7 compares a set of regional emission estimates based on different fire activity data. The first three bars in the two figures are our estimates. The last red bars are the estimates by the 2011 NEI, in which SO_2 , NO_x , and CO emission data are available. The error bars of the estimates based on *Melvin* [2012] represent a range corresponding to the burned area range as reported. Total uncertainties are not explicitly shown, in part because there is not enough information to estimate them quantitatively. The appropriate error would include error propagation from the non-crop-type specific EF data and the estimates of biomass burned.

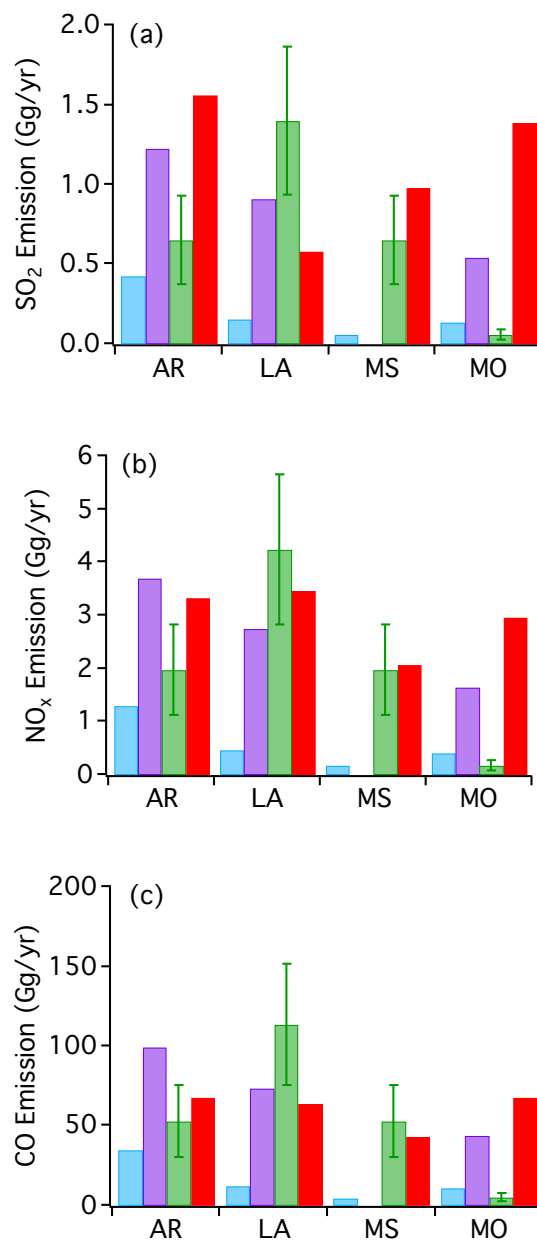
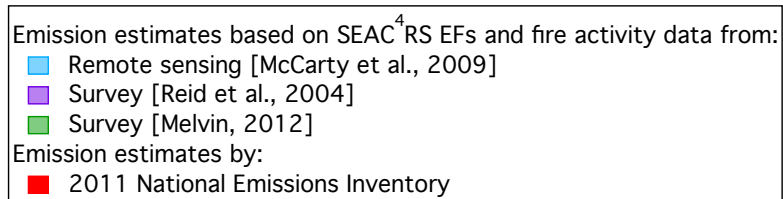


Figure 7 – Estimates of annual emissions of (a) SO₂, (b) NO_x, and (c) CO from crop residue burning in Arkansas, Louisiana, Mississippi, and Missouri. NO_x emission estimates are reported as NO₂. The green error bars of the estimates based on *Melvin* [2012] represent the ranges of the burned area reported and are smaller than the overall errors of the emission estimates.

In Figure 7, the estimated emissions of SO₂, NO_x, and CO vary with the fire activity data used. In general, the estimates based on *McCarty et al.* [2009] are the smallest emissions. Emissions estimated from *Reid et al.* [2004] and *Melvin* [2012] and by the 2011 NEI are generally close and they differ by less than a factor of 2.5 except for Missouri. The fire activity data are highly uncertain, as indicated by Figure 7. While there could have been some variability in fire activities of different years [*McCarty et al.*, 2009; *van der Werf et al.*, 2010], it is likely the different methods contributed most to the uncertainties in emissions. Three of the four estimates rank Arkansas as the state with the highest agricultural burning emissions among the studied states. Arkansas and Louisiana are also two of the several states that emitted the highest amounts of CO in the contiguous U.S. according to *McCarty* [2011]. Summing up the four states, the average annual SO₂, NO_x, and CO emissions from agricultural fires were ~2%, ~7%, and ~330% of coal combustion emissions estimated in the 2011 NEI. For NO_x and CO, the agricultural fire emissions were about ~1% and ~9% of mobile sources, respectively. These ratios are estimated to have uncertainties between factors of 2.1 and 2.4 by considering uncertainties in EFs and variations in burned areas. Further investigation is required to obtain realistic burning activities and crop-specific EFs for better emission estimation.

3.4 Conclusions

The emissions from 15 agricultural fires were measured over the southeastern U.S. from the NASA DC-8 research aircraft. Based on these measurements, this study reports a detailed set of EFs of a number of trace gases and fine particles from agricultural field burning. The aerosol light absorption coefficients measured by PSAP and the light

absorption measured from liquid extracts of aerosol implied that BrC was ubiquitous in these fires. The EFs as a function of MCE were examined. Whereas the EFs of VOCs generally showed good anti-correlation with MCE, the EFs of inorganic gases and particles were likely influenced more by fuel composition and fire variability than by MCE and thus had weak correlations with MCE. We also compared the EFs with the limited previous field and lab measurements of crop residue fires. In general, the average EFs of trace gases derived in this work agree well with those reported by *Akagi et al.* [2011], *Hayashi et al.* [2014], *Kudo et al.* [2014], and *Stockwell et al.* [2015]. As for the particle species, the agricultural fires studied here had significantly larger emissions than the lab burning of rice straw [*Hayashi et al.*, 2014].

With the measured EFs, we also roughly estimated the annual agricultural fire emissions of SO₂, NO_x, and CO from Arkansas, Louisiana, Mississippi, and Missouri. The estimated ratio of the annual primary emissions from agricultural burning to the annual primary emissions from major sources for these species follows: SO₂ (~2% of coal combustion), NO_x (~1% of mobile sources), and CO (~9% of mobile sources). However, these ratios are highly uncertain, about a factor of 2.1-2.4, since the EFs used for crop residues other than rice straw and the burning activity are uncertain. Future investigation of the EFs for different crop fuels, fuel loading, and fire activity will help address the uncertainties in agricultural burning emission inventories.

CHAPTER 4. EVOLUTION OF OZONE, REACTIVE NITROGEN, AND ORGANIC AEROSOL IN AGRICULTURAL FIRE PLUMES

This chapter examines the chemical evolution of the primary emissions in 7 agricultural fire plumes up to ~1.2 hr. A Lagrangian plume cross-section (LPCS) model was used to simulate the evolution of O₃, reactive nitrogen species, and OA.

4.1 Introduction

Chemical and physical transformations of primary fire emissions can lead to significant changes in the gaseous and particulate phase composition of the smoke [Hobbs *et al.*, 2003; Jost *et al.*, 2003; Yokelson *et al.*, 2009; Akagi *et al.*, 2012]. Therefore, understanding smoke evolution is an important issue. The chemical evolution of trace gases can influence the formation of O₃ and the conversion of NO_x to other reactive nitrogen (NO_y) species such as PAN and particulate nitrate. O₃ enhancement is common in tropical BB plumes, while both O₃ production and destruction have been observed in boreal BB plumes [Goode *et al.*, 2000; Hobbs *et al.*, 2003; Yokelson *et al.*, 2009; Alvarado *et al.*, 2010; Singh *et al.*, 2010; Jaffe and Wigder, 2012]. In temperate regions, the few available field studies of BB sampled prescribed fires and observed O₃ enhancement [Trentmann and Andreae, 2003; Akagi *et al.*, 2012; Akagi *et al.*, 2013; Müller *et al.*, 2016]. Jaffe and Wigder [2012] reviewed numerous factors that influence O₃ production from wildfires, including emissions of O₃ precursors such as NO_x and NMOCs, combustion efficiency, photochemistry, aerosol effects on chemistry and

radiation, and local and downwind meteorological patterns. PAN formation in the first few hours after emission has been observed in plumes of several types of BB, such as a chaparral fire in California, a small forest fire in Georgia, and boreal forest fires [Yokelson *et al.*, 2009; Alvarado *et al.*, 2010; Akagi *et al.*, 2012; Müller *et al.*, 2016]. The transport of PAN potentially influences O₃ formation downwind [Jacob *et al.*, 1992; Leung *et al.*, 2007; Jaffe and Wigder, 2012]. However, there are still questions regarding PAN photochemistry since some previous modeling studies were not able to successfully simulate the observed concentrations of O₃ and PAN in different BB plumes [Trentmann *et al.*, 2005; Alvarado and Prinn, 2009]. One exception is a recent study by Müller *et al.* [2016], which accurately modeled O₃ and PAN formation during the first hour of aging for a small forest fire in Georgia using the observations of 16 non-methane organic gases, CH₄, NO_x, nitrous acid (HONO), CO, and O₃. Another important plume process is the formation of secondary organic aerosol (SOA). Highly variable SOA formation rates in aging BB smoke have been reported, although limited net increase in OA mass is often observed [Capes *et al.*, 2008; Yokelson *et al.*, 2009; Cubison *et al.*, 2011; Hecobian *et al.*, 2011; Jolleys *et al.*, 2012; Vakkari *et al.*, 2014]. BrC, a component of OA that absorbs light in the UV and visible spectral regions, is associated with incomplete combustion and SOA formation [Hecobian *et al.*, 2011; Saleh *et al.*, 2013; Forrister *et al.*, 2015]. Recent studies indicate that BrC evolution in BB plumes is controlled by secondary processes such as chromophore formation and loss due to photobleaching, volatilization, and/or aerosol-phase reactions, leading to different evolution of BrC and bulk OA [Lee *et al.*, 2014a; Zhong and Jang, 2014; Forrister *et al.*, 2015; Zhao *et al.*, 2015]. Although

agricultural field burning is ubiquitous in the U.S., no field study to date has characterized the emissions and smoke chemistry of these fires.

This chapter examines in detail the evolution of O₃ and reactive nitrogen species (PAN, NO_x, HNO₃, and nitrate) in the agricultural fire plumes sampled during SEAC⁴RS. The changes of OA concentration and BrC absorption in the first 1.2 h of aging are also investigated. To evaluate our understanding of the rapid chemical evolution within fire plumes in a biogenically influenced environment, a Lagrangian plume cross-section (LPCS) model is used to simulate the formation of O₃, PAN, and nitrate. By implementing the simple parameterization proposed by *Hodzic and Jimenez* [2011], the model also simulates SOA and the change of atomic oxygen-to-carbon (O/C) ratios that characterize OA oxidation state.

4.2 Methods

4.2.1 *Characterizing Evolution with NEMRs*

As discussed in chapter 2, the ER has two important uses: (1) it can be used to calculate EFs; and (2) differences between the ERs measured at the source and the NEMRs measured downwind allow us to quantify post-emission gas and particulate phase chemistry and gas-particle partitioning. The long-axis sampling strategy used to sample agricultural fires often gave inter-instrument NEMRs at a series of typically 5-10 downwind ages up to ~1.2 hr. This enabled characterizing downwind plume evolution of reactive compounds using downwind NEMRs. However, besides plume evolution, the changes occurring downwind can also reflect changes at the source that occurred before the aircraft arrived. In most cases the source changes can be assumed to be small as the

fire burned through a homogeneous fuel bed in a single crop type. The cases where source combustion regime changes were contributing can be identified by looking at the $\Delta\text{BC}/\Delta\text{CO}$ ratio as a surrogate for the flaming to smoldering ratio [Yokelson *et al.*, 2009]. For all except one fire (Fire 12) in which BC was measured, the average $\Delta\text{BC}/\Delta\text{CO}$ ratios for the last few ages were similar to the $\Delta\text{BC}/\Delta\text{CO}$ ratios near the sources within measurement uncertainty. In addition, there was generally no apparent relationship between the observed small $\Delta\text{BC}/\Delta\text{CO}$ variations and the evolution of O_3 , PAN, or OA (r^2 of $\Delta\text{BC}/\Delta\text{CO}$ versus $\Delta\text{O}_3/\Delta\text{CO}$ or $\Delta\text{PAN}/\Delta\text{CO}$ ranged from 0.001 to 0.37). The exceptions are the relatively good correlations between $\Delta\text{BC}/\Delta\text{CO}$ and $\Delta\text{O}_3/\Delta\text{CO}$ ($r^2 = 0.61$) and $\Delta\text{PAN}/\Delta\text{CO}$ ($r^2 = 0.86$) for Fire 12 and that between $\Delta\text{BC}/\Delta\text{CO}$ and $\Delta\text{OA}/\Delta\text{CO}$ ($r^2 = 0.77$) for Fire 13. Except for these cases, we concluded that the downwind changes described here were driven mainly by chemical and physical evolution rather than source changes with time.

4.2.2 Lagrangian Plume Cross-Section Model

We developed a Lagrangian plume cross-section (LPCS) model based on the 1-D version of the Regional chEmical trAnsport Model (1-D REAM) [Wang *et al.*, 2007; Gray *et al.*, 2010; Liu *et al.*, 2010; Liu *et al.*, 2012; Zhang *et al.*, 2014; Zhang *et al.*, 2016]. This LPCS-REAM model was used to simulate the evolution of agricultural fire emissions. Differing from previous modeling approach that treated the plume as a well-mixed Lagrangian parcel [Mason *et al.*, 2006; Alvarado and Prinn, 2009] or performed 3-dimensional Eulerian simulations [Trentmann *et al.*, 2003; Alvarado *et al.*, 2009], the LPCS-REAM model simulated the cross-section of a fire plume along the cross-wind direction, so as to capture the strong concentration gradient within the plume. The cross-

section was discretized into 200 horizontal boxes, each 50 m wide. Both the photochemistry within individual boxes and the mixing among different boxes were computed alternately at a 15 s time step. The gas-phase O_3 - NO_x -hydrocarbon photochemistry mechanism was taken from the 1-D REAM, including 110 species and 400 reactions. Chemical kinetics data were updated following the latest compilation by *Sander et al.* [2011]. Additionally, the model implemented a new isoprene chemistry mechanism based on *Paulot et al.* [2009a] and *Paulot et al.* [2009b]. In our case, the use of the updated isoprene mechanism led to negligible differences for the species of interest (e.g., O_3 , PAN). The model used an implicit diffusion scheme to calculate the mixing process along the cross-wind direction [*Zhang et al.*, 2014]. The dilution parameters included the initial plume width and the cross-wind horizontal diffusion coefficient, K_y . The initial plume widths for all cases were set as 500 m, consistent with the typical field size observed during SEAC⁴RS, and were represented by the center 10 boxes in the model (the 96th -105th boxes). K_y was determined through a pretest, in which the model was run with various K_y (100, 500, 1000, 2000, 4000, 6000, and 10000 $\text{m}^2 \text{s}^{-1}$). When a plume was penetrated by the aircraft more than one time (Table 3), it was likely that the dilution conditions had changed and thus each pass was simulated separately. For each long-axis pass, we chose the K_y with which the simulated CO concentrations had the least sum of squared error compared with the peak-averaged CO observations. A sensitivity test confirmed that the chemical production of CO in the plume was <5%, thus negligible.

The model was constrained by aircraft measurements. Meteorological parameters such as temperature and humidity in-situ observations were used as model inputs.

Photolysis frequencies were calculated from measured actinic flux and laboratory-determined molecular cross sections and quantum yields [Shetter and Müller, 1999]. The initial concentrations in the center 10 boxes were set as fire emissions, i.e., the highest values measured in plumes near the fire sources. Note that in addition to the fast measurements, VOC data measured by WAS coupled with gas chromatography were also used as best estimates of the initial VOC emissions (Table 1). However, since WAS collected integrated air samples, the WAS VOC data tended to underestimate the actual fresh emissions. For other boxes, the initial values were specified with background concentrations. During mixing and aging processes, the boundary conditions (the 1st and 200st boxes) were specified with the background values identified from the dataset. The simulated results at different plume ages were averaged from the center 25 boxes to compare with the peak-averaged measurements.

To understand how VOC, oxygenated volatile organic compound (OVOC), and HONO emissions from the agricultural fires impact the production of PAN, a series of sensitivity tests were conducted by perturbing initial concentrations. Specifically, the sensitivities of PAN production to acetaldehyde, propene, isoprene, methylglyoxal, methyl ethyl ketone (MEK), diacetyl, and HONO emissions were examined. Since HONO and several important PAN precursors including methylglyoxal, MEK, and diacetyl [Liu *et al.*, 2010] were not measured in the campaign, the EFs for rice straw measured by Stockwell *et al.* [2015] were applied in order to estimate their initial concentrations by scaling with the observed CO.

In addition to gaseous species, nitrate, SOA, and the O/C ratios were also modeled. We estimated the nitrate production through the deposition of nitric acid (HNO₃) to the

aerosol surface using the formulation by *Dahneke* [1983], with an uptake coefficient assigned as 0.15 [*Sander et al.*, 2011]. The aerosol surface area was calculated based on measurements by a laser aerosol spectrometer (LAS, TSI Inc., St. Paul, MN). Dry deposition velocity of HNO_3 was set as 2 cm s^{-1} [*Zhang et al.*, 2009]. The wet deposition of HNO_3 and the dry/wet deposition of nitrate aerosols to land or clouds were not included in the simulation because of the short time span of the simulation ($\sim 1 \text{ hr}$) and the common clear sky conditions during the flights of interest. The SOA production was calculated following the simple parameterization by *Hodzic and Jimenez* [2011], using a mass emission ratio of 0.013 gram of a lumped SOA precursor per gram of CO based on *Cubison et al.* [2011], an SOA yield of one, and a rate constant with hydroxyl radical (OH) of $1.25 \times 10^{-11} \text{ cm}^3 \text{ molecule}^{-1} \text{ s}^{-1}$. Deriving the photochemical age from the simulated OH concentrations, the evolution of the O/C ratios of primary organic aerosol (POA) were also calculated with the following equation similar to the approach proposed by *Hodzic and Jimenez* [2011] for the evolution of urban emissions, but with different parameters,

$$O / C = 0.6 - 0.2 \exp\left(-\frac{A}{0.05}\right) \quad (7)$$

where A is days of photochemical age computed by dividing OH exposure by a typical OH concentration of $1.5 \times 10^6 \text{ molecules cm}^{-3}$, i.e. $A = (\int_0^t [\text{OH}] dt) / (1.5 \times 10^6 \text{ molecules cm}^{-3})$, and 0.05 in days is the aging time scale for the agricultural fires.

Due to plume tracking difficulties, plume intercepts were rarely perfect, posing challenges to model simulation. To realistically interpret the photochemical processes, the cases presented here were selected because (1) the dilution could be reasonably simulated with the model; (2) there are enough downwind data to compare with the modeled concentrations; and (3) the initial concentrations of important species, such as NO_x , are available. These cases include the 2nd pass of Fire 3, the two passes of Fire 4, and the 1st and 3rd passes of Fire 15.

4.3 Results

Among the 15 agricultural fires, 13 included at least one long-axis penetration providing samples of both the fresh and aged plume (Table 3). To study the evolution of reactive species, we selected all 7 fires that provided aged samples older than 20 min: Fires 1, 3, 4, 12, 13, 14, and 15. As discussed in section 4.2.1, the downwind changes discussed here were driven mainly by chemical and physical evolution rather than source changes. However, since the $\Delta\text{BC}/\Delta\text{CO}$ exhibited an increasing trend for Fire 12, it is possible that the downwind evolution of the species in this fire discussed here reflected both source changes to some extent and plume aging.

When using downwind NEMRs to illustrate evolution, we plot all available data for a single fire together to show the general trend even if these data were from multiple penetrations through the fire. The 1σ uncertainty in the estimated age is based on the variability of wind direction and wind speed. Absolute uncertainties of NEMRs are a result of error propagation from measurement uncertainties. The uncertainties of estimated age and NEMRs (or ERs) are only shown for one fresh and one aged

measurement for each fire as examples. Linear or polynomial fits were performed to the NEMRs versus smoke age plot as a simple representation of the evolution trend and also an estimation of the final NEMR at the age of the last measurement. The species we focus on include O_3 , reactive nitrogen species, OA, and BrC.

4.3.1 *Plume Evolution*

4.3.1.1 Ozone

In Figure 8, $\Delta O_3/\Delta CO$ for the 7 aged fires is plotted versus the estimated smoke age. The initial $\Delta O_3/\Delta CO$ is sometimes negative because the background O_3 can be depleted by fast reaction with freshly emitted NO. Negative initial $\Delta O_3/\Delta CO$ has been frequently observed in fresh BB plumes [Yokelson *et al.*, 2003; Akagi *et al.*, 2012]. In general, rapid O_3 formation was observed in 6 out of 7 agricultural fires. The only exception is Fire 3, in which the less-intense ultraviolet light in late afternoon likely retarded the photochemistry (local flight times are shown in Table 3). $\Delta O_3/\Delta CO$ for the other 6 fires increased from near zero to 0.03-0.05 in ~30 min after emission. For Fires 4, 14, and 15, the ratio reached over 0.10 or more in about 1h. Such a formation rate is comparable to that observed in prescribed fires in South Carolina [Akagi *et al.*, 2013] and tropical BB plumes as reviewed in Akagi *et al.* [2011] and faster than those observed in some mid- and high-latitude BB plumes [Goode *et al.*, 2000; Alvarado *et al.*, 2010; Akagi *et al.*, 2012].

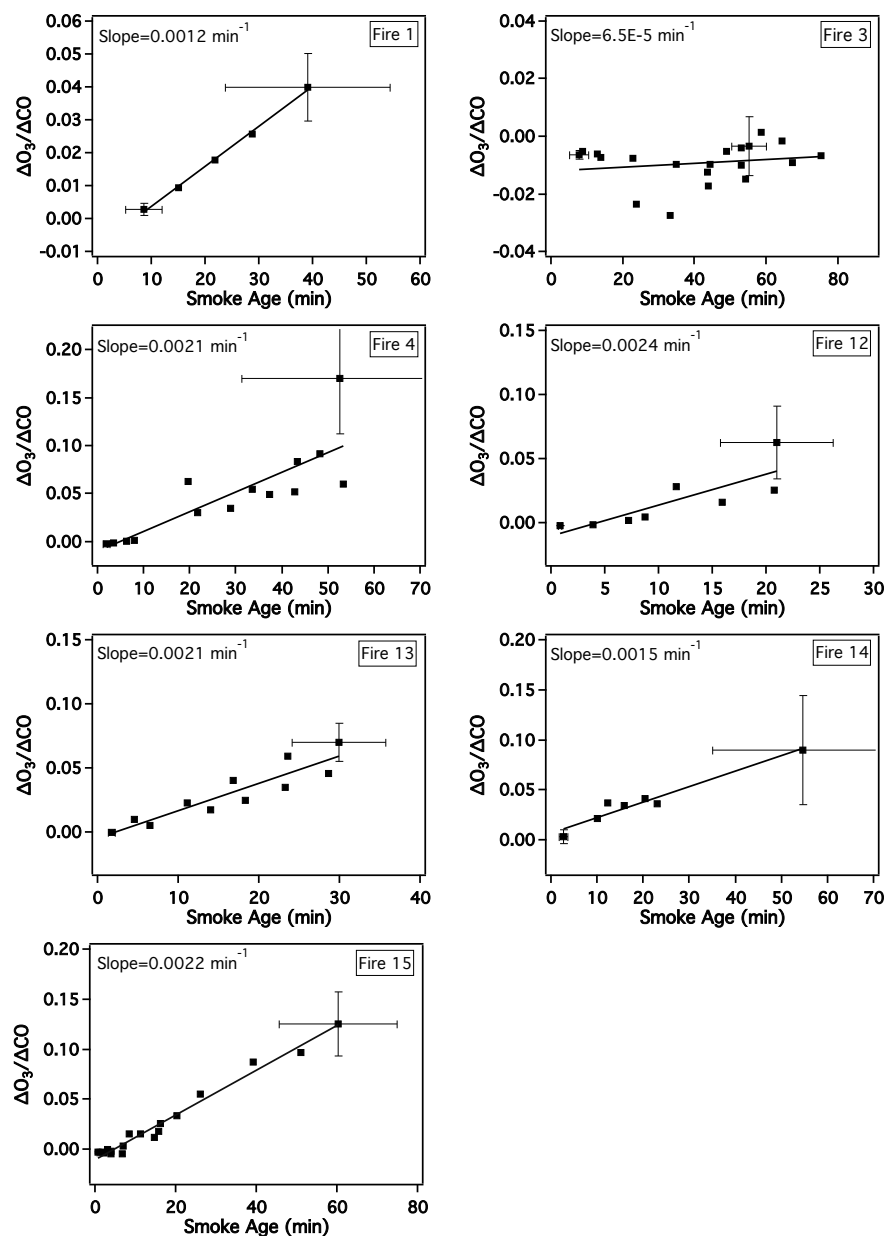


Figure 8 – Evolution of ozone in the 7 aged plumes. Data were fit to a linear trend line. Vertical error bars are a result of measurement uncertainties. Only error bars of one fresh and one aged measurement are shown as examples for each fire. Horizontal error bars represent the 1σ uncertainty in the estimated age based on the variability of wind direction and wind speed. Note that the downwind evolution of Fire 12 might reflect both source changes to some extent and plume aging.

4.3.1.2 Reactive Nitrogen Species

NO_x emitted from BB can be converted to HNO_3 , nitrate, peroxyacyl nitrates (PANs), alkyl nitrates, and other peroxy nitrates. Figure 9 shows the post-emission evolution of excess NO , NO_2 , PAN, HNO_3 , and nitrate normalized by measured excess NO_y for the selected 7 fires. These species constituted $\sim 0.82\text{--}0.96$ of the total measured NO_y . This fraction didn't show significant evolution during aging when compared to combined measurement uncertainty. Several organic nitrates produced by the first and second generation isoprene oxidation such as isoprene hydroxynitrates and MVK/MACR nitrates were also measured at high frequency but no significant elevation or evolution was seen in the plumes. Although not discussed in this section, their observations will be used to evaluate model performance in section 4.3.2.2. Other reactive nitrogen species were either not measured (such as HONO) or were measured at a lower time resolution so that such an evolution analysis is limited.

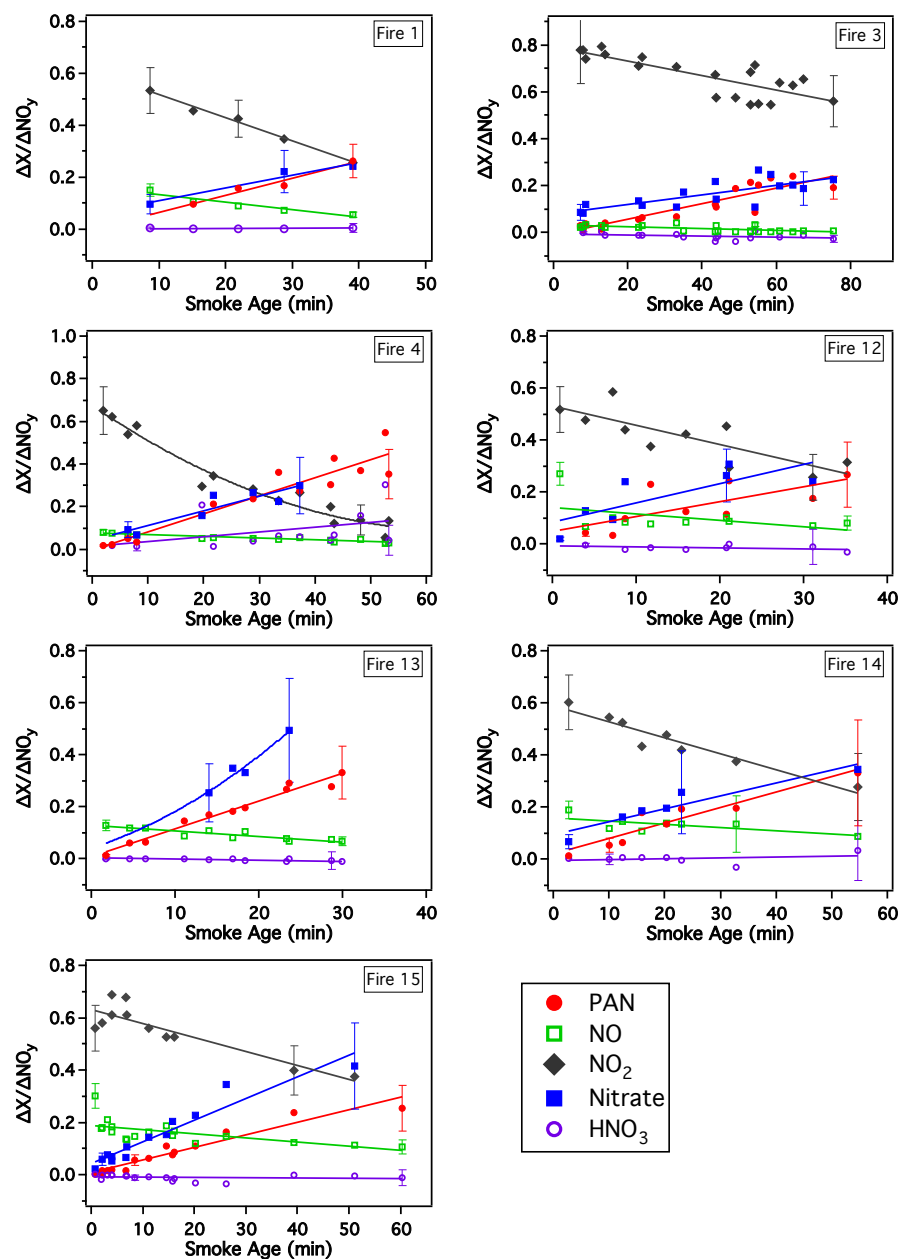


Figure 9 – Evolution of reactive nitrogen species in the 7 aged plumes. Data were fit to a linear or polynomial trend line. Vertical error bars are a result of measurement uncertainties. Only error bars of one fresh and one aged measurement are shown as examples for each fire. The 1σ uncertainty in the estimated age is same as that shown in Figure 8. NO₂ measurements are not available for Fire 13. Note that the downwind evolution of Fire 12 might reflect both source changes to some extent and plume aging.

Immediately after emission, NO_x constituted 0.69-0.82 of the total NO_y . The $\Delta\text{NO}_x/\Delta\text{NO}_y$ ratios decreased with smoke age. Similar to the trend of $\Delta\text{O}_3/\Delta\text{CO}$, the conversion of NO_x to other reactive nitrogen species was slow in the late afternoon smoke plume of Fire 3. The decrease of $\Delta\text{NO}_x/\Delta\text{NO}_y$ was much faster in the other 5 fires in which NO_x measurements were available. In these 5 plumes, NO_x loss ranged from ~26% to ~56% in about 30 min.

Figure 9 also shows the growth in $\Delta\text{PAN}/\Delta\text{NO}_y$. For all of the cases but Fire 3, the $\Delta\text{PAN}/\Delta\text{NO}_y$ ratios increased rapidly from less than 0.05 to ~0.3 in ~1 hr. Such a PAN formation rate is similar to that observed in a boreal smoke plume (Lake McKay) during ARCTAS-B [Alvarado *et al.*, 2010] and higher than in a Yucatan BB plume [Yokelson *et al.*, 2009] and in the chaparral fire in California [Akagi *et al.*, 2012]. Based on the increase in $\Delta\text{PAN}/\Delta\text{NO}_y$, PAN accounted for 51% to 74% of the loss of NO_x on a molar basis at the end of our aging measurements on each fire. No significant increasing trend was observed for HNO_3 . As the plumes aged, HNO_3 concentrations in general remained near background level. Although NH_3 was not measured in this campaign, significant amounts of NH_3 have been observed in other BB studies (Table 6), including crop residue burning [Akagi *et al.*, 2011; Stockwell *et al.*, 2014]. For example, Stockwell *et al.* [2014] measured an NH_3 EF of Asian rice straw as high as 1.12 ± 0.77 g/kg, adjusted to the SEAC⁴RS-averaged MCE. Therefore, HNO_3 formed from NO_2 oxidation might have been converted efficiently to nitrate due to the availability of NH_3 and aerosol surface area in the plumes. The trend in $\Delta\text{nitrate}/\Delta\text{NO}_y$ is most similar to that of $\Delta\text{PAN}/\Delta\text{NO}_y$, suggesting a rapid formation of nitrate particles in the first hour of aging. For the fires including Fires 1, 3, 4, 12, and 14, while $\Delta\text{PAN}/\Delta\text{NO}_y$ and $\Delta\text{nitrate}/\Delta\text{NO}_y$

increased at slightly different rates, the excess PAN and nitrate of the last few measurements accounted for roughly the same fraction of the excess NO_y . This suggests that during the ~ 1 h aging, approximately equal amounts of initial NO_x emissions were converted to PAN and to nitrate. For Fires 13 and 15, a larger fraction of NO_x was converted to nitrate than to PAN, with nitrate dominating the downwind NO_y budget. Our 1-hour $\Delta\text{nitrate}/\Delta\text{PAN}$ ratios equal to or slightly larger than 1 are the largest values reported to date. On a time scale of several hours, *Akagi et al.* [2012] and *Alvarado et al.* [2010] both observed an average $\Delta\text{nitrate}/\Delta\text{PAN}$ ratio of ~ 0.5 in the chaparral fire in California and in boreal forest fire plumes in Canada, respectively. It is also possible that PAN formation becomes increasingly dominant over HNO_3 /nitrate formation further downwind, as simulated by *Mason et al.* [2001], so that our $\Delta\text{nitrate}/\Delta\text{PAN}$ ratio may decrease as the plumes get older than 1 hr. PAN and nitrate together accounted for almost all NO_x loss, ranging from 100% to 140% if based on $\Delta\text{nitrate}/\Delta\text{PAN}$, $\Delta\text{PAN}/\Delta\text{NO}_y$, and $\Delta\text{NO}_x/\Delta\text{NO}_y$ ratios. However, such an estimate is uncertain since ΔNO_y is not a strictly conserved tracer in plumes. We will further discuss the conversion of NO_x to PAN and HNO_3 /nitrate and the branching between them in section 4.3.2.2 using our model simulations.

4.3.1.3 Organic Aerosol and Brown Carbon

The changes in $\Delta\text{OA}/\Delta\text{CO}$ were also measured for the 7 aged fires and were found to vary from fire to fire. The net formation of SOA may contribute to higher downwind $\Delta\text{OA}/\Delta\text{CO}$ while the net evaporation of semi-volatile OA may decrease OA mass during dilution and thus reduce $\Delta\text{OA}/\Delta\text{CO}$. The ratio may also stay approximately constant despite active oxidation chemistry, if the different processes approximately

cancel in terms of their changes of OA mass [Cubison *et al.*, 2011]. For Fires 12, 13, and 15 sampled on 23 September a possible net increase in $\Delta\text{OA}/\Delta\text{CO}$ might have been present. However, no significant increase was seen for the other fires. To represent the overall $\Delta\text{OA}/\Delta\text{CO}$ evolution, the changes in $\Delta\text{OA}/\Delta\text{CO}$ for all the 7 fires were compiled in a single box-and-whisker plot (25th-75th and 10th-90th percentiles), as shown by Figure 10. Within the first 15 min, the median $[\Delta\text{OA}/\Delta\text{CO}]_t/[\Delta\text{OA}/\Delta\text{CO}]_0$ is 0.96. In downwind plumes the median $[\Delta\text{OA}/\Delta\text{CO}]_t/[\Delta\text{OA}/\Delta\text{CO}]_0$ varies between 0.85 and 1.3 and is not significantly different from 1 or the freshest $[\Delta\text{OA}/\Delta\text{CO}]_t/[\Delta\text{OA}/\Delta\text{CO}]_0$. The fact that no significant change in the study-averaged $\Delta\text{OA}/\Delta\text{CO}$ was observed for the first ~ 1.2 h aging does not permit strong conclusions about consistent SOA formation in the plumes. Capes *et al.* [2008], Cubison *et al.* [2011], Hecobian *et al.* [2011], Akagi *et al.* [2012], Jolleys *et al.* [2012], and Forrister *et al.* [2015] also observed nearly constant $\Delta\text{OA}/\Delta\text{CO}$ with changes smaller than $\sim 20\%$ during aging in open BB plumes. In contrast, within a fire plume over the Yucatan, Yokelson *et al.* [2009] observed a significant enhancement in $\Delta\text{OA}/\Delta\text{CO}$ with a growth factor of 2.3 ± 0.85 at 1.4 h of aging. For 60 BB plumes in South Africa, Vakkari *et al.* [2014] observed that aged daytime $\Delta\text{OA}/\Delta\text{CO}$ was 4 times that of unprocessed nighttime $\Delta\text{OA}/\Delta\text{CO}$. Laboratory experiments have reported OA enhancement ratios between 0.75 and 3 as a result of photochemical oxidation after a few hours to a few days of exposure to typical atmospheric OH levels [Grieshop *et al.*, 2009; Hennigan *et al.*, 2011; Ortega *et al.*, 2013]. The reasons for the observed variability in net SOA formation from BB plumes are not well understood.

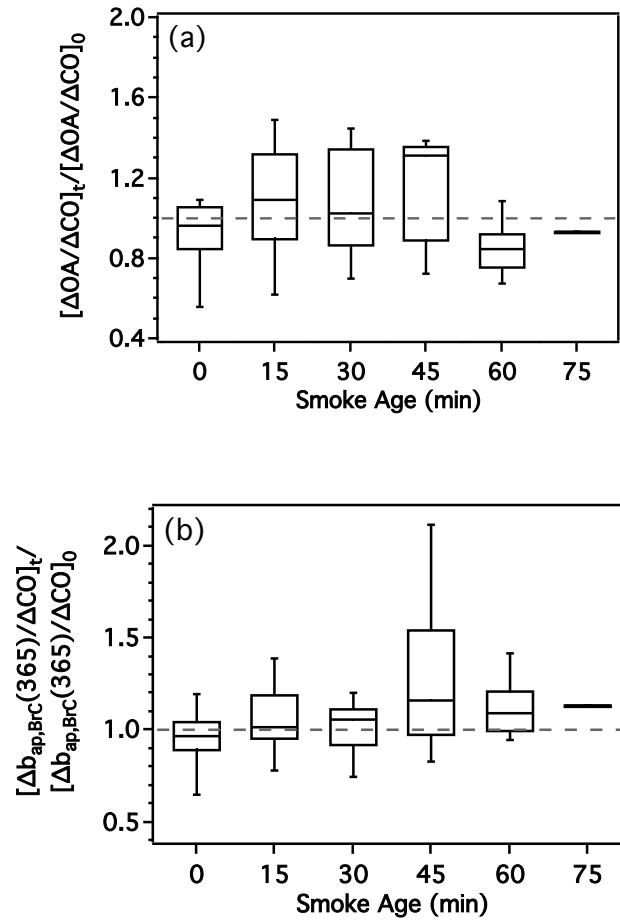


Figure 10 – Box-and-whisker plot of (a) $\Delta OA / \Delta CO$ change and (b) $\Delta b_{ap,BrC(365)} / \Delta CO$ change in the 7 aged plumes (boxes, 25th and 75th percentiles; whiskers, 10th and 90th percentiles; solid horizontal lines, medians; the two thick lines mean that only one data point is available for the corresponding age). Dashed horizontal lines represent a constant value of 1, i.e., no enhancement.

To investigate the chemical transformations of OA, we analyzed elemental ratios including oxygen-to-carbon (O/C) and hydrogen-to-carbon (H/C) ratios using data from the aerosol mass spectrometer (AMS) [Aiken *et al.*, 2008; Canagaratna *et al.*, 2015]. Figure 11 shows the evolution of these two elemental ratios and also background ratio values for 6 fires. Elemental ratios for Fire 12 were not available. The measurement uncertainties of O/C and H/C are 28% and 13%, respectively, based on Canagaratna *et al.* [2015]. The background H/C ratios were in the range of 1.5-1.7 and were always smaller than the H/C ratio near the burning sources, which were generally between 1.6 and 1.8. In contrast, the background O/C ratios (0.7-0.9) were higher than the O/C ratios for POA from the agricultural fires (0.3-0.5), which are similar to the values observed in BB plumes over the Mexico City basin [DeCarlo *et al.*, 2008]. Lower O/C and higher H/C values than background values suggest that POA produced by crop residue burning contained more-reduced and less-oxidized compounds than background OA. For all 6 plumes, a consistent increase in the O/C ratios and a decrease in the H/C ratios associated with aerosol aging was observed, although at different rates. Processes that could explain the observed elemental ratio trends include: (1) mixing with background OA, (2) chemical processing, and (3) the preferential evaporation of more reduced species. Although mixing with background OA would eventually increase O/C and decrease H/C toward the background values, this is likely not the dominant effect. For 5 out of the 6 cases, O/C ratios increased from around ~0.4 to 0.6–0.8 in less than 1 h. Since the measurements indicated that the excess OA concentrations in plumes were well beyond the background OA concentrations throughout this period, mixing alone could not have contributed enough background OA to account for such a rapid O/C increase (Figure 16,

as will be discussed in section 4.3.2.4). When combined with the approximately constant $[\Delta\text{OA}/\Delta\text{CO}]_t/[\Delta\text{OA}/\Delta\text{CO}]_0$ ratios, the observations in O/C and H/C ratios show that the addition of oxygen must be offset by the loss of carbon during aging so that both chemical processing and evaporation were contributing. Rapid O_3 formation also serves as evidence of photochemical activity within the plumes. Chemical processing could change elemental ratios by the addition of SOA of higher O/C ratios or the heterogeneous oxidation of POA. Not surprisingly, the changes of O/C and H/C ratios were slowest in the plume of Fire 3, which agrees with the overall slow photochemistry. This provides further evidence that in general SOA formation was active on this time scale and that not all the O/C changes can be explained by differential evaporation.

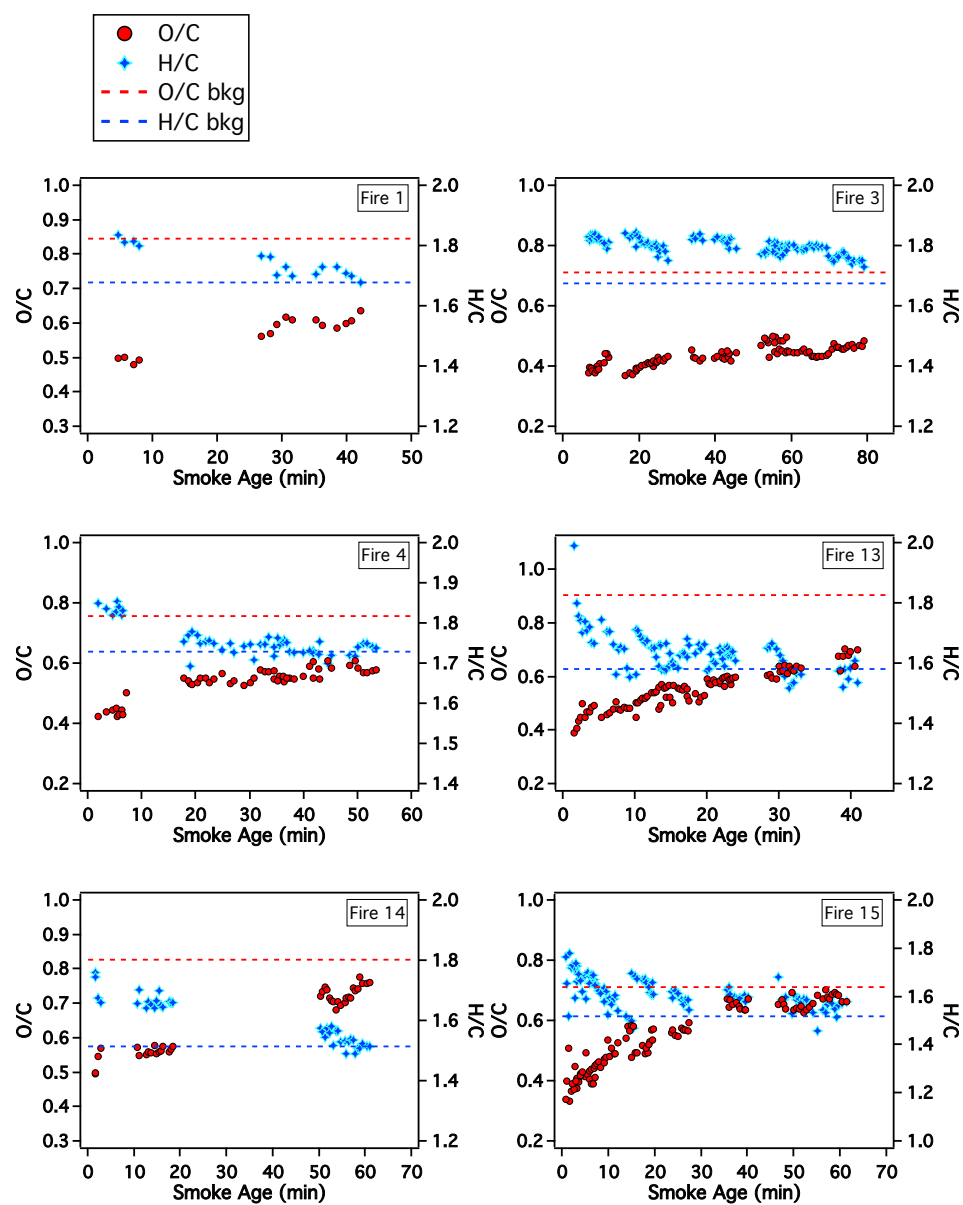


Figure 11 – Evolution of elemental ratios in particulate matter as measured by the AMS in 6 aged plumes (not available for Fire 12).

BrC in POA and SOA in BB plumes may also evolve. The aging effects on the light-absorbing properties of organic carbon vary among studies perhaps due to different aging times and oxidation conditions [Adler *et al.*, 2011; Saleh *et al.*, 2013; Zhong and Jang, 2014; Forrister *et al.*, 2015]. To investigate the influence of aging on short-wavelength light absorption, we plotted box-and-whisker plot of the changes in $\Delta b_{\text{ap,BrC}}(365)/\Delta \text{CO}$ for the 7 fires (Figure 10). $[\Delta b_{\text{ap,BrC}}(365)/\Delta \text{CO}]_t/[\Delta b_{\text{ap,BrC}}(365)/\Delta \text{CO}]_0$ was used to represent $\Delta b_{\text{ap,BrC}}(365)$ evolution. In Figure 10, the downwind $[\Delta b_{\text{ap,BrC}}(365)/\Delta \text{CO}]_t/[\Delta b_{\text{ap,BrC}}(365)/\Delta \text{CO}]_0$ exhibits slightly higher median values and upper limits than the fresher samples less than 15 min old. The slight increase in $\Delta b_{\text{ap,BrC}}(365)/\Delta \text{CO}$ suggests that the aged aerosols up to ~ 1.2 h old were more absorptive than fresh OA. This could possibly result from SOA formation, as implied by the O/C increase. Other processes could also be occurring, such as the loss of volatile BrC and photobleaching. On a similar time scale, Saleh *et al.* [2013] also reported that aged OC was more absorptive due to SOA formation in a smog chamber experiment. Zhong and Jang [2014] reported that chromophore formation and sunlight bleaching governed the change in the absorption of wood smoke aerosol. During a diurnal cycle, OA absorption was first enhanced by chromophore formation in the morning and then decreased by sunlight bleaching in the afternoon. On a longer time scale, Forrister *et al.* [2015] demonstrated that BrC emitted from wildfires was largely unstable and decayed in the plume with a half-life of 9 to 15 hr. Therefore, our measurements in agricultural fire plumes may have captured BrC evolution in the early stage before its loss exceeded possible secondary formation.

4.3.2 Model Simulations

Understanding the rapid chemical evolution in fire plumes is critical for evaluating the impact of agricultural fires on regional air quality, atmospheric composition, and climate. Here we use the LPCS-REAM model to simulate the evolution of O_3 , PAN, HNO_3 , nitrate, radicals, SOA, and the O/C ratios within young agricultural fire plumes.

Figure 12 shows the simulated CO mixing ratios using the best-fit dilution coefficient (K_y), one half of best-fit K_y , and twice of best-fit K_y , along with the observed CO mixing ratios. Despite the assumptions made for a single K_y value and the method of observation-model comparison, the simulated CO mixing ratios using the best-fit K_y reasonably represented the dilution trend when compared to the observations. The overall successful agreement enables us to further study the chemical evolution in the fire plumes.

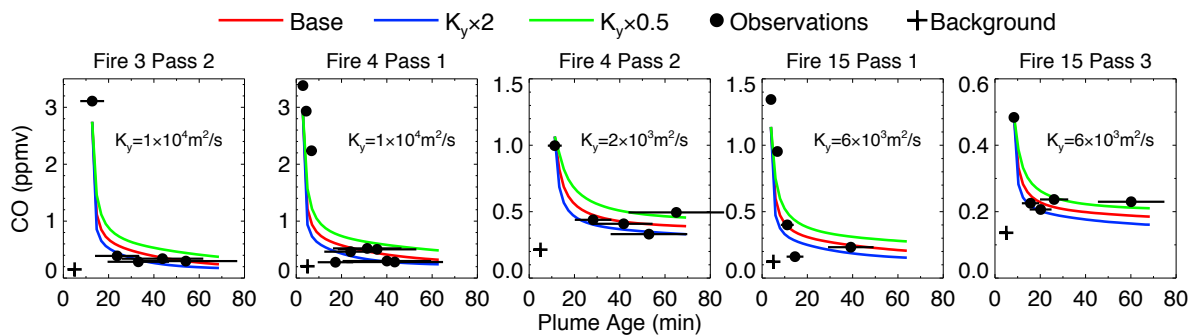


Figure 12 – CO mixing ratio vs. smoke age for the 5 selected cases. Green, red, and blue lines are for the slow, best fit, and fast plume dilution rates. Circles are the measured mixing ratios, with the horizontal error bars showing the uncertainty in the estimated age. Crosses are background CO concentrations outside the plumes.

4.3.2.1 Ozone

Figure 13 shows the evolution of the enhancement ratios of O_3 for the 5 selected cases. With the best-fit dilution coefficients, the model can reasonably simulate $\Delta O_3/\Delta CO$ to within $\sim 30\%$ in general. To quantify the photochemical O_3 production in an agricultural fire plume, we used the simulated results to calculate ozone production efficiency (OPE), defined as the number of O_3 molecules produced per number of NO_x molecules oxidized [Liu *et al.*, 1987; Lin *et al.*, 1988; Trainer *et al.*, 1993; Olszyna *et al.*, 1994]. In this study, we computed the OPEs during 1 h evolution by dividing the number of O_3 molecules produced by the number of NO_x molecules oxidized to PAN and HNO_3 +nitrate, given that PAN and HNO_3 +nitrate accounted for most of the measured

NO_x oxidation products (Figure 9). As shown in Table 7, the OPEs are in a range of 6.0 to 9.8 for the 5 cases. OPE values on the time scales of 0.5-4 days were estimated to be 5-17 for BB activities in Southeast Asia [Kondo *et al.*, 2004], South and Central Africa [Marion *et al.*, 2001; Yokelson *et al.*, 2003], Australia [Shirai *et al.*, 2003; Takegawa *et al.*, 2003], and western US [Baylon *et al.*, 2015]. The OPEs for the agricultural fires are in the lower end of the previously reported range. However, the OPEs in our cases will likely evolve as age increases beyond 1 hr. The thermal decomposition of PAN could also further promote O₃ production after the first 1 hr.

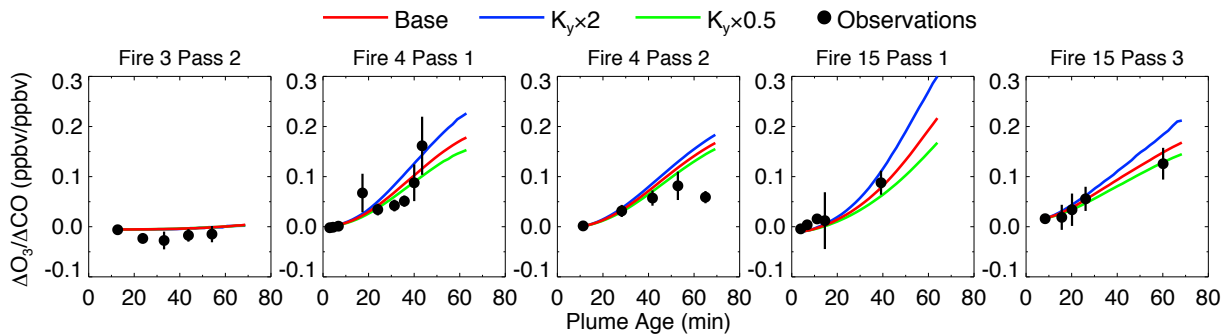


Figure 13 – Enhancement ratios of ΔO_3 to ΔCO vs. smoke age for the 5 selected cases. Green, red, and blue lines are for the slow, best fit, and fast plume dilution rates. Circles are the measured enhancement ratios, with the vertical error bars showing the uncertainty in the measurement. The uncertainty in the estimated age is not shown here but is same as in Figure 12.

Table 7 – Summary of the modeled evolution characteristics at an age of 1 h: ozone production efficiency (OPE), the ratio of NO_x oxidized to PAN to that oxidized to PAN plus HNO₃+nitrate (P_PAN/(P_HNO₃+P_PAN)), and radical concentrations.

Case	OPE	P_PAN/ (P_HNO ₃ +P_PAN)	OH		HO ₂		RO ₂	
			molecules cm ⁻³		molecules cm ⁻³		molecules cm ⁻³	
			Median	Average	Median	Average	Median	Average
Fire 3 Pass 2	6.0	0.65	5.6×10 ⁵	5.3×10 ⁵	1.5×10 ⁸	1.4×10 ⁸	6.7×10 ⁷	6.6×10 ⁷
Fire 4 Pass 1	7.0	0.66	1.7×10 ⁷	1.5×10 ⁷	1.2×10 ⁹	1.1×10 ⁹	3.8×10 ⁸	4.1×10 ⁸
Fire 4 Pass 2	9.8	0.50	1.9×10 ⁷	1.8×10 ⁷	1.0×10 ⁹	1.0×10 ⁹	2.8×10 ⁸	2.9×10 ⁸
Fire 15 Pass 1	6.3	0.39	1.5×10 ⁷	1.7×10 ⁷	2.5×10 ⁸	3.3×10 ⁸	8.9×10 ⁷	1.1×10 ⁸
Fire 15 Pass 3	7.2	0.62	7.5×10 ⁶	6.7×10 ⁶	3.9×10 ⁸	3.5×10 ⁸	1.4×10 ⁸	1.3×10 ⁸

4.3.2.2 Reactive Nitrogen Species

The simulated enhancement ratios of the major NO_x oxidation products, PAN, HNO₃, and nitrate, are shown in Figure 14. Note that the nitrate observations shown are the total nitrate measured by AMS while the modeled nitrate represents the sum of initial emissions plus those originating from HNO₃ condensation. As the AMS measurements indicated that the nitrate in all the fire plumes in this study was mainly comprised of inorganic nitrate (> 90%), comparing the evolution of measured total nitrate with that of the modeled inorganic nitrate is reasonable. Table 7 shows the ratio between NO_x oxidized to PAN and that oxidized to PAN plus HNO₃+nitrate. It can be seen from Figure

14 that the model in general underestimated the formation of PAN by up to ~50% of the observed $\Delta\text{PAN}/\Delta\text{CO}$. The simulated HNO_3 was generally lower than the observed HNO_3 as the simulated $\Delta\text{HNO}_3/\Delta\text{CO}$ decreased more rapidly with age than the observations. For nitrate, the model performance varied from case to case. For Fire 3 Pass 2 and Fire 4 Passes 1 and 2, the increase of $\Delta\text{nitrate}/\Delta\text{CO}$ was overestimated by the model by up to ~50%. In these three cases, the underestimation of HNO_3 and the overestimation of nitrate imply that the model exaggerated the gas-to-particle deposition of HNO_3 . In the other two cases, Fire 15 Passes 1 and 3, the model underestimated nitrate, although within measurement uncertainties. However, more downwind nitrate data are needed for better evaluation. Since modeling the partitioning between HNO_3 and nitrate is limited by the simplified treatment of HNO_3 deposition, it is also useful to compare the observed and the simulated sum of HNO_3 +nitrate. As also shown in Figure 14, the model made reasonable predictions for total HNO_3 +nitrate for the first three cases within measurement uncertainties but underestimated the concentrations of total HNO_3 +nitrate for the last two cases, although again more downwind nitrate data would be useful to better evaluate the model performance. Several reasons may explain the disagreement. First, the highest initial emissions of nitrate near the fire sources were not measured for the Fire 3 Pass 2 and Fire 4 Pass 1. The input of the freshly emitted nitrate was estimated using the $\text{EF}(\text{nitrate})$ from other transects of the same fire and measured CO peak, which is a source of uncertainty for downwind nitrate simulation. Second, errors in the modeled photochemistry, e.g., the modeled OH concentration, could bias the HNO_3 +nitrate predictions.

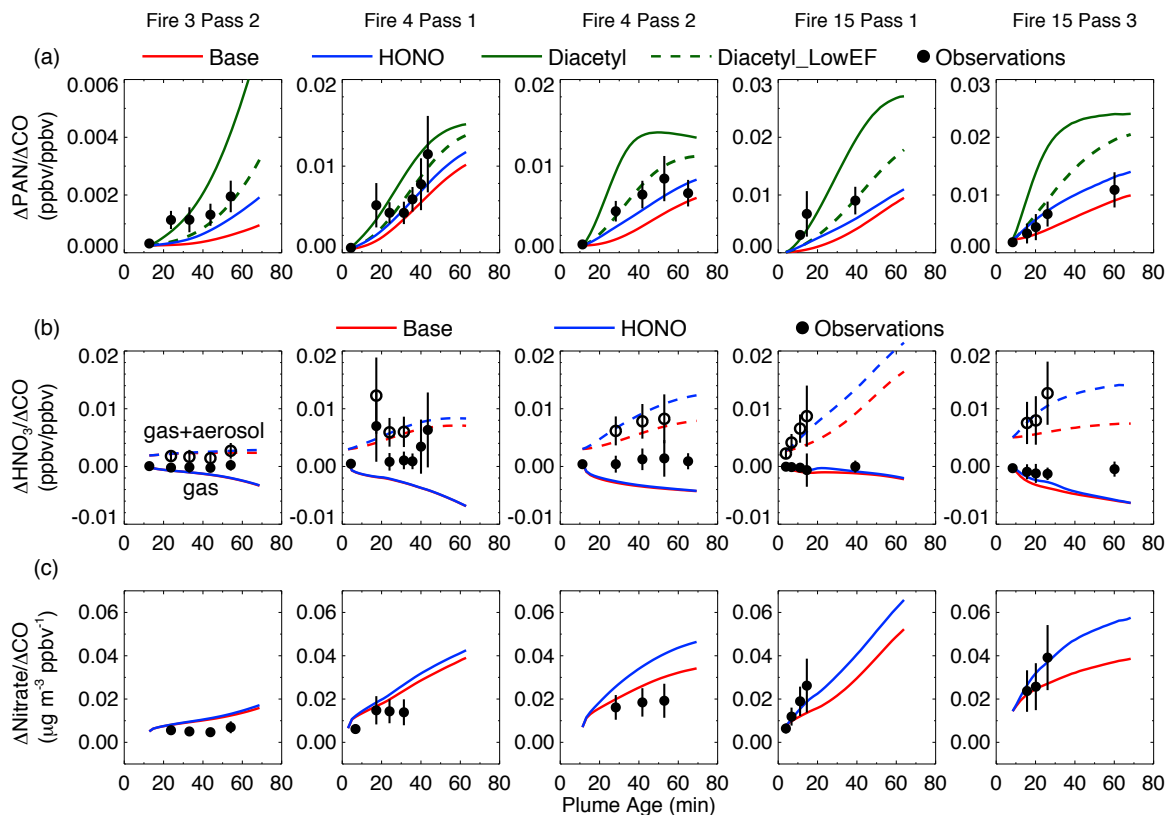


Figure 14 – Enhancement ratios of (a) ΔPAN to ΔCO , (b) ΔHNO_3 to ΔCO and $(\Delta\text{HNO}_3 + \Delta\text{nitrate})$ to ΔCO , and (c) $\Delta\text{nitrate}$ to ΔCO vs. smoke age for the 5 selected cases. Circles (solid circles for single NO_y species and open circles for HNO_3 by CIMS + nitrate by AMS) are the measured enhancement ratios, with the vertical error bars showing the uncertainty in the measurement. The uncertainty in the estimated age is not shown here but is same as in Figure 12. The red lines (solid and dashed) are base model results for the best-fit dilution rates. The blue (solid) and green (solid and dashed) lines are the results of the base model with estimated HONO (using FLAME-4 EF) and diacetyl (using FLAME-4 EF and one half of FLAME-4 EF) initial emissions.

The model output also includes other gaseous organic nitrate, including peroxypropionyl nitrate (PPN), peroxyacetyl nitrate (MPAN), $\text{NO}_3\text{CH}_2\text{PAN}$, isoprene organic nitrates, carbonyl nitrates from NO_3 +isoprene, methyl nitrate, and C_4 - and C_5 -alkyl nitrates. According to the simulation, the sum of these gaseous organic nitrates was elevated by 0.1-0.3 ppbv at an age of 1 h after accounting for dilution, which is minor compared to PAN or HNO_3 +nitrate formation. The available fast measurements of PPN and several organic nitrates produced from isoprene oxidation showed that their formation was of similar magnitude as predicted by the model. In addition, the organic nitrate fractions for all the fires in this study reported by the AMS were <10%, which indicates that the enhancement of particulate organic nitrate was smaller than or similar to that of gaseous organic nitrates. So it is likely that only a small amount of gaseous organic nitrates that formed, if any, partitioned to the particle phase.

Several sensitivity simulations were performed to explore possible reasons for the underestimation of PAN (all five cases) and HNO_3 +nitrate (the last two cases) formation (Figure 14). Since the VOCs measured at sampling rates ≥ 10 s (Table 1) likely missed the highest peak near fire sources and thus underestimated the initial emissions from the fires, additional model runs were performed with enhanced VOC initial concentrations. The results indicate that as expected, acetaldehyde had the most significant influence on PAN formation. However, doubling the acetaldehyde concentration still cannot fully explain the observed rapid formation of PAN (Figure 15). Simulations were conducted with additional unmeasured species, including HONO, methylglyoxal, diacetyl, and MEK. Their initial emissions were scaled using FLAME-4 EFs (adjusted to SEAC⁴RS MCE) and measured CO initial emissions [Stockwell *et al.*, 2015]. The results showed

that, with EFs from FLAME-4, HONO (0.35 ± 0.13 g/kg) and diacetyl (0.92 ± 1.00 g/kg) were significant contributors to PAN formation (Figure 14) while methylglyoxal (0.36 ± 0.31 g/kg) was relatively less important (Figure 15). A combined effect of adding HONO, diacetyl, and methylglyoxal is shown in Figure 15. Since PAN was very sensitive to diacetyl, the large variability of EF(diacetyl) could lead to a large uncertainty in the simulated PAN. We found that by reducing EF(diacetyl) by a factor of 2, the simulated $\Delta\text{PAN}/\Delta\text{CO}$ agreed well with the observed values (Figure 14). The addition of initial HONO also promoted the modeled HNO_3 +nitrate formation by ~30-70% and resulted in better agreements with observations especially for the last two cases. This suggests that the baseline simulation is likely missing some radical sources. The measured acetaldehyde, methylglyoxal, and diacetyl were also found to be the main precursors of peroxyacetyl radicals in the plume of the small forest understory fire in Georgia reported by Müller *et al.* [2016].

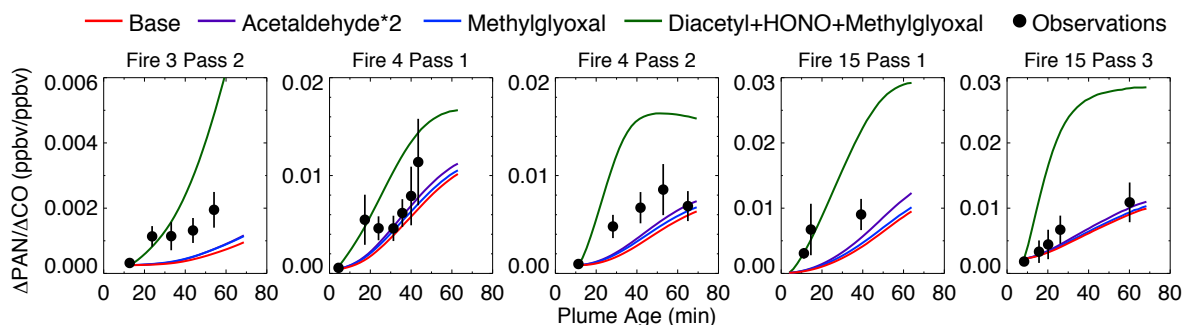


Figure 15 – Additional sensitivity test results of $\Delta\text{PAN}/\Delta\text{CO}$ vs. smoke age for the 5 selected cases. Circles are the measured enhancement ratios, with the vertical error bars showing the uncertainty in the measurement. The uncertainty in the estimated age is not shown but is same as in Figure 12. The red, purple, blue, and green lines are the results of the base model, the base model with doubled acetaldehyde input, the base model with estimated methylglyoxal using $\text{EF}(\text{methylglyoxal})$ by [Stockwell *et al.*, 2015], and the base model with estimated diacetyl, HONO, and methylglyoxal using EFs by [Stockwell *et al.*, 2015].

4.3.2.3 Radical Concentrations

BB greatly perturbs atmospheric oxidants. For example, the direct emissions and the secondary formation of hydrogen peroxide, formaldehyde, and other aldehydes from BB can be significant sources of hydrogen oxides (HO_x) [Lee *et al.*, 1998; Trentmann and Andreae, 2003; Yokelson *et al.*, 2009; Müller *et al.*, 2016]. In addition, the oxidation of emitted organic species produces organic peroxy radicals (RO_2), which can propagate HO_x and NO_x radical chains and thereby generate O_3 through subsequent photolysis of NO_2 [Orlando and Tyndall, 2012]. Although measurements of HO_x or RO_2 were not available, we present model estimates to characterize the oxidants within the agricultural

fire plumes. Table 7 lists the median and average concentrations of OH, hydroperoxyl radical (HO_2), and RO_2 during the 1 h simulation. For Fire 3 Pass 2, the low modeled radical concentrations agree with the overall slow photochemistry. For the other 4 cases, the average OH and HO_2 concentration were in the ranges of 6.7×10^6 to 1.8×10^7 molecules cm^{-3} and 3.3×10^8 to 1.1×10^9 molecules cm^{-3} , respectively. The photochemical production of the HO_x family in the plume was dominated by the photolysis of formaldehyde and the reaction of $\text{O}^1\text{D} + \text{H}_2\text{O}$ (from O_3 photolysis), which on average accounted for $\sim 60\%$ and $\sim 35\%$, respectively. As a comparison, *Hobbs et al.* [2003] inferred an average OH concentration of $\sim 1.7 \times 10^7$ molecules cm^{-3} from the relative rates of decrease for a number of chemical species in a savanna fire plume burned in South Africa in late morning. *Yokelson et al.* [2009] measured a similar OH level of 1.14×10^7 molecules cm^{-3} from a slightly aged plume that was 22-43 min old. Without being influenced by BB, the average noontime OH and HO_2 concentrations at the surface in the southeastern U.S. measured in summer 2013 were $\sim 2.4 \times 10^6$ (0.1 ppt) and $\sim 1.2 \times 10^9$ molecules cm^{-3} , respectively [*Xiong et al.*, 2015]. In short, the photochemical environment in the plumes studied here has similar levels of OH as those in *Hobbs et al.* [2003] and *Yokelson et al.* [2009] and generally higher OH, up to ~ 8 times higher, than the surface ambient air studied in *Xiong et al.* [2015]. The magnitude of simulated HO_2 in the plumes is similar to that in *Xiong et al.* [2015]. In the case of RO_2 , the average modeled concentration ranged from 6.6×10^7 to 4.1×10^8 molecules cm^{-3} , with methyl peroxy radical (CH_3O_2) accounting for $\sim 30\text{-}50\%$ of RO_2 . As discussed before, the radical concentrations reported here likely represent a lower limit on actual radical levels in the agricultural fire plumes.

4.3.2.4 SOA and O/C ratios

SOA formation in the plumes was calculated by a simplified parameterization, which was proposed based on urban pollution observations made in Mexico City [Hodzic and Jimenez, 2011] and Los Angeles [Hayes *et al.*, 2015], with parameters updated for biomass burning emissions based on Cubison *et al.* [2011]. Figure 16 shows the modeled $\Delta\text{OA}/\Delta\text{CO}$ versus plume age for the 5 individual passes. The simulated $\Delta\text{OA}/\Delta\text{CO}$ is the sum of the observed $\text{POA}/\Delta\text{CO}$ and the modeled $\text{SOA}/\Delta\text{CO}$, where POA is treated as non-volatile during the ~ 1 h aging considered here. The model parameters ensured that $\Delta\text{OA}/\Delta\text{CO}$ was generally conserved for all the 5 cases after considering dilution, indicating that SOA formed in 1 h was insignificant compared with POA emitted. Although there are discrepancies between the simulations and the observations, several factors limit a detailed parameter optimization. First, for Fire 3 Pass 2, Fire 4 Pass 1, and Fire 15 Pass 3 in Figure 16, POA emissions were not measured but were estimated from the EF(OA)s of the corresponding fires obtained from other transects, which may contribute to downwind discrepancies between modeled and observed $\Delta\text{OA}/\Delta\text{CO}$. Second, the short aging time and the limited number of downwind samples also make it less meaningful for a detailed parameter optimization. In our simulation, the EF of 0.013 g of the lumped SOA precursor per g of CO worked well for the agricultural fires, although a lower EF could have also worked due to the insignificant SOA formation observed. Since the ratio of the average EF for the VOCs listed in Table 4 to that of CO is already as high as 0.16 g g^{-1} , this implies a net SOA yield of the order of 10%.

The evolution of the O/C ratio due to oxidation was also empirically estimated using Equation (7). Note that since POA accounted for the majority of the mass of OA in

the plumes, Equation (7) can be regarded as a parameterization for the O/C increase in the bulk OA, which was composed of POA and some SOA. In Figure 16, the red lines are the O/C increases due to the mixing effect only and the blue lines represent the sum of mixing and chemical processing effects, both assuming a POA O/C ratio of 0.4 based on observations. In Fire 3 Pass 2, consistent with the low simulated OH, the slow increase of O/C was almost solely due to mixing with background air rather than chemical oxidation. In other cases with sufficient oxidation, our parameterization generally agreed with the observed O/C increases. Although highly uncertain, the photochemical aging time scale of 0.05 days used here (equivalent to OH exposure of 0.6×10^{10} molecules cm^{-3} s) is much smaller than that of 1.5 days (equivalent to OH exposure of 1.94×10^{11} molecules cm^{-3} s) for SOA in Mexico City [Hodzic and Jimenez, 2011] and Los Angeles [Hayes *et al.*, 2015] conditions. In other BB plumes, O/C aging time scales longer than 0.05 days were observed. For example, ~0.1-0.4 days were observed for forest fire plumes in field studies [Cubison *et al.*, 2011; Forrister *et al.*, 2015] and ~1.2 days when exposing smoke emitted from burning different types of biomass to OH and O₃ in a flow reactor [Ortega *et al.*, 2013]. By comparison, the rate of oxidation of OA in the agricultural fire plumes reported here is substantially faster than those in urban plumes, forest fire plumes, and smoke exposed in a flow reactor.

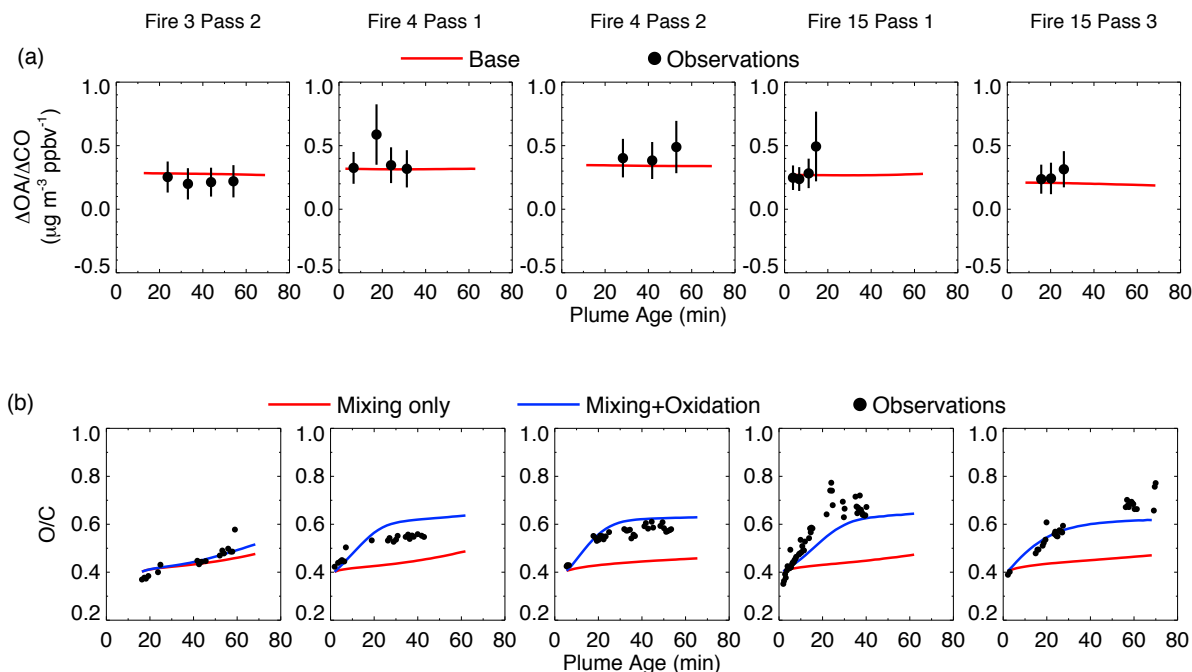


Figure 16 – (a) Enhancement ratios of ΔOA to ΔCO vs. smoke age for the 5 selected cases. Circles are the measured enhancement ratios, with the vertical error bars showing the uncertainty in the measurement. The uncertainty in the estimated age is not shown but is same as in Figure 12. The red lines are parameterization results for the best-fit dilution rates assuming OA is non-volatile. (b) Elemental O/C ratios vs. smoke age for the 5 selected cases. Dots are the measured O/C ratios. The red and blue lines are model results of mixing effects only and of both mixing and oxidation effects, respectively.

4.4 Conclusions

7 out of the 15 fire plumes allowed for a detailed investigation into the chemical evolution of the primary emissions during the first 1.2 h of aging. Rapid enhancement of O_3 was observed with $\Delta O_3 / \Delta CO$ reaching ~ 0.10 . Meanwhile, rapid conversion of NO_x to PAN and nitrate was also observed with the ratios of $\Delta PAN / \Delta NO_y$ and $\Delta nitrate / \Delta NO_y$

being generally similar and each reaching up to ~ 0.4 in about 1 hr. Although no significant evolution of OA mass and BrC absorption was seen on average, a consistent increase in O/C elemental ratios associated with aerosol aging indicated that chemical processing was ongoing and that SOA formation consistently occurred but was likely offset by the evaporation of OA. We used the LPCS-REAM model to simulate the chemistry within these young fire plumes. We found that the model reasonably simulated O_3 formation. The formation of PAN was generally underestimated by the model, which implied missing radical sources likely due to unidentified oxygenated compounds or underestimated initial VOC concentrations. Specifically, diacetyl, which is rarely measured in BB, could be a significant contributor to PAN formation. In the case of HNO_3 and nitrate, the model could not fully reproduce their branching. On the other hand, the modeled sums of HNO_3 +nitrate agreed with observations in three cases but were biased low in the other two cases. We speculated that the assumed HNO_3 uptake coefficient or the modeled photochemistry (e.g., no initial HONO) might be responsible for these discrepancies. As PAN and nitrate accounted for almost all observed NO_x loss, organic nitrates in the gas phase or the particulate phase were not formed efficiently in the agricultural fire plumes. The model also estimated radical concentrations within the fire plumes during the 1 h simulation, with high OH levels that sometimes reached over 1×10^7 molecules cm^{-3} . By implementing the simple empirical parameterization proposed by *Hodzic and Jimenez* [2011] with the parameters of *Cubison et al.* [2011], we modeled the evolution of OA mass. The OA parameterization was generally consistent with the measured OA, although the number of OA samples limited a thorough parameter optimization. After modifying the parameters used in *Hodzic and Jimenez* [2011] to adapt

to this study, our O/C parameterization indicated that the aerosol oxidation process within the agricultural fire plumes appeared to be much faster than that in urban atmospheres and forest fire plumes.

CHAPTER 5. WESTERN U.S. WILDFIRES: EMISSIONS AND AIR QUALITY TRADEOFFS WITH PRESCRIBED BURNING

This chapter presents an extensive set of EFs for over 80 gases and 5 components of PM₁ from three wildfires in the western U.S. These include some rarely, or never before, measured oxygenated volatile organic compounds and multifunctional organic nitrates. The EFs were used to estimate the annual wildfire emissions of CO, NO_x, total NMOC, and PM₁ from 11 western U.S. states.

5.1 Introduction

In the U.S., wildfires are the largest contributor to the annual total area burned and occur largely in the western continental states and Alaska (National Interagency Coordination Center, https://www.nifc.gov/fireInfo/fireInfo_statistics.html). While wildfires perform many beneficial ecosystem functions [Kilgore, 1981], they also degrade U.S. air quality [Park *et al.*, 2007; Jaffe *et al.*, 2008; Singh *et al.*, 2012; Brey and Fischer, 2016]. For example, summer wildfires produce a substantial fraction of the fine aerosol mass in the contiguous U.S. and their inter-annual variability dominates the fluctuations of carbonaceous aerosol concentrations [Park *et al.*, 2007]. In the 2011 National Emissions Inventory (NEI), open fires accounted for 37% of fine particulate matter (PM_{2.5}) emitted in the U.S., with wildfires contributing more than half of that amount. In addition, wildfires release substantial levels of gaseous pollutants including O₃ precursors [Andreae and Merlet, 2001; Akagi *et al.*, 2011]. O₃ production is common from wildfires in tropical and temperate regions, while both O₃ production and

destruction have been observed in boreal wildfire plumes [Goode *et al.*, 2000; Hobbs *et al.*, 2003; Alvarado *et al.*, 2010; Singh *et al.*, 2010; Jaffe and Wigder, 2012]. PM, O₃, and many other primary emissions and secondary products have negative health effects, which can be exacerbated when the smoke impacts populated areas [Künzli *et al.*, 2006; Naeher *et al.*, 2007; Delfino *et al.*, 2009]. A possible mechanism for PM's adverse health effect is a particle's ability to generate reactive oxygen species, referred to as oxidative potential [Donaldson *et al.*, 2005]. Recent studies based on dithiothreitol assay measurements find that BB plays a large role in PM_{2.5} oxidative potential, which is strongly associated with respiratory and cardiovascular diseases in epidemiological studies [Verma *et al.*, 2014; Fang *et al.*, 2016; Yang *et al.*, 2016]. This further points to the potential of BB PM_{2.5} for adverse health outcomes.

Prescribed burning is a commonly used land management practice implemented under specified fuel, meteorological, and dispersion conditions. It maintains the beneficial role of fire while minimizes smoke impacts, consumes accumulated fuels that could otherwise be conducive to wildfires, and thus reduces wildfire hazards [Biswell, 1999; Hardy *et al.*, 2001]. Currently, the understanding of the tradeoffs between the use of prescribed fires versus wildfires is limited, as it requires an integrated knowledge about fires and their emissions, climate change, and human activity [Marlon *et al.*, 2012]. Climate change has contributed to increases in wildfire size and frequency and to the length of the fire season in the western U.S. [Westerling *et al.*, 2006]. Other human activities, including land use change and wildfire management strategies, such as suppression, prevention, and fuel treatments, impact wildfire frequency and intensity as well [Savage and Swetnam, 1990; Belsky and Blumenthal, 1997; Stevens *et al.*, 2014]. In

addition, a detailed knowledge of the emissions and smoke chemistry of wildfires and prescribed burning is crucial to understand potential advantages of prescribed burns relative to wildfires. For example, wildfires typically consume more fuel per unit area than prescribed fires [*Campbell et al.*, 2007; *Turetsky et al.*, 2011; *Yokelson et al.*, 2013]. Higher fuel consumption coupled with potentially different EFs [*Urbanski*, 2013] suggests that prescribed fires and wildfires may have different total emissions and regional smoke impacts. Prescribed forest fire emissions were measured extensively between 2009-2011 across the U.S. temperate ecosystems in a series of studies [*Burling et al.*, 2011; *Akagi et al.*, 2013; *Yokelson et al.*, 2013; *May et al.*, 2014; *Müller et al.*, 2016]. However, the information available on wildfire emissions in temperate forests of the contiguous U.S. is limited to a few fires sampled from Oregon and Idaho in the 1980s, Montana in the 1990s, and from the northern Rocky Mountains recently [*Radke et al.*, 1991; *Friedli et al.*, 2001; *Urbanski*, 2013]. The goal of this study is to provide information about primary emissions from western U.S. wildfires to inform future fire management and atmospheric chemistry studies.

In the summer of 2013, two field campaigns sampled multiple wildfires in the western U.S. The Biomass Burning Observation Project (BBOP) deployed the DOE G-1 aircraft to identify the impact of wildfires and agricultural burns and how the impacts evolve with time. The G-1 aircraft was equipped with a suite of instruments for measuring aerosol, trace gases, and atmospheric parameters. Emissions from 17 wildfires in the western continental U.S. and over 24 agricultural burns in the southeastern U.S. were sampled from July to October 2013. Meanwhile, from August to September 2013, the SEAC⁴RS airborne field campaign intercepted plumes from 15 agricultural and over

10 forest fires in the western, central, and southeastern U.S. The heavily instrumented NASA DC-8 research aircraft was deployed during this mission, which enabled measurements of a wide variety of chemical species and physical parameters [Forrister *et al.*, 2015; Liu *et al.*, 2016; Toon *et al.*, 2016]. Here we focus on the initial emissions from the three wildfires where freshly emitted plumes were intercepted by the aircraft: the Colockum Tarps fire sampled during BBOP and the Big Windy Complex and the Rim Fire sampled during SEAC⁴RS. We also compare emissions from the three studied wildfires with those from other temperate and boreal wildfires and some prescribed fires obtained from aircraft. With the calculated EFs, we estimate the annual wildfire emissions of CO, NO_x, NMOCs, and PM₁ in the western U.S.

5.2 Methods

5.2.1 Fire Descriptions

Table 8 summarizes the locations, sizes, fuels, and local time of fresh plume intercepts of the three wildfires. Figure 17 shows the flight tracks near the fires, color-coded by measured CO concentrations. The Colockum Tarps fire started in the vicinity of Malaga, WA on 27 July 2013 and grew from 14,000 ha to 24,000 ha three days later on the day when its smoke was sampled. Fuels burned were mainly timber, grass, and brush. The G-1 aircraft sampled fresh and downwind plumes in both the morning and afternoon on 30 July 2013 southeast of Wenatchee, WA. The four fresh plumes used for this analysis, less than ~20 min old, were obtained near the source at 1.2 to 1.3 km above the ground. The Big Windy Complex started on 26 July 2013 and consisted of three large fires, which burned approximately 40 km northwest of Grants Pass, OR. On the day of

sampling (6 August 2013), the Big Windy Complex grew from 668 ha to 4,389 ha, burning timber and brush. Fresh plumes were intercepted by the NASA DC-8 aircraft at altitudes ranging from 1.5 to 2.3 km above the ground. The Rim Fire started on 17 August 2013 in the Stanislaus National Forest, about 3 km northeast of Buck Meadows, CA. On the day of sampling (26 August 2013), the fire was in its intense, primary burning period and burned more than 8,000 ha in one day [*Peterson et al.*, 2014; *Yates et al.*, 2016]. The Rim Fire fuel types included timber, brush, and chaparral. Fresh samples were obtained at ~2.6 km above the ground. For the two SEAC⁴RS fires, the DC-8 sampled smoke that extended tens of km during up to 6 min of duration (Table 8). The Big Windy Complex plumes used for analysis were estimated to be ~1 h after emission according to wind speeds measured aboard aircraft and the locations of burning spots detected from Moderate Resolution Imaging Spectroradiometer (MODIS). The Rim fires included near-source plume penetrations. The age of the relatively fresh Rim Fire smoke ranged from ~20 min to ~2 h as distance from source increased. Figure 18 shows examples of time series obtained from the three fires.

Table 8 – Details of the wildfires sampled in the western U.S.

Date	Fire Name	Latitude	Longitude	Final Area Burned (ha)	Location	Fuel Description	Fresh Plume Local Time
30 Jul 2013	Colockum Tarps	47.30	-120.11	32463	Malaga, WA	Timber (mixed conifer), grass, and brush	09:31-09:32, 10:33-10:35, 13:17-13:19, and 14:08-14:09
6 Aug 2013	Big Windy Complex	42.63	-123.86	10435	Grants Pass, OR	Timber (mixed conifer and oak) and brush	15:53-15:55, 16:17-16:20, 16:21-16:24, and 16:32-16:38
26 Aug 2013	Rim Fire	37.86	-120.09	104176	Buck Meadows, CA	Timber (mixed conifer and oak), brush, and chaparral	15:59-16:01, 16:03-16:07, and 16:13-16:19

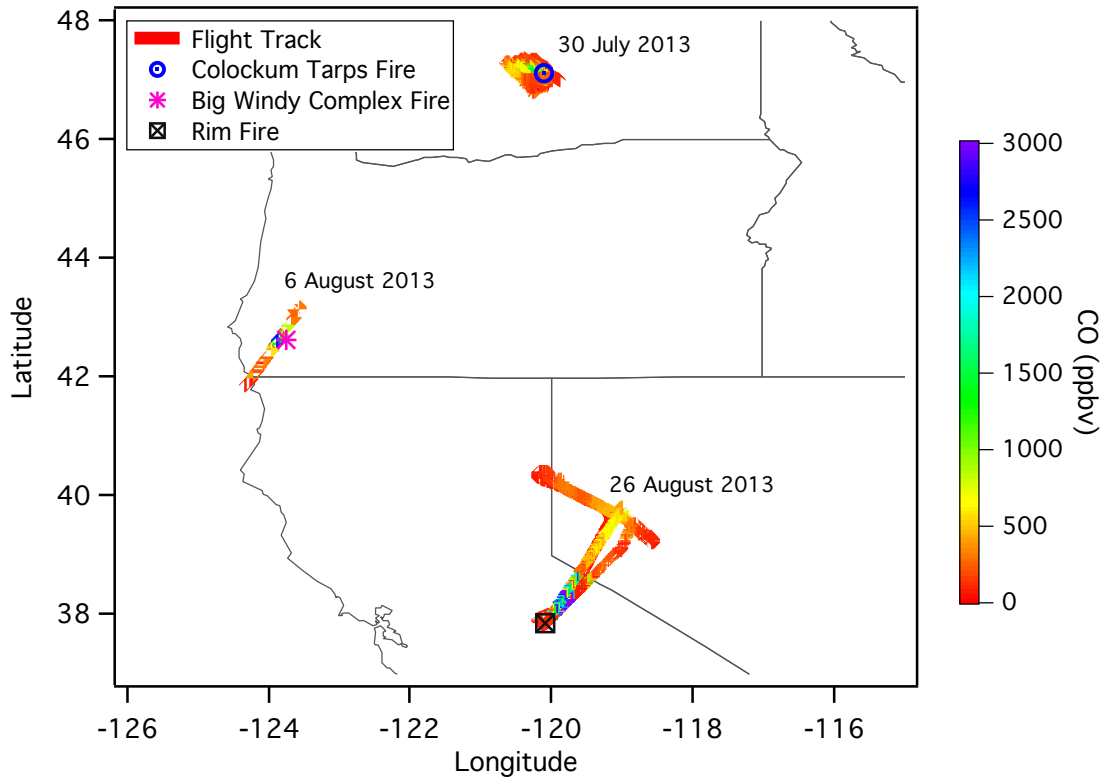


Figure 17 – Map of the three wildfires and flight tracks near the fire sources during BBOP and SEAC⁴RS. Flight tracks are colored by measured CO concentrations. The dates indicate the day each fire was sampled.

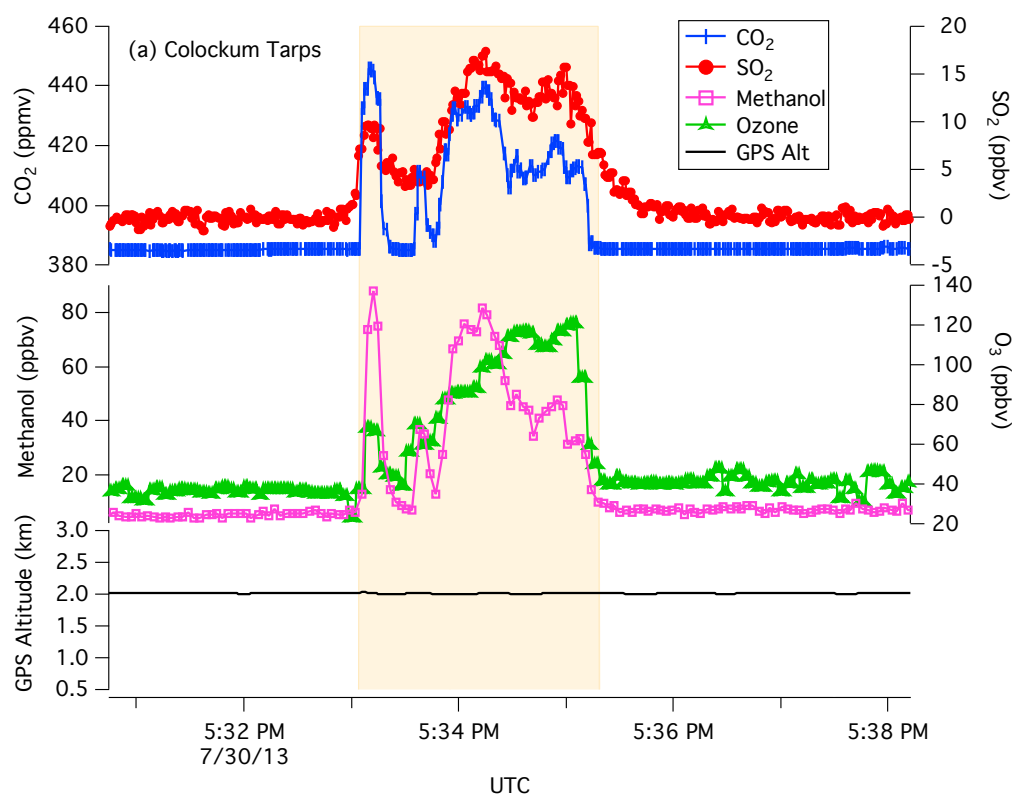


Figure 18 – Examples of time series of CO₂, SO₂, methanol, O₃, and GPS altitude for: (a) Colockum Tarps; (b) Big Windy Complex; and (c) Rim Fire. Shaded area shows the duration of fresh plume used for analysis.

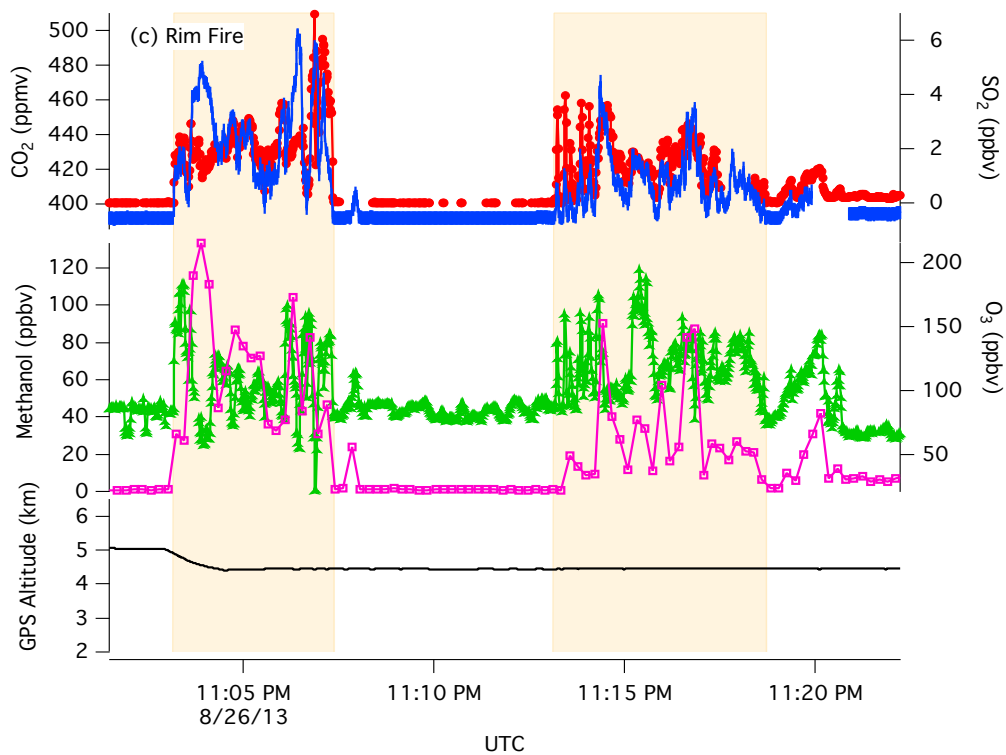
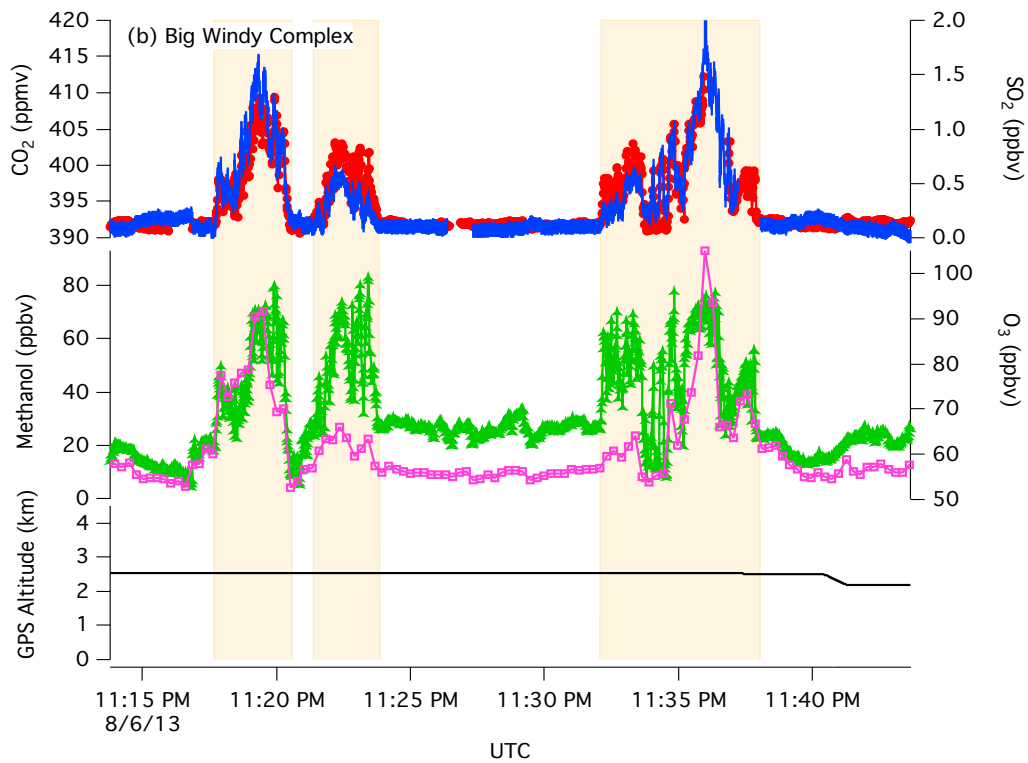


Figure 18 continued.

5.2.2 Calculation of ERs, EFs, and MCE

This study considers only fresh smoke samples as described above. For each fresh plume intercept, the average excess mixing ratio of a species X (ΔX) was calculated by subtracting the average mixing ratio of X in the background air from that in the fire plume. The background samples were taken just outside the plume at a similar location and altitude. We computed molar emission ratios (ERs) for gaseous species and mass ERs for particulate species for each fire as follows. During the two BBOP flights on 30 July 2013, four fresh, thick plumes from the Colockum Tarps fire with similar enhancement magnitudes were intercepted. To allow comparison between measurements with different time resolution and response times, we calculated plume-averaged ERs by dividing the integral of ΔX by the integral of simultaneously measured ΔCO_2 . The four plume-averaged ERs were subsequently used to calculate four plume-averaged EFs. The fire-average was calculated from the four plume samples. The fresh plume samples obtained for the Big Windy Complex and the Rim Fire during SEAC⁴RS consisted of both thick and thin plumes. To better weight larger excess mixing ratios that have higher signal-to-noise ratios, fire-averaged ERs for SEAC⁴RS were determined from the slope of the linear least-squares line of a plot of the integral of ΔX versus that of ΔCO_2 (or ΔCO) for each fire with the intercept forced to zero [Yokelson *et al.*, 2009]. This method works well for relatively fast measurements with time resolution ≤ 3 s, since the plume edges can be well defined. However, species measured by the WAS system were treated differently, since they were collected over a 0.5-1 min period every 1-2 min during plume encounters. A total of 8 and 11 WAS samples were collected for the Big Windy Complex and the Rim Fire, respectively. The fire-averaged ERs of WAS species were determined

as the slope (with the intercept forced to zero) of a plot of available discrete WAS ΔX versus WAS ΔCO . The fire-averaged ERs of the Big Windy Complex and the Rim Fire were then used for fire-averaged EF calculations. If we use the slope-based method to derive fire-averaged EFs for the Colockum Tarps fire, the difference is less than 10% compared to the plume-average method. The small difference was expected since the plumes of the Colockum Tarps fire were of similar sizes so the slope-based method weighted each plume similarly.

A set of ERs can be used to calculate a set of EFs, in units of grams of compound X emitted per kilogram of dry biomass burned. For the Colockum Tarps fire, we used its plume-averaged ERs to calculate a set of plume-averaged EFs and then derive the fire-averaged EFs by averaging the plume-averaged EFs. The fire-averaged EFs for the other two fires were derived using the single fire-averaged ERs. All EF calculations were based on the carbon mass balance method assuming that all of the volatilized carbon is detected [Yokelson *et al.*, 1999; Liu *et al.*, 2016]. The carbon mass fraction of consumed fuel was set as 45.7% [Santín *et al.*, 2015]. In a departure from previous studies that generally assume a fraction of 50% based on fuel elemental analysis [Susott *et al.*, 1996; Burling *et al.*, 2010], Santín *et al.* [2015] directly quantified C emitted to the atmosphere by a boreal forest fire. Since charcoal production may be significant for wildfires, using the percentage of carbon in the volatilized fuel is a preferred implementation of the carbon mass balance calculation when charcoal production is significant as discussed elsewhere [Bertschi *et al.*, 2003b]. Note that EFs scale linearly with the assumed carbon mass fraction. The sum of the emitted carbon was determined from the sum of measured gaseous and particulate carbon-containing compounds. This sum could underestimate the

total carbon by 1-2% due to unmeasured carbon, which would lead to an overestimation of EFs by 1-2% [Akagi *et al.*, 2011], which is small compared to the variability and uncertainty of these EFs. For the two SEAC⁴RS fires, we report the errors of individual EFs as combined uncertainties that vary by species and by fire and that could be quantified here, including: (1) the uncertainties in the integrated ΔX are assumed to be instrumental uncertainties given the significant enhancements in fresh plumes; and (2) the uncertainties in the slopes of ΔX versus ΔCO_2 (or ΔCO), which are usually $< 10\%$. For the Colockum Tarps fire, we used the standard deviations of the four plume-averaged EFs to represent EF errors, which are generally larger than the combined instrumental and slope uncertainties.

BB emissions also vary with flaming and smoldering combustion processes. MCE was calculated to describe the relative amount of flaming or smoldering.

5.3 Results

We use the airborne measurements to determine the composition of the emissions generated during major fire events, which could then lead to widespread air quality impacts via long-range transport. However, these airborne measurements did not capture smoke that was produced by residual smoldering combustion (RSC), during which smoke was not lofted by flame-induced convection [Bertschi *et al.*, 2003a]. The RSC emissions often contribute more to local (near-fire) impacts, but they also impact the total emissions over the lifetime of the fire. In general RSC would most often increase the whole fire EF for smoldering-dominated species. Thus, the EFs for smoldering-dominated species measured in this work may underestimate the total emissions from these fires. Another

factor that potentially influenced the EFs of some very reactive species (such as monoterpenes and NO_x) reported in this work is photochemical processing. Although only fresh samples were used, elevated O_3 (maximum ΔO_3 of 100 ppbv in the Rim Fire plumes) was observed for all three fires and elevated PAN up to ~ 9.4 ppbv for the two SEAC⁴RS fires where PAN measurements were available. Both O_3 and PAN formation indicated rapid photochemical processing. The observed $\Delta\text{O}_3/\Delta\text{CO}$ ratios in these plumes was approximately 0.01. Similar ERs of $\Delta\text{O}_3/\Delta\text{CO}$ have also been observed in prescribed forest and agricultural fire plumes less than ~ 20 min old [Akagi *et al.*, 2013; Liu *et al.*, 2016].

Table 9 shows the average EFs and MCEs for the three wildfires along with the study-averaged EFs and MCE. Among the chemical species that were quantified from the NASA DC-8 platform, we identified over 80 trace gases and 5 fine particle components that were significantly elevated within the wildfire plumes when compared with their background levels. Meanwhile, emissions of 14 gases and 5 fine particle components were acquired from the G-1 aircraft. This represents the most comprehensive suite of species measured in the field for U.S. wildfires to date. The fire-integrated MCEs derived in this work range from 0.877 to 0.935, corresponding to $\sim 41\%$ - 71% nominal flaming fractions.

Table 9 – Measured MCEs and emission factors (g kg^{-1}) for the three wildfires in the western U.S. and comparison with aircraft-measured EFs from previous forest fire studies. Values in parenthesis are errors for single fire and standard deviations for all available EFs for study averages.

Fire	Colockum Tarps	Big Windy Complex	Rim Fire	Study average	Temperate forests	Prescribed fires in South Carolina	Boreal forests
Reference	This work	This work	This work	This work	Akagi <i>et al.</i> [2011]	Akagi <i>et al.</i> [2013]	Simpson <i>et al.</i> [2011]
MCE	0.935	0.877	0.923	0.912	-	0.931	0.89
Compound	Formula						
Carbon dioxide	CO_2	1517 (20)	1367 (47)	1478 (11)	1454 (78)	1637 (71)	1675 (42)
Carbon monoxide	CO	67.6 (12.7)	122 (8)	78.7 (4.0)	89.3 (28.5)	89 (32)	79 (19)
Methane	CH_4	3.70 (0.31)	6.59 (0.35)	4.43 (0.25)	4.90 (1.50)	3.92 (2.39)	2.66 (1.77)
Hydrogen peroxide	H_2O_2	-	1.02 (0.35)	0.18 (0.06)	0.60 (0.60)	-	-
Sulfur dioxide	SO_2	0.75 (0.06)	0.11 (0.02)	0.11 (0.02)	0.32 (0.37)	2.03 (1.79)	-
Carbonyl sulfide	OCS	-	-	$5.9 (0.9) \times 10^{-3}$	$5.9 (0.9) \times 10^{-3}$	0.01 (0.003)	0.029 (0.007)
Dimethyl sulfide	$\text{C}_2\text{H}_6\text{S}$	-	$5.7 (1.2) \times 10^{-3}$	$5.6 (1.2) \times 10^{-4}$	$3.1 (3.6) \times 10^{-3}$	-	$2.3 (1.2) \times 10^{-3}$
Hydrochloric acid	HCl	-	$3.2 (1.1) \times 10^{-3}$	$4.6 (1.2) \times 10^{-3}$	$3.9 (1.0) \times 10^{-3}$	-	-
Methyl chloride	CH_3Cl	-	0.038 (0.005)	0.017 (0.002)	0.027 (0.015)	-	0.029 (0.007)
Dichloromethane	CH_2Cl_2	-	$1.9 (0.3) \times 10^{-3}$	$6.5 (1.8) \times 10^{-4}$	$1.3 (0.9) \times 10^{-3}$	-	-
1,2-dichloroethane	$\text{C}_2\text{H}_4\text{Cl}_2$	-	$1.1 (0.2) \times 10^{-3}$	$5.1 (1.3) \times 10^{-4}$	$8.2 (4.4) \times 10^{-4}$	-	$6.4 (5.1) \times 10^{-4}$
Methyl iodide	CH_3I	-	$5.5 (1.2) \times 10^{-4}$	$1.9 (0.4) \times 10^{-4}$	$3.7 (2.6) \times 10^{-4}$	-	$3.9 (0.9) \times 10^{-4}$
Methyl bromide	CH_3Br	-	$1.3 (0.2) \times 10^{-3}$	$2.9 (0.4) \times 10^{-4}$	$8.1 (7.3) \times 10^{-4}$	-	$1.8 (0.5) \times 10^{-3}$
Dibromomethane	CH_2Br_2	-	$2.0 (0.5) \times 10^{-4}$	$1.6 (0.3) \times 10^{-4}$	$1.8 (0.3) \times 10^{-4}$	-	$4.1 (8.0) \times 10^{-5}$
HCFC-141b ^a	$\text{C}_2\text{H}_3\text{Cl}_2\text{F}$	-	$1.4 (0.2) \times 10^{-3}$	$5.1 (1.1) \times 10^{-4}$	$9.7 (6.5) \times 10^{-4}$	-	-

Table 9 (continued).

Fire		Colockum Tarps	Big Windy Complex	Rim Fire	Study average	Temperate forests	Prescribed fires in South Carolina	Boreal forests
Reference		This work	This work	This work	This work	Akagi et al. [2011]	Akagi et al. [2013]	Simpson et al. [2011]
MCE		0.935	0.877	0.923	0.912	-	0.931	0.89
HCFC-142b ^a	C ₂ H ₂ ClF ₂	-	3.9 (1.2)×10 ⁻⁴	1.3 (0.3)×10 ⁻⁴	2.6 (1.8)×10 ⁻⁴	-	-	-
HFC-152a ^a	C ₂ H ₄ F ₂	-	1.1 (0.2)×10 ⁻³	2.4 (1.1)×10 ⁻⁴	6.8 (6.2)×10 ⁻⁴	-	-	-
Nitrogen monoxide	NO	0.23 (0.04)	8.0 (1.4)×10 ⁻³	0.094 (0.018)	0.11 (0.11)	-	0.32 (0.07)	-
Nitrogen dioxide	NO ₂	1.1 (0.4)	0.091 (0.011)	0.56 (0.09)	0.58 (0.50)	-	1.72 (0.32)	-
NO _x as NO	NO _x	0.94 (0.29)	0.067 (0.008)	0.46 (0.08)	0.49 (0.44)	2.51 (1.02)	1.31 (0.23)	-
Hydrogen cyanide	HCN	-	0.43 (0.22)	0.25 (0.13)	0.34 (0.12)	0.73 (0.19)	0.66 (0.27)	0.89 (0.29)
Acetonitrile	CH ₃ CN	0.39 (0.14)	0.23 (0.05)	0.13 (0.02)	0.25 (0.13)	-	-	0.3 (0.06)
Ethanal nitrate	C ₂ O ₄ H ₃ N	-	2.6 (1.3)×10 ⁻³	2.9 (1.5)×10 ⁻³	2.7 (0.3)×10 ⁻³	-	-	-
Ethene hydroxynitrate	C ₂ O ₄ H ₅ N	-	0.018 (0.010)	8.5 (4.3)×10 ⁻³	0.013 (0.007)	-	-	-
Propanone nitrate	C ₃ O ₃ H ₅ N	-	4.5 (2.5)×10 ⁻³	3.5 (1.8)×10 ⁻³	4.0 (0.7)×10 ⁻³	-	-	-
Propene hydroxynitrates	C ₃ O ₄ H ₇ N	-	0.027 (0.008)	0.015 (0.005)	0.021 (0.008)	-	-	-
Butadiene hydroxynitrates	C ₄ O ₄ H ₇ N	-	0.017 (0.008)	0.012 (0.006)	0.014 (0.003)	-	-	-
Butene hydroxynitrates	C ₄ O ₄ H ₆ N	-	0.034 (0.017)	0.024 (0.012)	0.029 (0.007)	-	-	-
Methyl vinyl ketone/mathacrolein hydroxynitrates	C ₄ O ₃ H ₇ N	-	0.024 (0.008)	0.017 (0.005)	0.021 (0.005)	-	-	-

Table 9 (continued).

Fire	Colockum Tarps	Big Windy Complex	Rim Fire	Study average	Temperate forests	Prescribed fires in South Carolina	Boreal forests
Reference	This work	This work	This work	This work	<i>Akagi et al.</i> [2011]	<i>Akagi et al.</i> [2013]	<i>Simpson et al.</i> [2011]
MCE	0.935	0.877	0.923	0.912	-	0.931	0.89
Nitroxyhydroperoxide/nitroxyhydroxypoxide	-	0.017 (0.009)	0.020 (0.010)	0.019 (0.002)	-	-	-
Isoprene hydroxynitrates	-	0.021 (0.007)	0.013 (0.004)	0.017 (0.006)	-	-	-
Methyl nitrate	-	1.7 (0.2) $\times 10^{-3}$	1.3 (0.2) $\times 10^{-3}$	1.5 (0.4) $\times 10^{-3}$	-	-	1.4 (0.9) $\times 10^{-3}$
Ethyl nitrate	-	1.3 (0.2) $\times 10^{-3}$	3.5 (0.5) $\times 10^{-4}$	8.4 (6.9) $\times 10^{-4}$	-	-	8.8 (4.5) $\times 10^{-4}$
<i>i</i> -Propyl nitrate	-	3.3 (0.5) $\times 10^{-3}$	5.8 (0.8) $\times 10^{-4}$	2.0 (2.0) $\times 10^{-3}$	-	-	1.6 (1.0) $\times 10^{-3}$
<i>n</i> -Propyl nitrate	-	7.3 (1.1) $\times 10^{-4}$	1.6 (0.2) $\times 10^{-4}$	4.4 (4.0) $\times 10^{-4}$	-	-	1.6 (1.2) $\times 10^{-4}$
2-Butyl nitrate	-	1.9 (0.3) $\times 10^{-3}$	2.6 (0.4) $\times 10^{-4}$	1.1 (1.1) $\times 10^{-3}$	-	-	1.9 (1.2) $\times 10^{-3}$
3-Methyl-2-butyl nitrate	-	6.7 (1.2) $\times 10^{-4}$	1.1 (0.1) $\times 10^{-4}$	3.9 (4.0) $\times 10^{-4}$	-	-	5.7 (4.6) $\times 10^{-4}$
3-Pentyl nitrate	-	4.4 (0.7) $\times 10^{-4}$	4.4 (1.0) $\times 10^{-5}$	2.4 (2.8) $\times 10^{-4}$	-	-	2.6 (1.7) $\times 10^{-4}$
2-Pentyl nitrate	-	5.2 (0.9) $\times 10^{-4}$	5.1 (0.8) $\times 10^{-5}$	2.8 (3.3) $\times 10^{-4}$	-	-	4.8 (3.1) $\times 10^{-4}$
Methanol	1.81 (0.44)	4.09 (0.93)	1.44 (0.22)	2.45 (1.43)	1.93 (1.38)	1.20 (0.49)	1.2 (0.3)
Formaldehyde	-	2.49 (0.26)	2.10 (0.21)	2.29 (0.27)	2.27 (1.13)	1.87 (0.27)	-
Acetaldehyde	1.64 (0.27)	2.16 (0.37)	1.12 (0.17)	1.64 (0.52)	-	-	-
Acetone/propanal	0.69 (0.13)	2.068 (0.359)	0.62 (0.03)	1.13 (0.82)	-	-	0.37 (0.10)

Table 9 (continued).

Fire	Colockum Tarps	Big Windy Complex	Rim Fire	Study average	Temperate forests	Prescribed fires in South Carolina	Boreal forests
Reference	This work	This work	This work	This work	<i>Akagi et al.</i> [2011]	<i>Akagi et al.</i> [2013]	<i>Simpson et al.</i> [2011]
MCE	0.935	0.877	0.923	0.912	-	0.931	0.89
Hydroxyacetone	C ₃ H ₆ O ₂	1.35 (0.55)	0.90 (0.36)	1.13 (0.31)	-	-	-
Furan	C ₄ H ₄ O	0.55 (0.05) ^b	0.46 (0.05) ^b	0.51 (0.06) ^b	0.20 (0.21)	0.27 (0.19)	0.28 (0.03)
Diacetyl	C ₄ H ₆ O ₂	-	-	2.10 (0.63)	-	-	-
MVK/MACR /crotonaldehyde	C ₄ H ₆ O	0.37 (0.05)	0.29 (0.03)	0.33 (0.06)	-	-	-
Isoprene hydroperoxyaldehy	C ₅ O ₃ H ₈	0.18 (0.09)	0.16 (0.08)	0.17 (0.02)	-	-	-
Hydroxymethylhydr ogenperoxide	CO ₃ H ₄	0.33 (0.17)	0.048 (0.024)	0.19 (0.20)	-	-	-
Peroxyacetic acid/hydroperoxy glycolaldehyde	C ₂ O ₃ H ₄	0.44 (0.24)	0.045 (0.023)	0.24 (0.28)	-	-	-
Hydroperoxy acetone	C ₃ O ₃ H ₆	0.13 (0.07)	0.043 (0.022)	0.086 (0.061)	-	-	-
C ₄ - dihydroxycarbonyls	C ₄ O ₃ H ₈	0.075 (0.039)	0.020 (0.010)	0.047 (0.039)	-	-	-
C ₄ - hydroxydicarbonyls	C ₄ O ₃ H ₆ /C ₅ O ₂ H ₁₀	0.12 (0.06)	0.090 (0.045)	0.11 (0.02)	-	-	-
Isoprene hydroxy hydroperoxides	C ₅ O ₃ H ₁₀	0.11 (0.04)	0.042 (0.013)	0.076 (0.047)	-	-	-
Ethane	C ₂ H ₆	0.89 (0.06)	0.54 (0.04)	0.72 (0.25)	1.12 (0.67)	0.489 (0.359)	0.56 (0.13)

Table 9 (continued).

Fire	Colockum Tarps	Big Windy Complex	Rim Fire	Study average	Temperate forests	Prescribed fires in South Carolina	Boreal forests
Reference	This work	This work	This work	This work	Akagi <i>et al.</i> [2011]	Akagi <i>et al.</i> [2013]	Simpson <i>et al.</i> [2011]
MCE	0.935	0.877	0.923	0.912	-	0.931	0.89
Ethene	-	1.03 (0.08)	0.79 (0.06)	0.91 (0.17)	1.12 (0.35)	-	0.82 (0.09)
Ethyne	-	0.26 (0.02)	0.21 (0.02)	0.24 (0.04)	0.29 (0.10)	-	0.22 (0.09)
Propane	-	0.32 (0.02)	0.17 (0.01)	0.24 (0.11)	0.26 (0.11)	0.153 (0.099)	0.23 (0.05)
Propene	-	0.36 (0.03)	0.35 (0.03)	0.35 (0.01)	0.95 (0.54)	-	0.38 (0.04)
<i>i</i> -Butane	-	0.023 (0.002)	0.010 (0.001)	0.016 (0.009)	-	0.010 (0.005)	0.021 (0.004)
<i>n</i> -Butane	-	0.084 (0.006)	0.038 (0.003)	0.061 (0.033)	0.083 (0.10)	0.036 (0.016)	0.076 (0.015)
1,2-Propadiene	-	0.011 (0.002)	0.011 (0.002)	0.011 (0.000)	-	0.015 (0.002)	-
<i>trans</i> -2-Butene	-	2.2 (0.2)×10 ⁻³	0.011 (0.002)	6.8 (6.5)×10 ⁻³	-	0.035 (0.018)	0.020 (0.003)
<i>cis</i> -2-Butene	-	2.0 (0.3)×10 ⁻³	0.011 (0.002)	6.7 (6.7)×10 ⁻³	-	0.028 (0.016)	0.015 (0.002)
1-Butene	-	0.079 (0.007)	0.080 (0.006)	0.080 (0.001)	-	0.131 (0.034)	0.077 (0.009)
<i>i</i> -Butene	-	0.043 (0.004)	0.043 (0.004)	0.043 (0.000)	-	0.088 (0.017)	0.056 (0.007)
1,3-Butadiene	-	0.043 (0.005)	0.067 (0.006)	0.055 (0.017)	-	-	0.070 (0.008)
<i>i</i> -Pentane	-	0.016 (0.002)	5.0 (0.5)×10 ⁻³	0.010 (0.008)	-	0.007 (0.002)	0.019 (0.005)
<i>n</i> -Pentane	-	0.043 (0.003)	0.017 (0.002)	0.030 (0.019)	-	0.019 (0.003)	0.042 (0.008)

Table 9 (continued).

Fire	Colockum Tarps	Big Windy Complex	Rim Fire	Study average	Temperate forests	Prescribed fires in South Carolina	Boreal forests
Reference	This work	This work	This work	This work	<i>Akagi et al.</i> [2011]	<i>Akagi et al.</i> [2013]	<i>Simpson et al.</i> [2011]
MCE	0.935	0.877	0.923	0.912	-	0.931	0.89
1-Pentene	C ₅ H ₁₀	-	0.029 (0.002)	0.022 (0.002)	0.026 (0.005)	-	0.030 (0.005)
Isoprene	C ₅ H ₈	-	0.043 (0.007)	0.032 (0.003)	0.038 (0.007)	-	0.14 (0.03)
2,3-Dimethylbutane	C ₆ H ₁₄	-	1.4 (0.1)×10 ⁻³	5.0 (0.6)×10 ⁻⁴	9.6 (6.4)×10 ⁻⁴	-	-
2+3-Methylpentane	C ₆ H ₁₄	-	8.2 (0.6)×10 ⁻³	4.0 (0.3)×10 ⁻³	6.1 (4.7)×10 ⁻³	-	0.010 (0.002)
<i>n</i> -Hexane	C ₆ H ₁₄	-	0.030 (0.002)	0.012 (0.001)	0.021 (0.012)	-	0.012 (0.003)
<i>n</i> -Heptane	C ₇ H ₁₆	-	0.014 (0.001)	-	0.014 (0.001)	-	0.008 (0.005)
Benzene	C ₆ H ₆	0.39 (0.11)	0.57 (0.04) ^c	0.34 (0.02) ^c	0.43 (0.12)	-	0.283 (0.043)
Toluene	C ₇ H ₈	0.25 (0.06)	0.29 (0.02) ^c	0.20 (0.02) ^c	0.24 (0.05)	-	0.199 (0.031)
Ethylbenzene	C ₈ H ₁₀	-	0.031 (0.003)	0.021 (0.002)	0.026 (0.007)	-	0.039 (0.016)
<i>m</i> + <i>p</i> -Xylene	C ₈ H ₁₀	-	0.086 (0.009)	0.085 (0.010)	0.086 (0.001)	-	0.080 (0.055)
<i>o</i> -Xylene	C ₈ H ₁₀	-	0.040 (0.004)	0.036 (0.004)	0.038 (0.003)	-	0.025 (0.011)
α -Pinene	C ₁₀ H ₁₆	-	0.017 (0.002)	0.018 (0.002)	0.017 (0.001)	-	0.094 (0.021)
β -Pinene	C ₁₀ H ₁₆	-	0.014 (0.003)	0.006 (0.001)	0.010 (0.006)	-	0.052 (0.013)
Monoterpenes	C ₁₀ H ₁₆	-	0.45 (0.08)	0.37 (0.07)	0.41 (0.06)	-	1.61 (1.00)
							-

Table 9 (continued).

Fire	Colockum Taps	Big Windy Complex	Rim Fire	Study average	Temperate forests	Prescribed fires in South Carolina	Boreal forests
Reference	This work	This work	This work	This work	<i>Akagi et al.</i> [2011]	<i>Akagi et al.</i> [2013]	<i>Simpson et al.</i> [2011]
MCE	0.935	0.877	0.923	0.912	-	0.931	0.89
Ammonium	NH ₄	0.19 (0.12)	0.49 (0.17)	0.34 (0.12)	0.34 (0.15)	-	-
Nitrate	NO ₃	0.73 (0.42)	0.99 (0.34)	0.90 (0.31)	0.87 (0.13)	-	-
Chloride	Chl	0.42 (0.12)	0.064 (0.022)	0.082 (0.029)	0.19 (0.20)	-	-
Sulfate	SO ₄	0.46 (0.10)	0.15 (0.05)	0.29 (0.10)	0.30 (0.16)	-	-
Organic aerosol	OA	23.3 (4.76)	30.9 (11.8)	18.8 (7.3)	24.3 (6.1)	-	-
Submicron aerosol	PM ₁	25.1 (4.8)	32.6 (11.8)	20.4 (7.3)	26.0 (6.2)	12.7 (7.5) ^d	-

^a HFCs and HCFCs are purely anthropogenic compounds that are not expected from BB.

^b EF for furan/pentadienes/cyclopentene, determined as the difference between PTR-MS measured isoprene/furan/pentadienes/cyclopentene and WAS measured isoprene.

^c Reported as PTR-MS and WAS averages.

^d Reported as PM_{2.5}-PM_{3.5}.

5.3.1 Initial Emissions of Trace Gases

For the Big Windy Complex and the Rim Fire, the emitted gases include CO₂, CO, CH₄, hydrogen peroxide (H₂O₂), sulfur species, HCl, six halocarbons, nitrogen-containing compounds, all the measured alkanes, alkenes, alkynes, and aromatics, and a variety of OVOCs. Benzene and toluene were measured by both WAS and PTR-MS. Good agreement was found between WAS and PTR-MS measurements of benzene (EFs within 8%) and toluene (EFs within 24%). We reported EFs of benzene and toluene as the averages of the two techniques. The gases that were measured, but deemed not to be emitted by the fires were primarily halocarbons that were either not enhanced or had weak correlations with CO ($r^2 < 0.6$). A list of these gases can be found in Table 4 of *Simpson et al.* [2011] with a few exceptions discussed in section 5.3.1.2. *Yates et al.* [2016] has also reported some Rim Fire EFs as measured on 26 August 2013 from the DC-8 aircraft, namely CO₂, CO, CH₄, methanol, acetonitrile (CH₃CN), acetone/propanal, benzene, and toluene. Despite potential differences in fresh plume selection and different assumptions made for the carbon mass balance method, our Rim Fire EFs agree with *Yates et al.* [2016] to within the stated uncertainties. For the Colockum Tarps fire, the emissions of 14 gases were measured: CO₂, CO, CH₄, SO₂, NO_x, two aromatics (benzene and toluene), CH₃CN, and five OVOCs.

Study-averaged EFs were calculated from the EFs of all three fires if available, or the two SEAC⁴RS fires if the species was not measured during BBOP. The three exceptions are carbonyl sulfide that was only emitted from the Rim Fire, *n*-heptane only emitted from the Big Windy Complex, and diacetyl only measured from the Colockum Tarps fire during BBOP. The uncertainties reported for the study averages are the

standard deviations of the EFs for single fires and thus represent fire-to-fire variability. Note that for a few species that were measured by CIMS and were associated with measurement uncertainties of 30-50%, such as HCN, the fire-to-fire variability is smaller than the single-fire uncertainty (Table 9).

According to the study-averaged EFs, the major gaseous emissions by mass are (EF > 0.5 g kg⁻¹; Table 9; Figure 19): CO₂ (1454 ± 78), CO (89.3 ± 28.5), CH₄ (4.90 ± 1.50), methanol (2.45 ± 1.43), formaldehyde (2.29 ± 0.27), diacetyl (2.10 ± 0.63), acetaldehyde (1.64 ± 0.52), acetone/propanal (1.13 ± 0.82), hydroxyacetone (1.13 ± 0.31), ethene (0.91 ± 0.17), ethane (0.72 ± 0.25), H₂O₂ (0.60 ± 0.60), NO₂ (0.58 ± 0.50), and furan (0.51 ± 0.06). Also listed in Table 9 are average gaseous EFs from previous airborne studies of forest fires: boreal forest fires over Canada [*Simpson et al.*, 2011], seven prescribed fires burning pine-forest understory in longleaf pine stands in South Carolina [*Akagi et al.*, 2013], and a compilation by *Akagi et al.* [2011] of temperate evergreen forest fires (which included only two confirmed wildfires) in North America. Detailed discussion of the emissions of different compounds and their comparison with these previous airborne measurements is presented below.

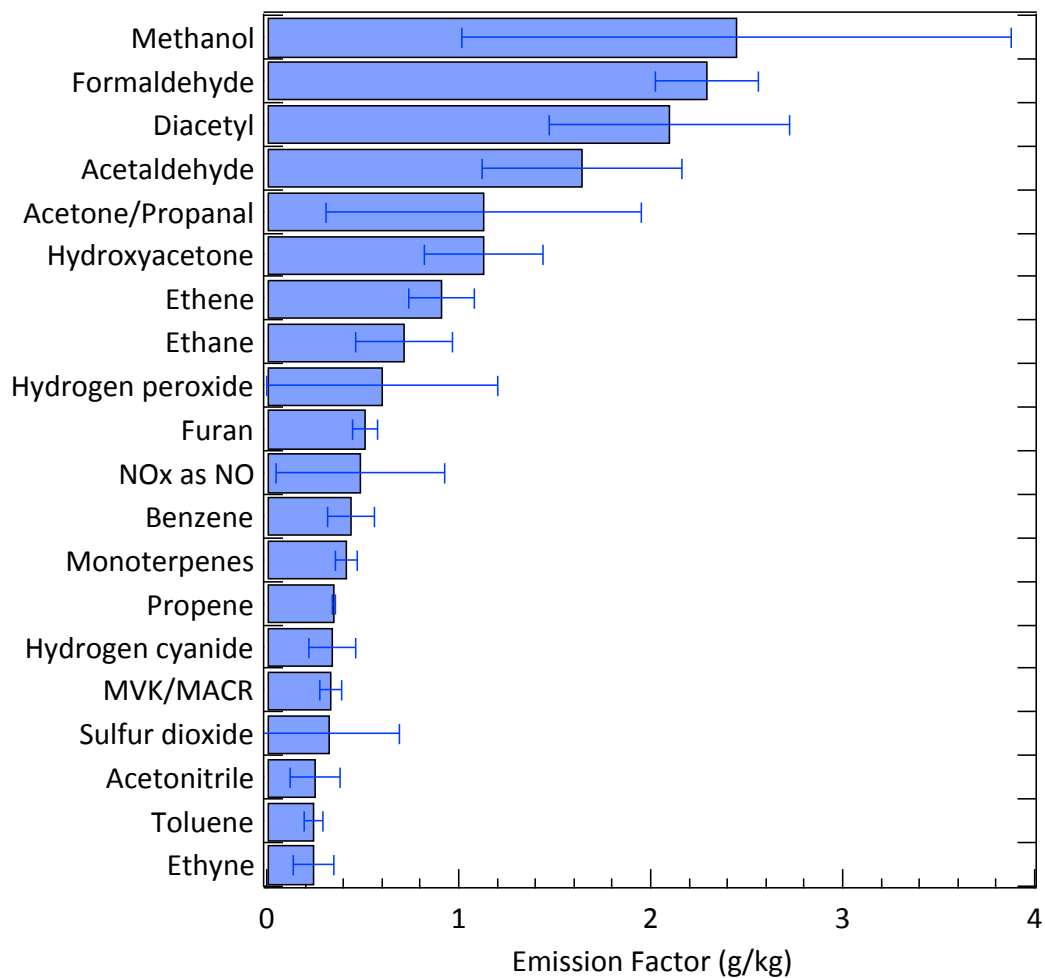


Figure 19 – The average emission factors (boxes) and standard deviations (whiskers) for the 20 most abundant trace gases (excluding CO₂, CO, CH₄) measured from the three wildfires.

5.3.1.1 Sulfur Compounds

SO₂ was the main sulfur-containing gas measured from the three fires, followed by significantly less dimethyl sulfide (DMS) and carbonyl sulfide (OCS). The study average EF(SO₂) (0.32 ± 0.37 g kg⁻¹) is smaller than the average EF(SO₂) (2.03 ± 1.79 g kg⁻¹) for various temperate evergreen fires [Akagi *et al.*, 2011] and (0.795 ± 0.377 g kg⁻¹) for 15 agricultural fires sampled during SEAC⁴RS [Liu *et al.*, 2016], though the differences are not statistically significant. Note that the uncertainty in the SO₂ EF is large because it represents fire-to-fire variability, whereas the uncertainty in the EF for each individual fire is tightly constrained (Table 9). Since SO₂ emissions are found to be highly dependent on fuel sulfur content [Burling *et al.*, 2010; Stockwell *et al.*, 2014], the reason for our low EF(SO₂) relative to other studies is presumably lower sulfur content for the plants burned, especially for those burned in the two SEAC⁴RS fires. Since there could be SO₂ oxidation to particulate sulfate given high levels of H₂O₂ in the SEAC⁴RS plumes, summing up the emitted SO₂ and sulfate may better reflect fuel sulfur content. The resulted average sulfur emissions from the SEAC⁴RS fires (0.21-0.31 g kg⁻¹) were still lower than the cited average SO₂ EFs.

DMS was clearly released from the two SEAC⁴RS fires as it was strongly correlated with CO ($r^2 > 0.97$). OCS was also highly correlated with CO for the Rim Fire ($r^2 = 0.91$). However, OCS from the Big Windy Complex had no measurable elevation and weak correlation with excess CO ($r^2 = 0.14$). Both DMS and OCS have been measured previously from prescribed [Akagi *et al.*, 2013] and boreal forest fire plumes [Yokelson *et al.*, 1997; Simpson *et al.*, 2011] with EFs ranged from 0.0023-0.008 g kg⁻¹ and 0.01-0.029 g kg⁻¹, respectively (Table 9). While the Big Windy Complex EF(DMS)

($0.0057 \pm 0.0012 \text{ g kg}^{-1}$) is within the range observed from the few available studies, the Rim Fire EF(DMS) (0.00056 ± 0.00012) and EF(OCS) (0.0059 ± 0.0009) are both lower than the literature values.

5.3.1.2 Chlorine Compounds and Halocarbons

The chlorine-containing gases emitted from the two SEAC⁴RS fires are HCl and six halocarbons, methyl chloride (CH_3Cl), dichloromethane (CH_2Cl_2), 1,2-dichloroethane, methyl iodide (CH_3I), methyl bromide (CH_3Br), and dibromomethane (CH_2Br_2). In addition, hydrochlorofluorocarbon (HCFC)-142b, HCFC-141b, and hydrofluorocarbon (HFC)-152a were also measurably enhanced in the plumes, as discussed below. The HCl emission was very low, with an average EF of $0.0039 \pm 0.0010 \text{ g kg}^{-1}$. This value is almost the smallest of the existing HCl emissions from various fuel types burned in field or laboratory, which range from 0.008 to 3.61 g kg^{-1} [Akagi *et al.*, 2011; Stockwell *et al.*, 2014]. As also shown in Table 9, particulate chloride EFs from these two fires ($0.064\text{--}0.082 \text{ g kg}^{-1}$) were near the lower end of a range of EFs from prescribed fires of different ecosystems (0.13 to 1.3 g kg^{-1}) [May *et al.*, 2014]. HCl and chloride emissions were found in laboratory studies to have a significant dependence on fuel composition for a variety of biomass fuels [Christian *et al.*, 2003; Hosseini *et al.*, 2013; Stockwell *et al.*, 2014]. For example, oak, one of the fuels burned in the two SEAC⁴RS fires, was found to have low Cl content and low EF(chloride) when compared to some other southwestern U.S. fuels [Hosseini *et al.*, 2013]. Thus, low EFs of HCl and chloride observed in these two fires may imply a low chlorine fraction of the fuels burned.

The nine halocarbons included in Table 9 showed reasonable correlations with CO ($0.61 < r^2 < 0.99$) and measurable enhancements compared to the background air. The emissions of CH₃Cl, CH₃I, CH₃Br, CH₂Br₂, and 1,2-dichloroethane have been previously reported by *Simpson et al.* [2011] from Canadian forest fire plumes. Except for a factor of four higher value of EF(CH₂Br₂) and a factor of two lower value of CH₃Br, the average EFs measured in this work are similar to (within 5-28% of) those reported by *Simpson et al.* [2011]. In addition, CH₂Cl₂ was also emitted with an average ER to CO of $(4.0 \pm 1.8) \times 10^{-6}$ by volume, which is in between the ERs $< (1-6) \times 10^{-7}$ measured in Tasmania [*Simmonds et al.*, 2006] and the ER = $(2.5 \pm 0.6) \times 10^{-5}$ measured in Africa [*Rudolph et al.*, 1995]. Note that the more smoldering Big Windy Complex consistently emitted more of these halocarbons than the Rim Fire. Methyl halides (CH₃Cl, CH₃Br, and CH₃I) are thought to form predominantly from smoldering and also reflect halogen content in fuels burned [*Reinhardt and Ward*, 1995; *Andreae and Merlet*, 2001]. It is also known that in the Pacific Northwest, chlorine and bromine concentrations in vegetation decrease with distance from the coast [*McKenzie et al.*, 1996]. Therefore both the burning condition and the closer proximity to ocean could possibly account for higher halocarbon emissions from the Big Windy Complex.

HFCs, CFCs, and HCFCs are produced exclusively by anthropogenic activities and are not expected from BB. A possible explanation for their enhanced concentrations in the wildfire plumes could be a re-suspension after being deposited previously onto the forests. *Hegg et al.* [1990] also observed variable CFC-12 (CF₂Cl₂) emissions from seven fires in North America, most pronounced in the Los Angeles basin. In contrast, *Simpson et al.* [2011] did not see any elevated HFCs or HCFCs over remote regions of Canada.

Our observations may suggest the deposition of HFCs and HCFCs on vegetation in the regions studied. However, since these compounds are highly volatile, their enhancements in wildfire plumes may result from other unknown mechanisms.

5.3.1.3 Nitrogen Compounds

Freshly emitted gaseous nitrogen-containing compounds measured in the plumes are (in descending order) NO_2 , NO_x , HCN, CH_3CN , NO, multifunctional organic nitrates usually derived from the oxidation of isoprene and other alkenes [Paulot *et al.*, 2009a; Lee *et al.*, 2014b; Teng *et al.*, 2015], and C_1 - C_5 saturated alkyl nitrates. Similar to many other BB studies [Yokelson *et al.*, 2009; Alvarado *et al.*, 2010; Liu *et al.*, 2016], the observed HNO_3 was not significantly elevated within the fresh wildfire plumes.

Since NO and NO_2 are rapidly interconverted, it is also useful to report an EF for NO_x as NO. In Table 9, the derived EFs of NO, NO_2 , and NO_x from the three wildfires are all the smallest among the studies listed. The Big Windy Complex emitted extremely small amounts of NO_x ($0.067 \pm 0.008 \text{ g kg}^{-1}$). One reason could be that the smoldering-dominated burning conditions did not favor NO_x emission [Lobert *et al.*, 1991; Yokelson *et al.*, 1996; Goode *et al.*, 2000]. However, as the samples of the Big Windy Complex and the Rim Fire included smoke up to ~1-2 h old, the freshly emitted NO_x might have partially transformed to other reactive nitrogen species such as PAN and particulate nitrate. In support of this, elevated PAN was observed for both fires while a decrease in $\Delta\text{NO}_x/\Delta\text{CO}$ was seen in the Rim Fire plumes as the distance from fire sources increased. So the NO_x EFs for the two fires are likely lower limits.

HCN and CH₃CN are commonly recognized as BB tracers and their ER, $\Delta\text{CH}_3\text{CN}/\Delta\text{HCN}$, ranges between 0.30-0.56 for a wide range of fuels burned in the laboratory and field [Li *et al.*, 2000; Christian *et al.*, 2003; de Gouw *et al.*, 2003; Yokelson *et al.*, 2008; Crounse *et al.*, 2009; Yokelson *et al.*, 2009; Simpson *et al.*, 2011]. The average EF(HCN), $0.34 \pm 0.12 \text{ g kg}^{-1}$, from the two SEAC⁴RS fires is low compared to the other forest fires listed in Table 9 ($0.66\text{-}0.89 \text{ g kg}^{-1}$). Note that the small uncertainty, 0.12 g kg^{-1} , only reflects the standard deviation of the two SEAC⁴RS EFs, whereas the measurement uncertainty is as high as 50%. Previously, forest fire CH₃CN emissions were measured mostly from boreal and tropical regions but rarely from temperate regions [Akagi *et al.*, 2011; Simpson *et al.*, 2011; Müller *et al.*, 2016]. A typical range for forest fire CH₃CN EFs in the literature is 0.2 to 0.6 g kg^{-1} . While the CH₃CN emission from the Rim Fire ($\text{EF} = 0.13 \pm 0.02 \text{ g kg}^{-1}$) was below this range, those from the other two fires are both within it. Note that the Rim Fire also had a relatively low EF(HCN) of $0.25 \pm 0.13 \text{ g kg}^{-1}$. The ERs of $\Delta\text{CH}_3\text{CN}/\Delta\text{HCN}$ for the two SEAC⁴RS fires, 0.31 and 0.35, are at the lower end of the generally observed range, 0.30-0.56.

Alkyl nitrate formation is an important feature of NO_x–VOC chemistry and it also affects OA formation [Perring *et al.*, 2013; Lee *et al.*, 2016]. In general, the average EFs of the saturated C₁-C₅ alkyl nitrates from the two SEAC⁴RS wildfires are similar to those measured from boreal forest fire plumes [Akagi *et al.*, 2011; Simpson *et al.*, 2011]. In addition, we report the first EFs of multifunctional organic nitrates (isoprene/butadiene/butene/propene/ethene hydroxynitrates, methyl vinyl ketone/mathacrolein hydroxynitrates, propanone nitrate, ethanal nitrate, and nitroxyhydroperoxide + nitroxyhydroxyepoxide) from BB. In the fresh plumes of the two

SEAC⁴RS fires, most of these nitrates were elevated over background by less than 200 pptv, corresponding to ERs to CO on the order of 10^{-6} - 10^{-5} . Although relatively minor in concentrations, they exhibited excellent correlations with HCN with r^2 generally larger than 0.95, indicating a clear BB source. The summed emissions of these measured alkyl nitrates are 0.18 g kg^{-1} (8.5% of HCN by molar ratio) and 0.12 g kg^{-1} (9.6% of HCN by molar ratio) for the Big Windy Complex and the Rim Fire, respectively.

5.3.1.4 Non-methane Organic Compounds (NMOCs)

Open biomass burning is the second largest global source of NMOCs after biogenic emissions [Yokelson *et al.*, 2008]. The emitted NMOCs can greatly influence the production of ozone and secondary organic compounds. Additional NMOCs, especially OVOCs, have been measured by recent work, which can then improve photochemical model performance [Stockwell *et al.*, 2015; Liu *et al.*, 2016; Müller *et al.*, 2016]. The extensive measurements during SEAC⁴RS enable the development of a detailed set of EFs of NMOCs for wildfires. The PTR-MS onboard the G-1 aircraft also measured several important NMOCs from the Colockum Tarps fire. Among the common species, the Big Windy Complex had higher emissions for a variety of OVOCs measured by PTR-MS and CIMS. Its smoldering-dominated burning condition could have contributed to the higher OVOC EFs, although this observation cannot be fully explained without knowing differences in fuels.

The most abundant NMOCs emitted from the wildfires were methanol, formaldehyde, acetaldehyde, acetone/propanal, and hydroxyacetone. They are also often the most abundant OVOCs emitted by other types of BB [Akagi *et al.*, 2011; Stockwell *et*

al., 2014; *Stockwell et al.*, 2015; *Liu et al.*, 2016]. Although not measured here, acetic acid is often another major NMOC emitted from forest fires [*Akagi et al.*, 2011; *Yokelson et al.*, 2013]. In general, our average EFs of the measured compounds (except for hydroxyacetone) agree within a factor of ~2 with the other studies listed in Table 9 and from burning different plants as compiled by *Akagi et al.* [2011]. Hydroxyacetone emissions from a prescribed forest fire have recently been reported by *Müller et al.* [2016] with an average EF of $0.28 \pm 0.15 \text{ g kg}^{-1}$. The two SEAC⁴RS fires produced relatively high amounts of hydroxyacetone, with an average EF of $1.13 \pm 0.31 \text{ g kg}^{-1}$, which is higher than those for a variety of common fire types studied during FLAME-4 except for crop residual fuels.

Diacetyl has been found to be an important precursor of peroxyacetyl radicals through photolysis and has large effects on modeled plume chemistry [*Liu et al.*, 2016; *Müller et al.*, 2016]. We report an EF(diacetyl) of $2.10 \pm 0.63 \text{ g kg}^{-1}$ for the Colockum Tarps fire, which was the second most abundant NMOC after formaldehyde for that fire, even higher than methanol and acetaldehyde. This EF is much higher than the measured $0.44 \pm 0.18 \text{ g kg}^{-1}$ from a small prescribed fire in Georgia [*Müller et al.*, 2016], $0.73 \pm 0.22 \text{ g kg}^{-1}$ for some tropical deforestation fires [*Yokelson et al.*, 2008], and $\sim 0.2\text{--}1.2 \text{ g kg}^{-1}$ for a variety of fuels burned in laboratory [*Yokelson et al.*, 2008; *Stockwell et al.*, 2015]. Such high primary diacetyl emissions significantly promote peroxyacetyl nitrate (PAN) formation in downwind plumes.

The SEAC⁴RS data extend previously published emissions by including a few OVOCs that are also important products from the oxidation of biogenic emissions such as isoprene [*Paulot et al.*, 2009a; *Paulot et al.*, 2009b; *Crounse et al.*, 2011; *Crounse et al.*,

2013; Bates *et al.*, 2016]. These species consist of peroxyacetic acid (PAA) and hydroperoxy glycolaldehyde (HPGLYC), hydroperoxy acetone, organic peroxides (hydroxymethylhydrogenperoxide (HMHP) and isoprene hydroxy hydroperoxides and epoxydiols), isoprene hydroperoxyaldehydes (HPALDs), and some other hydroxy compounds (C₄-dihydroxycarbonyls, C₄-hydroxydicarbonyls, and C₅-alkenediols). These intermediate compounds are of particular interest because they are known to affect the atmosphere's oxidative capacity and form SOA [Lelieveld *et al.*, 2008; Surratt *et al.*, 2010]. PAA/HPGLYC, HMHP, and HPALDs are the three compounds that had the highest average EFs: 0.24 ± 0.28 , 0.19 ± 0.20 , and 0.17 ± 0.02 g kg⁻¹. HPALDs were also found to be abundant in agricultural fire plumes, with a higher average EF of 0.406 ± 0.229 g kg⁻¹ [Liu *et al.*, 2016]. While the EF(HPALD) values were similar for the Big Windy Complex and Rim Fire, EF(PAA/HPGLYC) and EF(HMHP) showed strong fire-to-fire variability, with EFs 7-10 times higher from the Big Windy Complex.

Among the NMHCs quantified from the SEAC⁴RS fires, the shorter-chained alkanes and alkenes (C₂-C₃) were most abundant in the plumes on a molar basis, as also found in other BB studies [Akagi *et al.*, 2011; Simpson *et al.*, 2011]. Benzene and toluene ranked highest among the longer-chained hydrocarbons (\geq C₄) based on both ERs and EFs. Most of the NMHC EFs were comparable to the other forest fires listed in Table 9. The NMHCs that had lower EFs for both the two SEAC⁴RS fires than some literature values are mainly terpenes including isoprene, α -pinene, β -pinene, and total monoterpenes. The average EF(α -pinene) and EF(β -pinene) in this study are lower by over 5 times and 40 times those obtained from prescribed forest fires in South Carolina [Akagi *et al.*, 2013] and boreal forest fires in Canada [Simpson *et al.*, 2011], respectively.

The highest pinene EFs from the boreal forest fires is consistent with their stronger association with coniferous than deciduous ecosystems [Fuentes *et al.*, 2000]. However, since western forests burned here are also predominantly coniferous, vegetation type alone may not be able to account for the difference in pinene emissions. Additionally, Akagi *et al.* [2013] suggests that α -pinene and β -pinene may be preferentially released from fuels on the ground (duff, dead-down woody fuels, etc.) that burn largely by RSC, and temperate forests tend to have a smaller loading of dead-down woody fuels than boreal forests. Compared to the boreal fire plumes, the lower EF(pinenes) determined here may be partially explained by the fact that less emissions from such fuels were lofted and sampled. However, other factors such as fire variability and photochemical processing are also expected to contribute to the difference.

5.3.2 Initial Emissions of PM_1

PM emissions from temperate fuels have been measured mainly from prescribed fires and in laboratory studies [Hosseini *et al.*, 2013; May *et al.*, 2014]. Very recently, Collier *et al.* [2016] reported aerosol enhancement ratios from 32 wildfire plumes originating from the Pacific Northwest region during BBOP, which were sampled at a fixed site located in central Oregon as well as from the G-1 aircraft. BB OA has been shown to contain substantial amounts of light-absorbing BrC, which has potential impacts on climate forcing [Saleh *et al.*, 2013; Forrister *et al.*, 2015; Washenfelder *et al.*, 2015; Liu *et al.*, 2016]. Forrister *et al.* [2015] has presented a detailed examination of BrC evolution in the smoke of the Rim Fire. Here we report a suite of emissions of non-refractory components of PM_1 from western wildfires. It is known that the measured fine PM emissions for similar fuel types often vary between field-measured prescribed burns

and laboratory-based burns due to different burning control and fuel conditions such as moisture content [May *et al.*, 2014]. Similarly, fine PM variability may also exist between prescribed fires and uncontrolled wildfires. However, little information is available for a detailed comparison. Therefore we also compare our EF(PM₁) with previous airborne and ground-based studies that measured the same PM₁ species from prescribed fires (Table 10).

Table 10 – Comparison of aerosol EFs (g kg⁻¹) and ERs to Δ(CO₂+CO) for temperate fuels measured from aircraft.

Fire	Western wildfires (this work)		Prescribed chaparral fires (<i>May et al.</i> [2014])	Prescribed montane fires (<i>May et al.</i> [2014])	Prescribed SE coastal plain fires (<i>May et al.</i> [2014])	Western wildfires (<i>Collier et al.</i> [2016])
MCE	0.912 (0.031)		0.924 (0.019)	0.899 (0.020)	0.936 (0.014)	0.91 (0.046)
	EF (g kg ⁻¹)	ER to Δ(CO ₂ +CO) (μg m ⁻³ ppm ⁻¹)	EF (g kg ⁻¹)	EF (g kg ⁻¹)	EF (g kg ⁻¹)	ER to Δ(CO ₂ +CO) (μg m ⁻³ ppm ⁻¹)
OA	24.3 (6.1)	30.0 (8.1)	3.9 (1.8)	11.2 (2.7)	2.8 (1.6)	31 (24)
BC	-	-	1.43 (0.13)	0.59 (0.13)	1.11 (0.67)	-
NH ₄	0.34 (0.15)	0.42 (0.19)	0.05 (0.05)	0.06 (0.00)	0.07 (0.03)	0.32 (0.32)
NO ₃	0.87 (0.13)	1.08 (0.18)	0.08 (0.07)	0.20 (0.00)	0.09 (0.03)	0.81 (0.94)
Chl	0.19 (0.20)	0.23 (0.24)	0.08 (0.05)	0.01 (0.00)	0.09 (0.15)	-
SO ₄	0.30 (0.16)	0.37 (0.18)	0.01 (0.01)	0.01 (0.00)	0.17 (0.10)	-
PM ₁	26.0 (6.2)	32.1 (8.2)	5.5 (1.7)	12.1 (2.9)	4.4 (2.0)	-

The major particulate species emitted from all three fires are primary OA (POA), with an average EF of $24.3 \pm 6.1 \text{ g kg}^{-1}$ (Table 9). The Big Windy Complex had the largest EF(OA) among the three studied fires ($30.9 \pm 11.8 \text{ g kg}^{-1}$). This high EF(OA) was possibly related to the smoldering burning conditions, although it could also be affected by gas-particle partitioning of semivolatile compounds during dilution processes. Another complication is the net formation of SOA that could contribute to higher downwind $\Delta\text{OA}/\Delta\text{CO}$, which could be important for the SEAC⁴RS plumes as they involved smoke as old as 1-2 h. Highly variable SOA formation rates in aging BB plumes have been reported, although limited net increase in OA mass is often observed [Capes *et al.*, 2008; Yokelson *et al.*, 2009; Cubison *et al.*, 2011; Liu *et al.*, 2016]. In the case of the Rim Fire, besides the relatively fresh plumes (~20-120 min), it also provided samples > 4 h old. We found that in the fresh Rim Fire plumes that ranged from ~20-120 min old, $\Delta\text{OA}/\Delta\text{CO}$ and the O/C ratio remained at 0.24 g g^{-1} and ~0.5, respectively, without significant variation. In contrast, in the ~4 h plumes, $\Delta\text{OA}/\Delta\text{CO}$ decreased to 0.11 g g^{-1} while the average O/C ratio increased to ~0.8. This indicated that between ~2-4 h, the net effect of oxidation and evaporation resulted in a 54% decrease in OA mass. Forrister *et al.* [2015] found that $\Delta\text{OA}/\Delta\text{CO}$ exhibited little change afterwards in more aged Rim Fire plumes up to ~50 h. Similarly, constant $\Delta\text{OA}/\Delta\text{CO}$ and O/C ratio were also seen in the fresh Big Windy Complex plumes. Therefore, the OA EFs in this study represent freshly emitted OA (< 2 h) that did not undergo a significant change in mass.

For all three fires, OA emissions represented the majority of the mass (>90%) of the emitted PM₁. Such a high OA fraction was also observed from montane prescribed fires and from burning pines and dense fuels such as duff and peat in laboratory studies

[May *et al.*, 2014]. Based on aircraft observations, May *et al.* [2014] observed significantly smaller EF(OA) from prescribed fires for three temperate ecosystems, namely maritime chaparral ($3.9 \pm 1.8 \text{ g kg}^{-1}$), montane ($11.2 \pm 2.7 \text{ g kg}^{-1}$), and southeastern coastal plain ($2.8 \pm 1.6 \text{ g kg}^{-1}$). By contrast, by calculating enhancement ratios as $\Delta\text{OA}/\Delta(\text{CO}_2+\text{CO})$, we find that our average value, $30.0 \pm 8.1 \text{ } \mu\text{g m}^{-3} \text{ ppm}^{-1}$, agrees well with the average of $31 \pm 24 \text{ } \mu\text{g m}^{-3} \text{ ppm}^{-1}$ for the 32 plumes reported by Collier *et al.* [2016]. Cubison *et al.* [2011], Jolleys *et al.* [2012], and Jolleys *et al.* [2015] summarize some field BB datasets for boreal and tropical wildfires and conclude that fresh $\Delta\text{OA}/\Delta\text{CO}$ often ranged from ~ 0.02 to 0.33 g g^{-1} . In this study, the ERs of $\Delta\text{OA}/\Delta\text{CO}$ for the three fires ranged between 0.24 - 0.34 g g^{-1} , which lies in the upper end of the previously reported range.

The dominant inorganic aerosol species measured by the AMS are ammonium, nitrate, chloride, and sulfate, with average EFs of 0.34 ± 0.15 , 0.87 ± 0.13 , 0.19 ± 0.20 , and $0.30 \pm 0.16 \text{ g kg}^{-1}$. All these average EFs are larger than the aircraft-measured EFs from U.S. prescribed fires reported by May *et al.* [2014] (Table 10). For tropical forest fires, wide ranges of sulfate (~ 0.05 - 0.21 g kg^{-1}) and chloride (~ 0.07 - 0.51 g kg^{-1}) EFs have been measured in the field [Yokelson *et al.*, 2009; Akagi *et al.*, 2011]. Compared to the tropical fires, our average EF(sulfate) is relatively high while the average EF(chloride) is within the observed range of chloride emissions. Nitrate and ammonium are often found to be minor components of the emitted nitrogen species when compared to NO_x and NH_3 from various BB studies, with EFs generally less than $\sim 0.2 \text{ g kg}^{-1}$ [McMeeking *et al.*, 2009; Akagi *et al.*, 2011]. In our work, the emitted nitrogen as nitrate and ammonium accounted for 87% and 116% of that as NO_x on average, respectively. Collier *et al.*

[2016] also observed significant nitrate and ammonium emissions, which were both ~25% lower than our observations based on ERs to $\Delta(\text{CO}_2+\text{CO})$.

We combined our EF measurements of non-refractory species to investigate the total PM_{10} emission from the temperate wildfires. The average $\text{EF}(\text{PM}_{10})$ for the three fires is $26.0 \pm 6.2 \text{ g kg}^{-1}$, which is more than 2 times larger than the average for the montane prescribed fires and ~5-6 times larger than those for the chaparral and coastal plain fires (Table 10). Although black carbon (BC) is not included in our $\text{EF}(\text{PM}_{10})$, we expect the comparison to be roughly the same since our $\text{EF}(\text{PM}_{10})$ is dominated by OA. Our $\text{EF}(\text{PM}_{10})$ is also substantially larger than the temperate forest average reviewed by *Akagi et al.* [2011], which takes into account two wildfires and many prescribed fires (Table 9). Although the analysis is limited, our overall higher $\text{EF}(\text{PM}_{10})$ may reflect differences between emissions from prescribed fires and wildfires due to differences in fuel content and condition, burning condition, and fire size and intensity. For example, inorganic EFs are often found to have a strong dependence on fuel composition [*Christian et al.*, 2003; *Burling et al.*, 2010; *May et al.*, 2014] and OA is mainly produced by smoldering combustion [*Reid et al.*, 2005]. Since the observed wildfire MCEs of both this work and *Collier et al.* [2016] fall within the range of MCEs that is commonly measured for prescribed fires (Table 10), other reasons besides the smoldering to flaming ratio of the fire are needed to explain the higher production of OA from wildfires. For example, prescribed fires often occur within restricted meteorological and fuel moisture conditions designed to maintain containment of the fire while still burning a significant fraction of the fuel [*Radke et al.*, 1991]. Different conditions that drive the wildfire intensity and movement may result in different PM EFs. In addition, wildfires tend to burn more

dead/down fuels and live, moist canopy fuels, both of which can promote high OA emissions [Yokelson *et al.*, 2008; May *et al.*, 2014]. In short, this work suggests that the aircraft-measured EF(PM₁) from wildfires is more than 2 times that of prescribed fires.

In addition, wildfires typically consume more fuel than prescribed fires [Campbell *et al.*, 2007; Turetsky *et al.*, 2011; Yokelson *et al.*, 2013]. Higher PM EFs and higher fuel consumption for wildfires suggest that it is possible to reduce overall PM emissions by prescribed burning. However, this assumes that prescribed burning will significantly reduce the prevalence of wildfires.

5.3.3 Relationship between EF and MCE

BB emissions often vary with different combustion processes such as flaming and smoldering. For this reason, we examined the correlation between MCEs and the derived EFs for the three wildfires sampled in this study. Since BB studies for similar western fuels are rare, we also compare our data to the previous U.S. prescribed fire and boreal fire studies of Burling *et al.* [2011], Simpson *et al.* [2011], Akagi *et al.* [2013], and May *et al.* [2014]. The species we chose are CH₄, 16 out of the 20 most abundant gases in Figure 19, and the 5 PM₁ components, all of which comprise at least three data points obtained from this work and/or the selected prescribed fire studies. Despite differences in fuels and burning environments in these studies, we examined EFs as a function of MCE using all available data to provide a general idea about whether variability in MCE can describe the variability in EFs.

Figure 20 shows all gaseous species with a linear regression slope significantly different from zero, including NO_x, CH₄, methanol, benzene, toluene, formaldehyde,

furan, and propene. EF(NO_x) increases as MCE increases, consistent with its primary emission from flaming combustion [Yokelson *et al.*, 1996; Lobert *et al.*, 1999; Goode *et al.*, 2000]. All NMOCs in Figure 20 are negatively correlated with MCE, consistent with their emission from smoldering combustion. Variability in the EF versus MCE relationship does exist among the different studies. For example, the EF(NO_x) and MCE correlation ($r^2 = 0.29$) might have been degraded by other factors such as fuel nitrogen content [McMeeking *et al.*, 2009; Burling *et al.*, 2010] and photochemical aging. In addition, the EFs for propene from this work and Simpson *et al.* [2011] clearly lie below the overall fit and all other EFs at a similar MCE range (0.87-0.93).

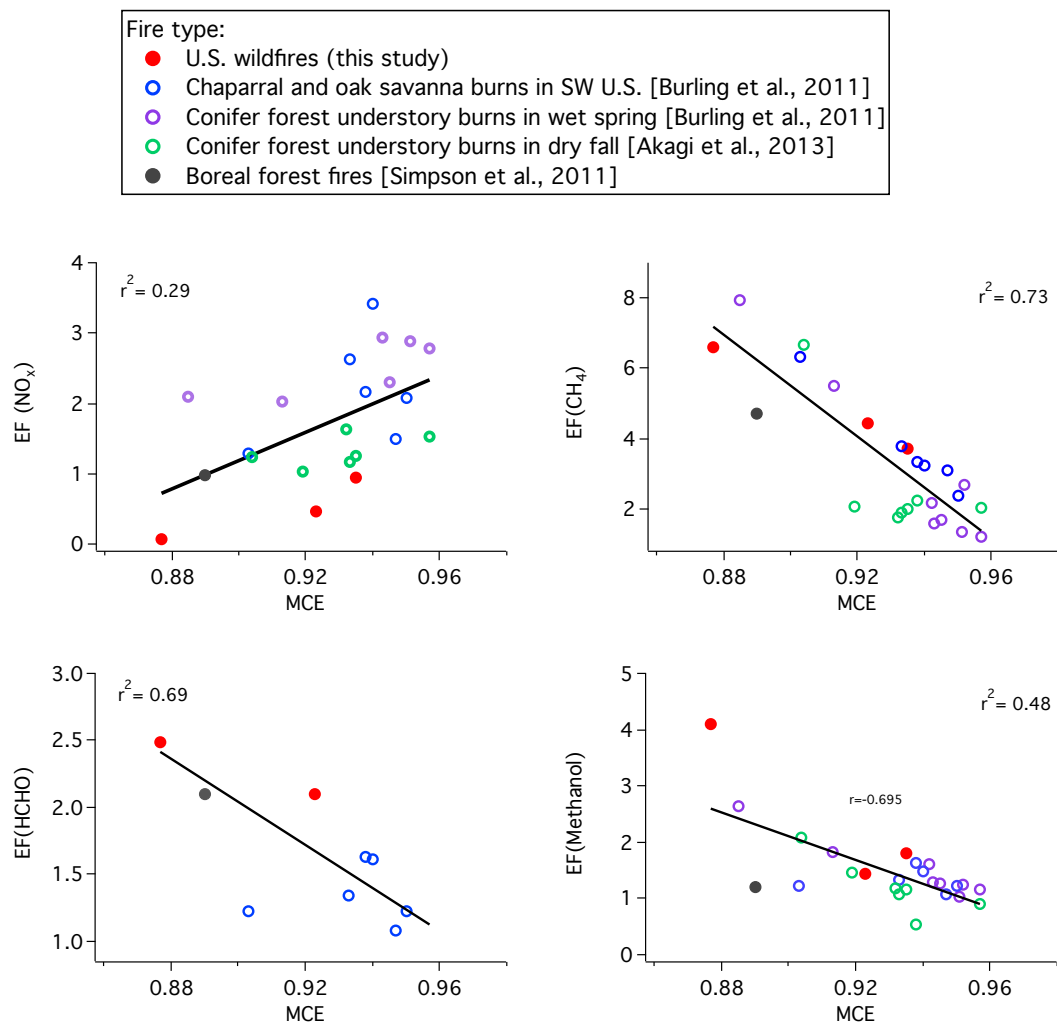


Figure 20 – Emission factors (g kg^{-1}) of gaseous species as a function of MCE for the three wildfires of this study, the boreal forest fires of *Simpson et al.* [2011], and the prescribed fires of *Burling et al.* [2011] and *Akagi et al.* [2013]. Gases shown here are associated with slopes that are significantly different from zero. Correlation coefficients (r^2) were derived from bivariate linear regressions of all plotted data.

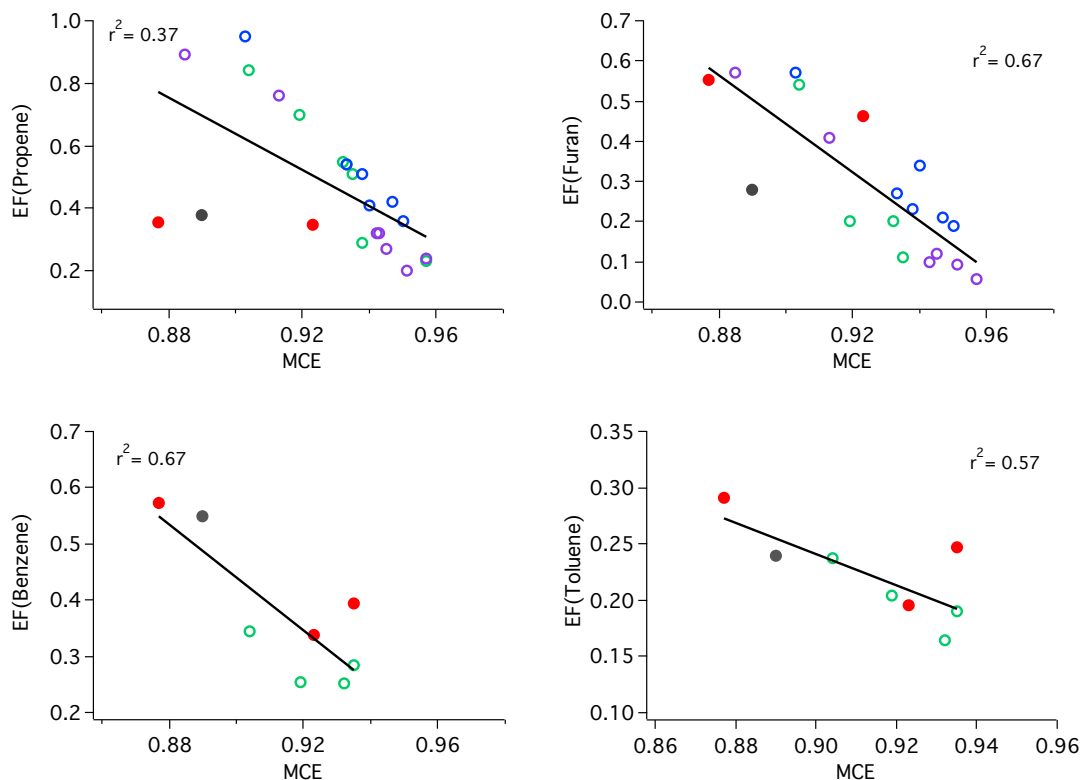


Figure 20 continued.

Ethane, ethene, ethyne, HCN, CH_3CN , SO_2 , acetone/propanal, MVK/MACR, and acetaldehyde are associated with EF-versus-MCE slopes that are not significantly different from zero (Figure 21). For these species, data from different studies are more scattered. Ethane, ethene, HCN, CH_3CN , acetone, MVK/MACR, and acetaldehyde are primarily released from smoldering combustion [McMeeking *et al.*, 2009; Burling *et al.*, 2011; Akagi *et al.*, 2013]. Except for CH_3CN and MVK/MACR, the EFs of these species showed negative correlations, however not strong, with MCE ($r^2 \leq 0.55$). SO_2 has been

established as a flaming combustion product [Yokelson *et al.*, 1996; Andreae and Merlet, 2001]. In agreement with this, the slope of our linear fit of EF(SO₂) as a function of MCE is positive, although not significant. The unexplained variability in EF(SO₂) may partly be due to the influence of fuel sulfur content and possible oxidation. Ethyne also has a positive slope ($r^2 = 0.09$) and it has been known as a product of both flaming and smoldering combustion [Yokelson *et al.*, 2008; Burling *et al.*, 2011; Yokelson *et al.*, 2011].

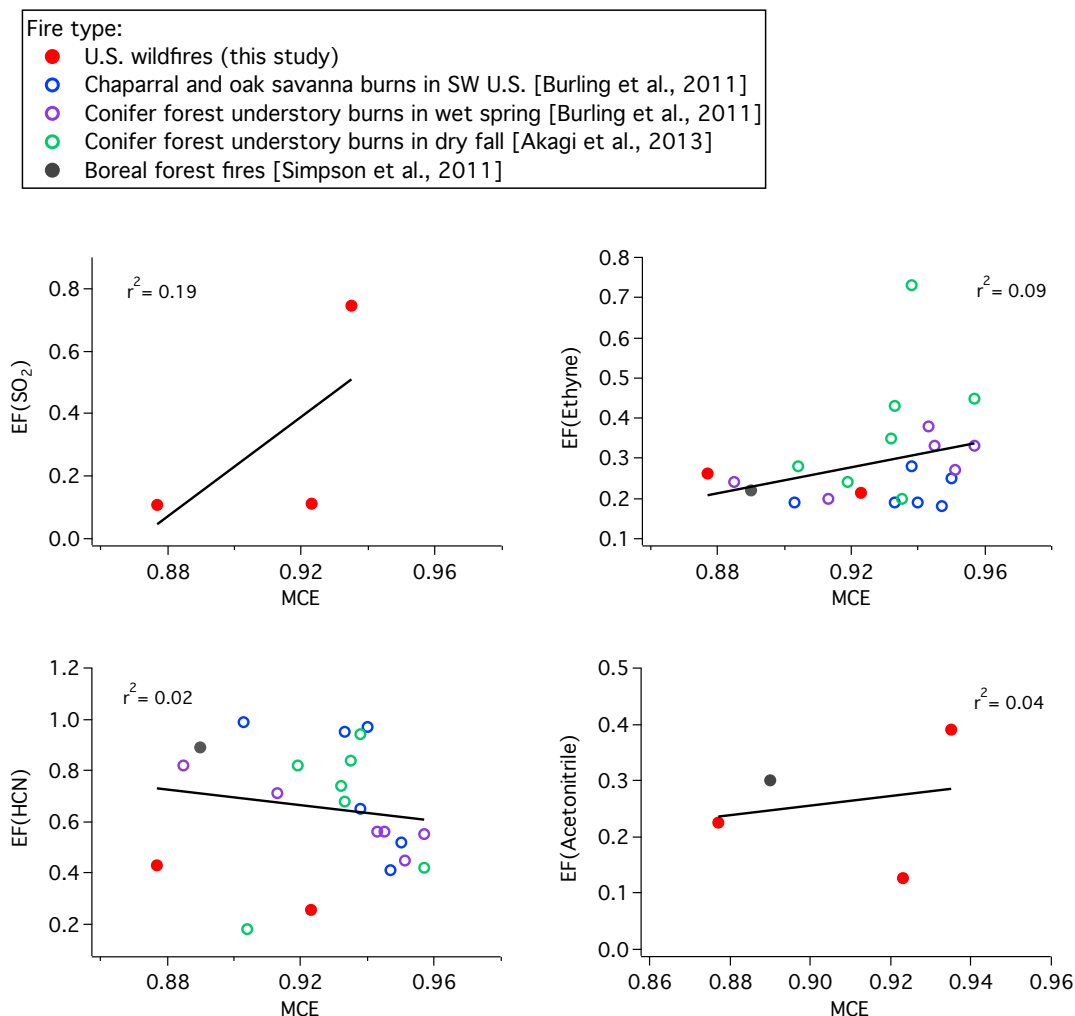


Figure 21 – Emission factors (g kg^{-1}) of gaseous species as a function of MCE for the three wildfires of this study, the boreal forest fires of *Simpson et al.* [2011], and the prescribed fires of *Burling et al.* [2011] and *Akagi et al.* [2013]. Gases shown here are associated with slopes that are not significantly different from zero. Correlation coefficients (r^2) were derived from bivariate linear regressions of all plotted data.

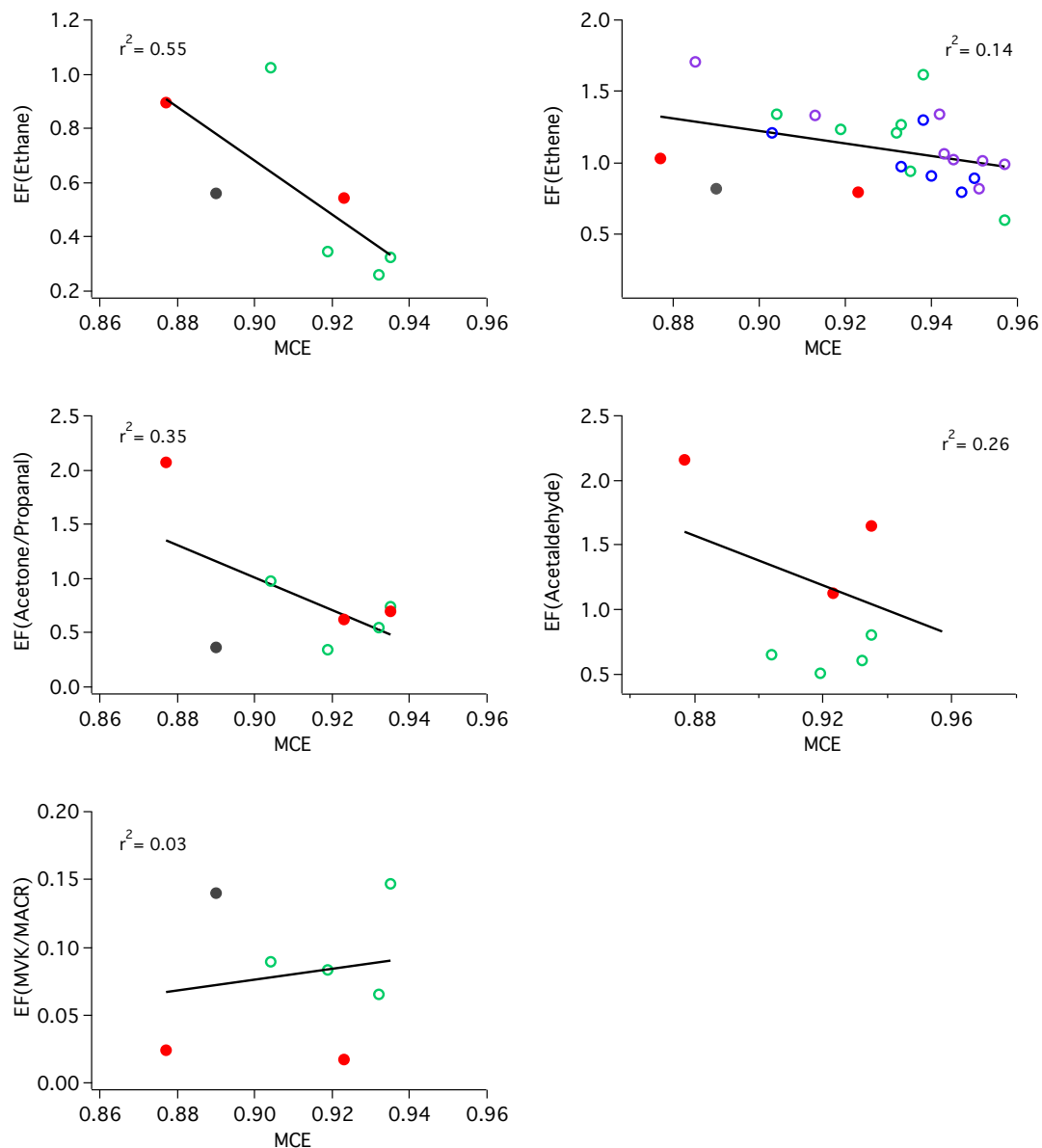


Figure 21 continued.

Except for chloride, other PM_{10} components emitted from wildfires generally follow their own separate and higher trend lines (Figure 22). When plotted with prescribed fire data, OA is the only component that had a slope significantly different

from zero, which is negative and signifies production mainly by smoldering combustion. Inorganic PM_{10} EFs are less dependent on MCE and likely more dependent on fuel composition. As shown by the regression results, numerous factors could affect the variability in emissions, which limits the predictive power of the EF and MCE relationship.

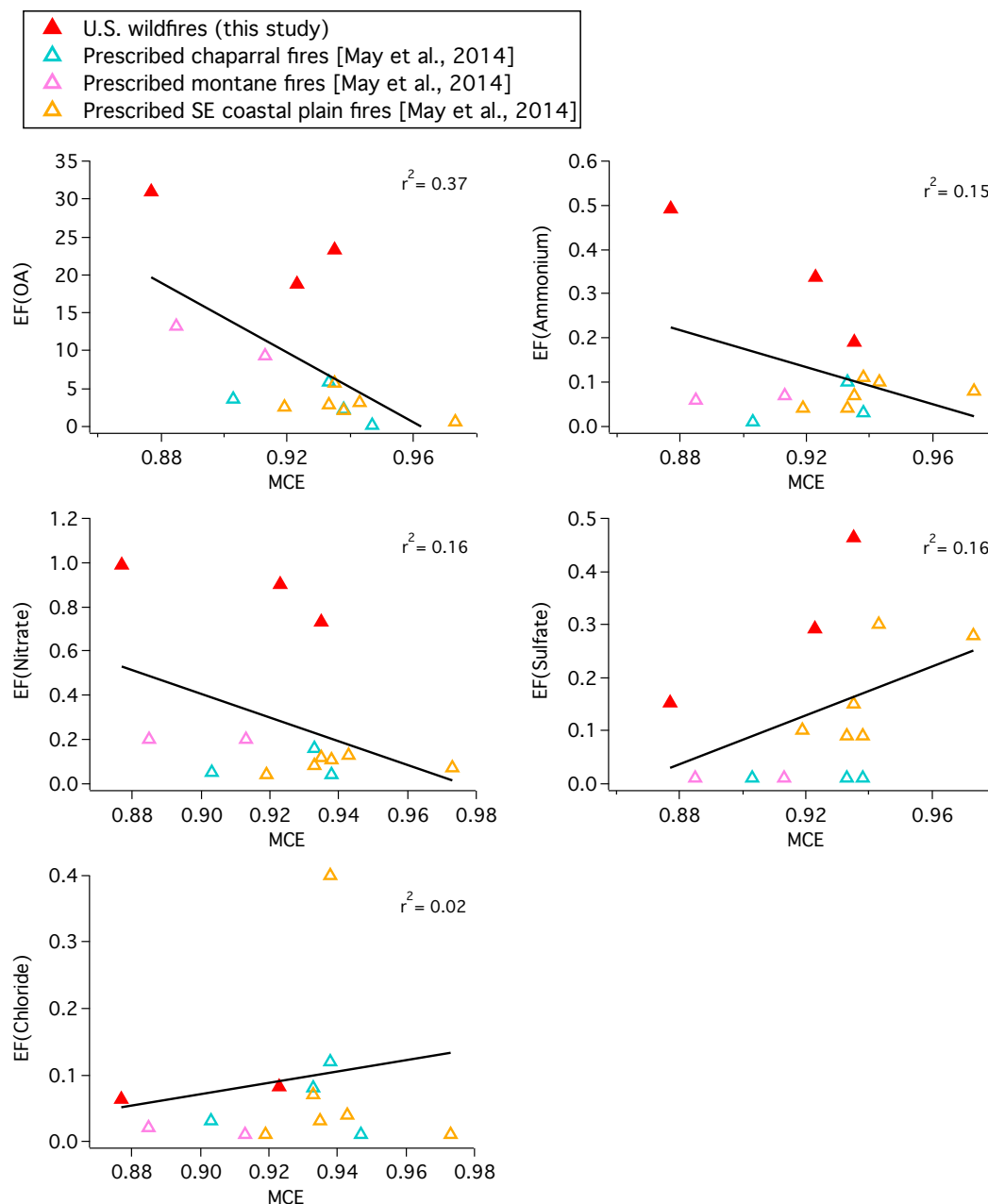


Figure 22 – Emission factors (g kg^{-1}) of all fine particle species as a function of MCE for the three wildfires of this study and the prescribed fire data of *May et al.* [2014]. Correlation coefficients (r^2) were derived from bivariate linear regressions of all plotted data. Only the slope of EF(OA) versus MCE is significantly different from zero.

5.3.4 Emission Estimates from Western U.S. Wildfires

We used the measured EFs to estimate the annual emissions of CO, NO_x, SO₂, total NMOC, and PM₁ from wildfires in the western contiguous U.S. (defined here as 11 states: Arizona, California, Colorado, Idaho, Montana, Nevada, New Mexico, Oregon, Utah, Washington, and Wyoming). The wildfire season in the western U.S. is June–October [Urbanski, 2013]. Thus the EFs of this study, which were derived within the wildfire season, may serve as reasonable estimates for typical wildfires in the western region. BB emissions are typically estimated as the product of EF, area burned, and fuel consumption [Seiler and Crutzen, 1980]. The burned area by state from 2011 to 2015 was obtained from the National Interagency Fire Center (NIFC; http://www.nifc.gov/fireInfo/fireInfo_statistics.html). Fuel consumption depends on the biomass available to burn and the fraction of biomass consumed by fire. Fuel consumption likely varies across different western U.S. ecosystems. For example, compared with the Colockum Tarps fire, the Big Windy Complex and the Rim Fire were in more humid forests with more large trees and surface (e.g., dead wood) and ground fuels (e.g., duff and litter). Thus, the Big Windy Complex and the Rim Fire possibly had higher fuel consumption than the Colockum Tarps fire. However, fuel consumption for western wildfires is not well quantified [van Leeuwen *et al.*, 2014]. Here we averaged the field-measured fuel consumptions of a large wildfire in western Oregon (41.6 Mg ha⁻¹ if assuming a carbon fraction of 45.7%) [Campbell *et al.*, 2007] and a prescribed boreal forest fire in Northwest Territories, Canada (27.6 ± 8.7 Mg ha⁻¹) [Santín *et al.*, 2015], which gave 34.6 ± 9.9 Mg ha⁻¹, to represent the average fuel consumption for western wildfires. The components used for emission estimates can all contribute to uncertainty in

emission estimates. Quantitative assessments of overall uncertainty in emissions are difficult to make due to limited knowledge about EFs of different fuels and wildfire fuel consumption in different ecosystems. We estimated the emission uncertainty by combining the variations in our EFs and in the two fuel consumption measurements. As mentioned before, the airborne EFs for smoldering species are likely underestimated without including RSC emissions. This could cause our central estimates for CO, total NMOC, and PM₁ (dominated by OA) to be conservative.

Table 11 lists the estimated annual emissions of gases and fine particles from the 11 western states between 2011 and 2015. Also listed are the emissions from wildfires and all other sources in these western states reported by the 2011 NEI (<http://www.epa.gov/air-emissions-inventories/2011-national-emissions-inventory-nei-data>), which is the most recent NEI that has detailed technical documentation available. The 2011 NEI estimated wildfire emissions using EFs from the Fire Emissions Prediction Simulator (FEPS) v2 that relies on EFs from the literature apportioned by flaming and smoldering combustion, fire activity data from multiple sources based on survey and remote sensing, fuel loading from the Fuel Characteristic Classification System, and fuel consumed estimated by the CONSUME model. The 2011 NEI also states that they have compared acres burned by state to the NIFC data to make sure the values are within a reasonable range. The NIFC burned area in 2011 in these western states is 4,069,072 acres, which is very close to (6.6% less than) the NEI wildfire area (4,355,613 acres). Note that the NIFC five-year average (4,196,133 acres) is also similar to the 2011 NEI burned area (Table 11). Since uncertainties associated with the NEI estimates are not

available, the following comparisons are solely based on the NIFC five-year average and the NEI values.

Table 11 – Acres burned and estimated annual emissions (Gg yr⁻¹) by western U.S. wildfires.

	This work	NEI wildfire	NEI all other sources	This work wildfire/NEI wildfire	This work wildfire/NEI all other sources
Year	2011-2015	2011	2011	-	-
Acres burned	4196133 ^a	4355613	-	0.96	-
Emission by species					
CO	5240 (2240)	4894	13222	1.07	0.40
NO _x as NO ₂	44 (41)	62	2588	0.71	0.02
SO ₂	19 (22)	35	352	0.54	0.05
NMOC	905 (437) ^b	1153	14361	0.78	0.06
PM ₁ or PM _{2.5} ^c	1530 (570)	418	858	3.66	1.78

^a Source: NIFC, http://www.nifc.gov/fireInfo/fireInfo_statistics.html.

^b Identified NMOC only.

^c PM₁ and PM_{2.5} were estimated by this work and the 2011 NEI, respectively.

Given similar areas burned, the five-year averaged gas emissions using our EFs show considerable consistency with the 2011 NEI estimates, especially for CO (Table 11). Our estimated flux of CO from wildfires is 5240 ± 2240 Gg yr⁻¹ and accounts for

~40% of emissions from all other sources. The total NMOC estimates were based on the EFs measured for the two SEAC⁴RS fires, which had a more complete suite of NMOC measurements as compared to BBOP. In view of the fact that some important but unmeasured NMOCs (such as acetic acid) were not incorporated into our estimate, the annual emission of 905 ± 437 Gg is likely to be a lower limit. NO_x and SO_2 emissions from western wildfires are 44 ± 41 and 19 ± 22 Gg yr^{-1} , respectively, and are both smaller than the NEI estimates, although not statistically different. The wildfire emissions of NMOC, NO_x , and SO_2 are on the order of a few percent of the total emissions from all other sources.

On the other hand, the western wildfires significantly contribute to the emission of fine particles. Our PM_{10} emission of 1530 ± 570 Gg yr^{-1} is over three times the NEI $\text{PM}_{2.5}$ estimate and almost twice the $\text{PM}_{2.5}$ emitted from all other sources. We investigated the possible reason causing our much higher fine PM estimate. As mentioned before, the burned areas used in this work and by the 2011 NEI are close. In addition, the NEI-used $\text{EF}(\text{CO})$ given by the FEPS user's guide is ~ 107 g kg^{-1} at our average combustion efficiency (~ 0.87) [Anderson *et al.*, 2004], which is $\sim 20\%$ larger than our average $\text{EF}(\text{CO})$ of 89.3 ± 28.5 g kg^{-1} . Given similar burned areas, $\text{EF}(\text{CO})$ s, and total CO estimates, we would presume that our fuel consumption term should also be similar to that of the NEI, despite our simplified assumptions. Thus it is likely that our high fine PM emission is due to higher EF than the values used by the NEI. This is also supported by the FEPS user's guide [Anderson *et al.*, 2004], in which $\text{EF}(\text{PM}_{2.5})$ is only ~ 9 g kg^{-1} at our average combustion efficiency, according to the provided empirical equation of EF as a function of combustion efficiency, as opposed to our average

EF(PM₁) of $26.0 \pm 6.2 \text{ g kg}^{-1}$. The higher fine PM EFs and the magnitude of biomass consumed by western U.S. wildfires indicate that the primary fine PM emitted from wildfires may have important implications for the management of regional air quality. As OA constitutes the majority of aerosol mass, a better understanding of wildfire impacts downwind requires future emission estimates to account for gas-particle partitioning and photochemical processing of POA emissions.

5.4 Conclusions

This study significantly updates and expands the range of species measured from temperate wildfires. This work presents EFs of over 80 trace gases and 5 fine particle components, which will improve emission estimates and the modeling of smoke chemistry and air quality impacts. The EFs of multifunctional organic nitrates and a few OVOCs that are important products from isoprene oxidation were measured for the first time from BB plumes. We also compared our EFs with those from the limited airborne measurements of temperate wildfires, boreal forest fires, and temperate prescribed fires. Among the commonly measured species, most of the NMOC EFs were comparable to the other forest fires listed in Table 9, while the discrepancies in some other NMOCs and sulfur-, nitrogen-, and chlorine-containing gases may be explained by fire variability, chemical and physical properties of fuels, combustion conditions, and photochemical aging. This work also suggests that the aircraft-measured EF(PM₁) from wildfires is substantially larger than that from prescribed fires, which may reflect different fire behavior and fuel conditions between prescribed fires and wildfires. The EFs as a function of MCE were also examined by including data from previous boreal forest fire and prescribed fire studies in North America. The linear fit for EF versus MCE showed

good correlation (or anti-correlation) and slopes significantly different from zero for NO_x, CH₄, several NMOCs, and OA. The EFs of other gases and inorganic PM₁ components are less dependent on MCE and probably more influenced by fuel characteristics and fire variability.

The annual emissions of CO, NO_x, SO₂, total NMOC, and PM₁ from western wildfires in the U.S. were estimated using the observed EFs. The estimated gas emissions are generally comparable with the 2011 NEI. However, due to the high EF(PM₁) measured in this study, our regional PM₁ emissions are over three times larger than the NEI PM_{2.5} estimate and almost two times larger than the NEI PM_{2.5} emitted from all other sources.

The findings of the large PM EFs and annual emissions from western U.S. wildfires could better inform fire management and support the practice of prescribed burning to reduce the impact of PM on air quality. A detailed assessment of the tradeoffs between wildfires and prescribed fires will require the efficacy of attempting to reduce wildfire events through managed burning practice.

CHAPTER 6. CONCLUSIONS

This chapter concludes the thesis and summarizes the findings. Potential future research on BB is also discussed.

6.1 Summary of Findings

This thesis improves the understanding of under-sampled BB, including agricultural fires and wildfires in the U.S., by utilizing airborne measurements of a wide variety of chemical species and physical parameters. These measurements provided valuable information on emissions near the source including some previously rarely measured species and on evolution up to ~ 1.2 h in downwind plumes. This work will promote accurate representation of BB's impacts on climate, atmospheric chemistry, and air quality in regional and global models.

Emissions from 15 agricultural fires in the southeastern U.S. were reported, including 25 trace gases and 6 fine particle species. Observed EFs are generally consistent with previous measurements of crop residue burning, but the fires studied here emitted high amounts of SO_2 and fine particles, especially primary OA and chloride. Filter-based measurements of aerosol light absorption implied that BrC was ubiquitous in the plumes. With the calculated EFs, total annual SO_2 , NO_x , and CO emissions from agricultural fires in Arkansas, Louisiana, Mississippi, and Missouri were estimated (within a factor of ~ 2) to be equivalent to $\sim 2\%$ SO_2 from coal combustion and $\sim 1\%$ NO_x and $\sim 9\%$ CO from mobile sources.

The chemical evolution of the primary emissions in 7 out of 15 agricultural plumes was examined in detail for ~1.2 hr. A Lagrangian plume cross-section model was used to simulate the evolution of O₃, reactive nitrogen species, and OA. In aged plumes, rapid production of O₃, PAN, and nitrate were observed with $\Delta\text{O}_3/\Delta\text{CO}$, $\Delta\text{PAN}/\Delta\text{NO}_y$, and $\Delta\text{nitrate}/\Delta\text{NO}_y$ reaching ~0.1, ~0.3, and ~0.3. For 5 selected cases, the model reasonably simulated O₃ formation but underestimated PAN formation. No significant evolution of OA mass or BrC absorption was observed. However, a consistent increase in oxygen-to-carbon (O/C) ratios of OA indicated that OA oxidation in the agricultural fire plumes was much faster than in urban and forest fire plumes.

In addition, plumes from three wildfires in the western U.S. were measured from aircraft during SEAC⁴RS and BBOP, both in summer 2013. An extensive set of EFs for over 80 gases and 5 components of PM₁ from temperate wildfires were presented here. These include some rarely, or never before, measured oxygenated volatile organic compounds and multifunctional organic nitrates. The EFs from three wildfires are compared with those from previous airborne measurements of temperate wildfires, boreal forest fires, and temperate prescribed fires. These wildfires emitted high amounts of PM₁ (in which OA comprised most of the mass) with an average EF that is over two times of prescribed fire EFs. The EFs were used to estimate the annual wildfire emissions of CO, NO_x, total NMOC, and PM₁ from 11 western U.S. states. Whereas the estimated gas emissions are generally comparable with the 2011 NEI, our PM₁ emission estimate (1530 ± 570 Gg yr⁻¹) is over three times that of the NEI PM_{2.5} estimate mainly due to our high EF(PM₁) and also higher than the PM_{2.5} emitted from all other sources in these states

according to NEI. This result supports the practice of prescribed burning that could reduce fine particle emissions.

6.2 Future Research

While this thesis has expanded our knowledge of agricultural fires and wildfires, it also points to the necessity of further improving characterization of these fires and their impacts. Some limitations and future research directions are summarized below.

1. The current research has discussed emission variability due to natural fire variability, combustion efficiency, and fuel composition, but there were not enough data or information to fully understand all the factors that determined emissions. For example, the reason for the high EF(OA) from the western wildfires remains unclear. Future research is needed to investigate whether the emissions and evolution reported here are representative and what underlying factors influence BB emissions.
2. A variety of NMOCs have been identified in both agricultural and forest fire plumes. The Lagrangian simulations indicate that some unmeasured NMOCs such as diacetyl and methylglyoxal could be significant contributors to PAN formation. Future identification of these reactive species will help improve the capability of photochemical models to simulate the chemical process and impacts of smoke.
3. Airborne sampling of fires involves some limitations such as plume tracking difficulties, freshness of smoke samples, limited instrumentation, and limited fire samples under specific conditions. Therefore laboratory studies could be utilized to complement field studies and acquire more information under well-controlled conditions. In addition, aircraft was not able to sample unlofted emissions from RSC. To realistically represent

the total smoldering-dominated emissions over the lifetime of a fire, ground-based sampling of these RSC emissions could be utilized in addition to airborne measurements.

4. This work provides new information about BB sources of a variety of species and reasonable predictions on gas-phase photochemistry in young plumes. However, predictions of the prevalence or impacts of some BB emissions cannot simply be inferred from measurements conducted at or near the sources without considering complex aging processes on longer time scales. For example, the unclear mechanisms governing BB OA and BrC evolution in the atmosphere are important to determine their atmospheric burden on regional and global scales. Future studies should continue to advance the characterization of primary emissions and focus on the poorly characterized physical and chemical processes to accurately predict the distributions of BB emissions and thus the associated air quality and climate impacts. In particular, this thesis indicates that wildfires may produce more POA than all other sources in the western U.S. Therefore current models may have significantly underestimated the attribution of the percentage of OA loading from BB sources.

REFERENCES

- Adler, G., J. M. Flores, A. Abo Riziq, S. Borrmann, and Y. Rudich (2011), Chemical, physical, and optical evolution of biomass burning aerosols: a case study, *Atmos. Chem. Phys.*, *11*(4), 1491-1503, doi: 10.5194/acp-11-1491-2011.
- Aiken, A. C., et al. (2008), O/C and OM/OC Ratios of Primary, Secondary, and Ambient Organic Aerosols with High-Resolution Time-of-Flight Aerosol Mass Spectrometry, *Environ. Sci. Technol.*, *42*(12), 4478-4485, doi: 10.1021/es703009q.
- Akagi, S. K., R. J. Yokelson, C. Wiedinmyer, M. J. Alvarado, J. S. Reid, T. Karl, J. D. Crounse, and P. O. Wennberg (2011), Emission factors for open and domestic biomass burning for use in atmospheric models, *Atmos. Chem. Phys.*, *11*(9), 4039-4072, doi: 10.5194/acp-11-4039-2011.
- Akagi, S. K., et al. (2012), Evolution of trace gases and particles emitted by a chaparral fire in California, *Atmos. Chem. Phys.*, *12*(3), 1397-1421, doi: 10.5194/acp-12-1397-2012.
- Akagi, S. K., et al. (2013), Measurements of reactive trace gases and variable O₃ formation rates in some South Carolina biomass burning plumes, *Atmos. Chem. Phys.*, *13*(3), 1141-1165, doi: 10.5194/acp-13-1141-2013.
- Alvarado, M. J., and R. G. Prinn (2009), Formation of ozone and growth of aerosols in young smoke plumes from biomass burning: 1. Lagrangian parcel studies, *J. Geophys. Res.*, *114*(D9), doi: 10.1029/2008jd011144.
- Alvarado, M. J., C. Wang, and R. G. Prinn (2009), Formation of ozone and growth of aerosols in young smoke plumes from biomass burning: 2. Three-dimensional Eulerian studies, *J. Geophys. Res. Atmos.*, *114*(D9), doi: 10.1029/2008JD011186.
- Alvarado, M. J., et al. (2010), Nitrogen oxides and PAN in plumes from boreal fires during ARCTAS-B and their impact on ozone: an integrated analysis of aircraft and satellite observations, *Atmos. Chem. Phys.*, *10*(20), 9739-9760, doi: 10.5194/acp-10-9739-2010.
- Anderson, G. K., D. V. Sandberg, and R. A. Norheim (2004), Fire Emission Production Simulator (FEPS) user's guide version 1.0, Pacific Northwest Research Station, the USDA Forest Service, Seattle, WA.
- Andreae, M. O., and P. Merlet (2001), Emission of trace gases and aerosols from biomass burning, *Global Biogeochem. Cy.*, *15*(4), 955-966, doi: 10.1029/2000gb001382.
- Atkinson, R., and J. Arey (2003), Atmospheric Degradation of Volatile Organic Compounds, *Chem. Rev.*, *103*(12), 4605-4638, doi: 10.1021/cr0206420.

- Atkinson, R., D. L. Baulch, R. A. Cox, J. N. Crowley, R. F. Hampson, R. G. Hynes, M. E. Jenkin, M. J. Rossi, J. Troe, and I. Subcommittee (2006), Evaluated kinetic and photochemical data for atmospheric chemistry: Volume II-gas phase reactions of organic species, *Atmos. Chem. Phys.*, 6(11), 3625-4055, doi: 10.5194/acp-6-3625-2006.
- Bai, J., C. Yu, L. Li, P. Wu, Z. Luo, and M. Ni (2013), Experimental Study on the NO and N₂O Formation Characteristics during Biomass Combustion, *Energy Fuels*, 27(1), 515-522, doi: 10.1021/ef301383g.
- Bates, K. H., T. B. Nguyen, A. P. Teng, J. D. Crounse, H. G. Kjaergaard, B. M. Stoltz, J. H. Seinfeld, and P. O. Wennberg (2016), Production and Fate of C₄ Dihydroxycarbonyl Compounds from Isoprene Oxidation, *J. Phys. Chem. A*, 120(1), 106-117, doi: 10.1021/acs.jpca.5b10335.
- Baylon, P., D. A. Jaffe, N. L. Wigder, H. Gao, and J. Hee (2015), Ozone enhancement in western US wildfire plumes at the Mt. Bachelor Observatory: The role of NO_x, *Atmos. Environ.*, 109, 297-304, doi: 10.1016/j.atmosenv.2014.09.013.
- Becidan, M., Ø. Skreiberg, and J. E. Hustad (2007), NO_x and N₂O Precursors (NH₃ and HCN) in Pyrolysis of Biomass Residues, *Energy Fuels*, 21(2), 1173-1180, doi: 10.1021/ef060426k.
- Belsky, A. J., and D. M. Blumenthal (1997), Effects of Livestock Grazing on Stand Dynamics and Soils in Upland Forests of the Interior West, *Conserv. Biol.*, 11(2), 315-327, doi: 10.1046/j.1523-1739.1997.95405.x.
- Bergstrom, R. W., P. B. Russell, and P. Hignett (2002), Wavelength Dependence of the Absorption of Black Carbon Particles: Predictions and Results from the TARFOX Experiment and Implications for the Aerosol Single Scattering Albedo, *J. Atmos. Sci.*, 59(3), 567-577, doi: 10.1175/1520-0469(2002)059<0567:WDOTAO>2.0.CO;2.
- Bertschi, I., R. J. Yokelson, D. E. Ward, R. E. Babbitt, R. A. Susott, J. G. Goode, and W. M. Hao (2003a), Trace gas and particle emissions from fires in large diameter and belowground biomass fuels, *J. Geophys. Res. Atmos.*, 108(D13), doi: 10.1029/2002JD002100.
- Bertschi, I. T., R. J. Yokelson, D. E. Ward, T. J. Christian, and W. M. Hao (2003b), Trace gas emissions from the production and use of domestic biofuels in Zambia measured by open-path Fourier transform infrared spectroscopy, *J. Geophys. Res. Atmos.*, 108(D13), doi: 10.1029/2002JD002158.
- Biswell, H. (1999), *Prescribed Burning in California Wildlands Vegetation Management*, Univ. of California Press, Berkeley, CA.
- Blake, N. J., et al. (2003), NMHCs and halocarbons in Asian continental outflow during the Transport and Chemical Evolution over the Pacific (TRACE-P) Field

- Campaign: Comparison With PEM-West B, *J. Geophys. Res.*, *108*(D20), doi: 10.1029/2002jd003367.
- Bond, T. C., D. G. Streets, K. F. Yarber, S. M. Nelson, J.-H. Woo, and Z. Klimont (2004), A technology-based global inventory of black and organic carbon emissions from combustion, *J. Geophys. Res. Atmos.*, *109*(D14), doi: 10.1029/2003JD003697.
- Bond, T. C., et al. (2013), Bounding the role of black carbon in the climate system: A scientific assessment, *J. Geophys. Res. Atmos.*, *118*(11), 5380-5552, doi: 10.1002/jgrd.50171.
- Brey, S. J., and E. V. Fischer (2016), Smoke in the City: How Often and Where Does Smoke Impact Summertime Ozone in the United States?, *Environ. Sci. Technol.*, *50*(3), 1288-1294, doi: 10.1021/acs.est.5b05218.
- Burling, I. R., et al. (2010), Laboratory measurements of trace gas emissions from biomass burning of fuel types from the southeastern and southwestern United States, *Atmos. Chem. Phys.*, *10*(22), 11115-11130, doi: 10.5194/acp-10-11115-2010.
- Burling, I. R., R. J. Yokelson, S. K. Akagi, S. P. Urbanski, C. E. Wold, D. W. T. Griffith, T. J. Johnson, J. Reardon, and D. R. Weise (2011), Airborne and ground-based measurements of the trace gases and particles emitted by prescribed fires in the United States, *Atmos. Chem. Phys.*, *11*(23), 12197-12216, doi: 10.5194/acp-11-12197-2011.
- Butkovskaya, N. I., N. Pouvesle, A. Kukui, Y. Mu, and G. Le Bras (2006), Mechanism of the OH-Initiated Oxidation of Hydroxyacetone over the Temperature Range 236-298 K, *J. Phys. Chem. A*, *110*(21), 6833-6843, doi: 10.1021/jp056345r.
- Campbell, J., D. Donato, D. Azuma, and B. Law (2007), Pyrogenic carbon emission from a large wildfire in Oregon, United States, *J. Geophys. Res. Biogeo.*, *112*(G4), doi: 10.1029/2007JG000451.
- Canagaratna, M. R., et al. (2007), Chemical and microphysical characterization of ambient aerosols with the aerodyne aerosol mass spectrometer, *Mass Spectrom. Rev.*, *26*(2), 185-222, doi: 10.1002/mas.20115.
- Canagaratna, M. R., et al. (2015), Elemental ratio measurements of organic compounds using aerosol mass spectrometry: characterization, improved calibration, and implications, *Atmos. Chem. Phys.*, *15*(1), 253-272, doi: 10.5194/acp-15-253-2015.
- Capes, G., B. Johnson, G. McFiggans, P. I. Williams, J. Haywood, and H. Coe (2008), Aging of biomass burning aerosols over West Africa: Aircraft measurements of chemical composition, microphysical properties, and emission ratios, *J. Geophys. Res.*, *113*, doi: 10.1029/2008jd009845.

- Cazorla, M., G. M. Wolfe, S. A. Bailey, A. K. Swanson, H. L. Arkinson, and T. F. Hanisco (2015), A new airborne laser-induced fluorescence instrument for in situ detection of formaldehyde throughout the troposphere and lower stratosphere, *Atmos. Meas. Tech.*, *8*(2), 541-552, doi: 10.5194/amt-8-541-2015.
- Chan, K. R., J. Dean-Day, S. W. Bowen, and T. P. Bui (1998), Turbulence measurements by the DC-8 Meteorological Measurement System, *Geophys. Res. Lett.*, *25*(9), 1355-1358, doi: 10.1029/97gl03590.
- Chang, D., and Y. Song (2010), Estimates of biomass burning emissions in tropical Asia based on satellite-derived data, *Atmos. Chem. Phys.*, *10*(5), 2335-2351, doi: 10.5194/acp-10-2335-2010.
- Chen, Y., and T. C. Bond (2010), Light absorption by organic carbon from wood combustion, *Atmos. Chem. Phys.*, *10*(4), 1773-1787, doi: 10.5194/acp-10-1773-2010.
- Christian, T. J., B. Kleiss, R. J. Yokelson, R. Holzinger, P. J. Crutzen, W. M. Hao, B. H. Saharjo, and D. E. Ward (2003), Comprehensive laboratory measurements of biomass-burning emissions: 1. Emissions from Indonesian, African, and other fuels, *J. Geophys. Res.*, *108*(D23), doi: 10.1029/2003jd003704.
- Christian, T. J., R. J. Yokelson, B. Cárdenas, L. T. Molina, G. Engling, and S. C. Hsu (2010), Trace gas and particle emissions from domestic and industrial biofuel use and garbage burning in central Mexico, *Atmos. Chem. Phys.*, *10*(2), 565-584, doi: 10.5194/acp-10-565-2010.
- Collier, S., et al. (2016), Regional Influence of Aerosol Emissions from Wildfires Driven by Combustion Efficiency: Insights from the BBOP Campaign, *Environ. Sci. Technol.*, *50*(16), 8613-8622, doi: 10.1021/acs.est.6b01617.
- Cox, R. A., and J. A. Cole (1985), Chemical aspects of the autoignition of hydrocarbon-air mixtures, *Combustion and Flame*, *60*(2), 109-123, doi: 10.1016/0010-2180(85)90001-X.
- Crosson, E. R. (2008), A cavity ring-down analyzer for measuring atmospheric levels of methane, carbon dioxide, and water vapor, *Appl. Phys. B*, *92*(3), 403-408, doi: 10.1007/s00340-008-3135-y.
- Crounse, J. D., K. A. McKinney, A. J. Kwan, and P. O. Wennberg (2006), Measurement of Gas-Phase Hydroperoxides by Chemical Ionization Mass Spectrometry, *Anal. Chem.*, *78*(19), 6726-6732, doi: 10.1021/ac0604235.
- Crounse, J. D., et al. (2009), Biomass burning and urban air pollution over the Central Mexican Plateau, *Atmos. Chem. Phys.*, *9*(14), 4929-4944, doi: 10.5194/acp-9-4929-2009.

- Crounse, J. D., F. Paulot, H. G. Kjaergaard, and P. O. Wennberg (2011), Peroxy radical isomerization in the oxidation of isoprene, *Phys. Chem. Chem. Phys.*, *13*(30), 13607-13613, doi: 10.1039/C1CP21330J.
- Crounse, J. D., L. B. Nielsen, S. Jørgensen, H. G. Kjaergaard, and P. O. Wennberg (2013), Autoxidation of Organic Compounds in the Atmosphere, *J. Phys. Chem. Lett.*, *4*(20), 3513-3520, doi: 10.1021/jz4019207.
- Crutzen, P. J., and M. O. Andreae (1990), Biomass Burning in the Tropics: Impact on Atmospheric Chemistry and Biogeochemical Cycles, *Science*, *250*(4988), 1669-1678, doi: 10.1126/science.250.4988.1669.
- Cubison, M. J., et al. (2011), Effects of aging on organic aerosol from open biomass burning smoke in aircraft and laboratory studies, *Atmos. Chem. Phys.*, *11*(23), 12049-12064, doi: 10.5194/acp-11-12049-2011.
- Dahneke, B. (1983), Simple kinetic theory of Brownian diffusion in vapors and aerosols, in *Theory of Dispersed Multiphase Flow*, edited by R. E. Meyer, pp. 97-133, Academic Press, New York.
- de Gouw, J. A., C. Warneke, D. D. Parrish, J. S. Holloway, M. Trainer, and F. C. Fehsenfeld (2003), Emission sources and ocean uptake of acetonitrile (CH₃CN) in the atmosphere, *J. Geophys. Res. Atmos.*, *108*(D11), doi: 10.1029/2002JD002897.
- DeCarlo, P. F., et al. (2008), Fast airborne aerosol size and chemistry measurements above Mexico City and Central Mexico during the MILAGRO campaign, *Atmos. Chem. Phys.*, *8*(14), 4027-4048, doi: 10.5194/acp-8-4027-2008.
- Delfino, R. J., et al. (2009), The relationship of respiratory and cardiovascular hospital admissions to the southern California wildfires of 2003, *Occup. Environ. Med.*, *66*(3), 189-197.
- Dennis, A., M. Fraser, S. Anderson, and D. Allen (2002), Air pollutant emissions associated with forest, grassland, and agricultural burning in Texas, *Atmos. Environ.*, *36*(23), 3779-3792, doi: 10.1016/S1352-2310(02)00219-4.
- Diskin, G. S., J. R. Podolske, G. W. Sachse, and T. A. Slate (2002), Open-path airborne tunable diode laser hygrometer, *Proceedings of the International Society for Optics and Photonics (SPIE)*, *4817*, 196-204, doi: 10.1117/12.453736.
- Donahue, N. M., A. L. Robinson, C. O. Stanier, and S. N. Pandis (2006), Coupled Partitioning, Dilution, and Chemical Aging of Semivolatile Organics, *Environ. Sci. Technol.*, *40*(8), 2635-2643, doi: 10.1021/es052297c.
- Donaldson, K., L. Tran, L. A. Jimenez, R. Duffin, D. E. Newby, N. Mills, W. MacNee, and V. Stone (2005), Combustion-derived nanoparticles: A review of their toxicology following inhalation exposure, *Particle and Fibre Toxicology*, *2*(1), 1-14, doi: 10.1186/1743-8977-2-10.

- Fang, T., et al. (2016), Oxidative potential of ambient water-soluble PM_{2.5} in the southeastern United States: contrasts in sources and health associations between ascorbic acid (AA) and dithiothreitol (DTT) assays, *Atmos. Chem. Phys.*, *16*(6), 3865-3879, doi: 10.5194/acp-16-3865-2016.
- Fischer, E. V., et al. (2014), Atmospheric peroxyacetyl nitrate (PAN): a global budget and source attribution, *Atmos. Chem. Phys.*, *14*(5), 2679-2698, doi: 10.5194/acp-14-2679-2014.
- Forrister, H., et al. (2015), Evolution of brown carbon in wildfire plumes, *Geophys. Res. Lett.*, *42*(11), 4623-4630, doi: 10.1002/2015GL063897.
- Friedli, H. R., E. Atlas, V. R. Stroud, L. Giovanni, T. Campos, and L. F. Radke (2001), Volatile organic trace gases emitted from North American wildfires, *Global Biogeochem. Cy.*, *15*(2), 435-452, doi: 10.1029/2000GB001328.
- Goode, J. G., R. J. Yokelson, D. E. Ward, R. A. Susott, R. E. Babbitt, M. A. Davies, and W. M. Hao (2000), Measurements of excess O₃, CO₂, CO, CH₄, C₂H₄, C₂H₂, HCN, NO, NH₃, HCOOH, CH₃COOH, HCHO, and CH₃OH in 1997 Alaskan biomass burning plumes by airborne Fourier transform infrared spectroscopy (AFTIR), *J. Geophys. Res. Atmos.*, *105*(D17), 22147-22166, doi: 10.1029/2000JD900287.
- Gray, B. A., Y. Wang, D. Gu, A. Bandy, L. Mauldin, A. Clarke, B. Alexander, and D. D. Davis (2010), Sources, transport, and sinks of SO₂ over the equatorial Pacific during the Pacific Atmospheric Sulfur Experiment, *J. Atmos. Chem.*, *68*(1), 27-53, doi: 10.1007/s10874-010-9177-7.
- Grieshop, A. P., N. M. Donahue, and A. L. Robinson (2009), Laboratory investigation of photochemical oxidation of organic aerosol from wood fires 2: analysis of aerosol mass spectrometer data, *Atmos. Chem. Phys.*, *9*(6), 2227-2240, doi: 10.5194/acp-9-2227-2009.
- Grosjean, D., E. L. Williams, and E. Grosjean (1993), Atmospheric chemistry of isoprene and of its carbonyl products, *Environ. Sci. Technol.*, *27*(5), 830-840, doi: 10.1021/es00042a004.
- Hardy, C. C., R. D. Ottmar, J. L. Peterson, J. E. Core, and P. Seamon (2001), Smoke management guide for prescribed and wildland fire: 2001 edition, National Wildfire Coordination Group, Boise, ID.
- Hawbaker, T. J., V. C. Radeloff, A. D. Syphard, Z. Zhu, and S. I. Stewart (2008), Detection rates of the MODIS active fire product in the United States, *Remote Sens. Environ.*, *112*(5), 2656-2664, doi: 10.1016/j.rse.2007.12.008.
- Hayashi, K., K. Ono, M. Kajiuura, S. Sudo, S. Yonemura, A. Fushimi, K. Saitoh, Y. Fujitani, and K. Tanabe (2014), Trace gas and particle emissions from open burning of three cereal crop residues: Increase in residue moistness enhances

- emissions of carbon monoxide, methane, and particulate organic carbon, *Atmos. Environ.*, *95*, 36-44, doi: 10.1016/j.atmosenv.2014.06.023.
- Hayes, P. L., et al. (2015), Modeling the formation and aging of secondary organic aerosols in Los Angeles during CalNex 2010, *Atmos. Chem. Phys.*, *15*(10), 5773-5801, doi: 10.5194/acp-15-5773-2015.
- Hecobian, A., et al. (2011), Comparison of chemical characteristics of 495 biomass burning plumes intercepted by the NASA DC-8 aircraft during the ARCTAS/CARB-2008 field campaign, *Atmos. Chem. Phys.*, *11*(24), 13325-13337, doi: 10.5194/acp-11-13325-2011.
- Hegg, D. A., L. F. Radke, P. V. Hobbs, R. A. Rasmussen, and P. J. Riggan (1990), Emissions of some trace gases from biomass fires, *J. Geophys. Res. Atmos.*, *95*(D5), 5669-5675, doi: 10.1029/JD095iD05p05669.
- Hennigan, C. J., et al. (2011), Chemical and physical transformations of organic aerosol from the photo-oxidation of open biomass burning emissions in an environmental chamber, *Atmos. Chem. Phys.*, *11*(15), 7669-7686, doi: 10.5194/acp-11-7669-2011.
- Hobbs, P. V., P. Sinha, R. J. Yokelson, T. J. Christian, D. R. Blake, S. Gao, T. W. Kirchstetter, T. Novakov, and P. Pilewskie (2003), Evolution of gases and particles from a savanna fire in South Africa, *J. Geophys. Res.*, *108*(D13), doi: 10.1029/2002jd002352.
- Hodzic, A., and J. L. Jimenez (2011), Modeling anthropogenically controlled secondary organic aerosols in a megacity: a simplified framework for global and climate models, *Geosci. Model Dev.*, *4*(4), 901-917, doi: 10.5194/gmd-4-901-2011.
- Hosseini, S., et al. (2013), Laboratory characterization of PM emissions from combustion of wildland biomass fuels, *J. Geophys. Res. Atmos.*, *118*(17), 9914-9929, doi: 10.1002/jgrd.50481.
- Huang, X., M. Li, J. Li, and Y. Song (2012), A high-resolution emission inventory of crop burning in fields in China based on MODIS Thermal Anomalies/Fire products, *Atmos. Environ.*, *50*, 9-15, doi: 10.1016/j.atmosenv.2012.01.017.
- Huey, L. G., et al. (2004), CIMS measurements of HNO₃ and SO₂ at the South Pole during ISCAT 2000, *Atmos. Environ.*, *38*(32), 5411-5421, doi: 10.1016/j.atmosenv.2004.04.037.
- Jacob, D. J., et al. (1992), Summertime photochemistry of the troposphere at high northern latitudes, *J. Geophys. Res. Atmos.*, *97*(D15), 16421-16431, doi: 10.1029/91JD01968.

- Jaffe, D., D. Chand, W. Hafner, A. Westerling, and D. Spracklen (2008), Influence of Fires on O₃ Concentrations in the Western U.S, *Environ. Sci. Technol.*, 42(16), 5885-5891, doi: 10.1021/es800084k.
- Jaffe, D. A., and N. L. Wigder (2012), Ozone production from wildfires: A critical review, *Atmos. Environ.*, 51, 1-10, doi: 10.1016/j.atmosenv.2011.11.063.
- Jolleys, M. D., et al. (2012), Characterizing the aging of biomass burning organic aerosol by use of mixing ratios: a meta-analysis of four regions, *Environ. Sci. Technol.*, 46(24), 13093-13102, doi: 10.1021/es302386v.
- Jolleys, M. D., H. Coe, G. McFiggans, G. R. McMeeking, T. Lee, S. M. Kreidenweis, J. L. Collett, and A. P. Sullivan (2014), Organic aerosol emission ratios from the laboratory combustion of biomass fuels, *J. Geophys. Res. Atmos.*, 119(22), 12,850-812,871, doi: 10.1002/2014JD021589.
- Jolleys, M. D., et al. (2015), Properties and evolution of biomass burning organic aerosol from Canadian boreal forest fires, *Atmos. Chem. Phys.*, 15(6), 3077-3095, doi: 10.5194/acp-15-3077-2015.
- Jost, C., J. Trentmann, D. Sprung, M. O. Andreae, J. B. McQuaid, and H. Barjat (2003), Trace gas chemistry in a young biomass burning plume over Namibia: Observations and model simulations, *J. Geophys. Res. Atmos.*, 108(D13), doi: 10.1029/2002JD002431.
- Kilgore, B. M. (1981), Fire in ecosystem distribution and structure : western forests and scrublands, in *Proceedings of the Conference: Fire Regimes and Ecosystem Properties*, edited by H. A. Mooney, T. M. Bonnicksen and N. L. Christensen, pp. 58-89, USDA Forest Service, General Technical Report WO-GTR-26.
- Kirchstetter, T. W., T. Novakov, and P. V. Hobbs (2004), Evidence that the spectral dependence of light absorption by aerosols is affected by organic carbon, *J. Geophys. Res. Atmos.*, 109(D21), doi: 10.1029/2004JD004999.
- Kondo, Y., et al. (2004), Impacts of biomass burning in Southeast Asia on ozone and reactive nitrogen over the western Pacific in spring, *J. Geophys. Res. Atmos.*, 109(D15), doi: 10.1029/2003JD004203.
- Kudo, S., et al. (2014), Emissions of nonmethane volatile organic compounds from open crop residue burning in the Yangtze River Delta region, China, *J. Geophys. Res. Atmos.*, 119(12), 7684-7698, doi: 10.1002/2013jd021044.
- Künzli, N., et al. (2006), Health Effects of the 2003 Southern California Wildfires on Children, *Am. J. Respir. Crit. Care Med.*, 174(11), 1221-1228, doi: 10.1164/rccm.200604-519OC.

- Lack, D. A., J. M. Langridge, R. Bahreini, C. D. Cappa, A. M. Middlebrook, and J. P. Schwarz (2012), Brown carbon and internal mixing in biomass burning particles, *Proc. Natl. Acad. Sci. USA*, *109*(37), 14802-14807.
- Lack, D. A., and J. M. Langridge (2013), On the attribution of black and brown carbon light absorption using the Ångström exponent, *Atmos. Chem. Phys.*, *13*(20), 10535-10543, doi: 10.5194/acp-13-10535-2013.
- Lee, A. K. Y., M. D. Willis, R. M. Healy, T. B. Onasch, and J. P. D. Abbatt (2015), Mixing state of carbonaceous aerosol in an urban environment: single particle characterization using the soot particle aerosol mass spectrometer (SP-AMS), *Atmos. Chem. Phys.*, *15*(4), 1823-1841, doi: 10.5194/acp-15-1823-2015.
- Lee, B. H., et al. (2016), Highly functionalized organic nitrates in the southeast United States: Contribution to secondary organic aerosol and reactive nitrogen budgets, *Proc. Natl. Acad. Sci. USA*, *113*(6), 1516-1521.
- Lee, H. J., P. K. Aiona, A. Laskin, J. Laskin, and S. A. Nizkorodov (2014a), Effect of solar radiation on the optical properties and molecular composition of laboratory proxies of atmospheric brown carbon, *Environ. Sci. Technol.*, *48*(17), 10217-10226, doi: 10.1021/es502515r.
- Lee, L., A. P. Teng, P. O. Wennberg, J. D. Crounse, and R. C. Cohen (2014b), On Rates and Mechanisms of OH and O₃ Reactions with Isoprene-Derived Hydroxy Nitrates, *J. Phys. Chem. A*, *118*(9), 1622-1637, doi: 10.1021/jp4107603.
- Lee, M., B. G. Heikes, and D. J. Jacob (1998), Enhancements of hydroperoxides and formaldehyde in biomass burning impacted air and their effect on atmospheric oxidant cycles, *J. Geophys. Res. Atmos.*, *103*(D11), 13201-13212, doi: 10.1029/98JD00578.
- Lelieveld, J., et al. (2008), Atmospheric oxidation capacity sustained by a tropical forest, *Nature*, *452*(7188), 737-740, doi: 10.1038/nature06870.
- Leung, F.-Y. T., J. A. Logan, R. Park, E. Hyer, E. Kasischke, D. Streets, and L. Yurganov (2007), Impacts of enhanced biomass burning in the boreal forests in 1998 on tropospheric chemistry and the sensitivity of model results to the injection height of emissions, *J. Geophys. Res.*, *112*(D10), doi: 10.1029/2006jd008132.
- Li, Q., D. J. Jacob, I. Bey, R. M. Yantosca, Y. Zhao, Y. Kondo, and J. Notholt (2000), Atmospheric hydrogen cyanide (HCN): Biomass burning source, ocean sink?, *Geophys. Res. Lett.*, *27*(3), 357-360, doi: 10.1029/1999GL010935.
- Li, Q., D. J. Jacob, R. M. Yantosca, C. L. Heald, H. B. Singh, M. Koike, Y. Zhao, G. W. Sachse, and D. G. Streets (2003), A global three-dimensional model analysis of the atmospheric budgets of HCN and CH₃CN: Constraints from aircraft and

- ground measurements, *J. Geophys. Res. Atmos.*, 108(D21), doi: 10.1029/2002JD003075.
- Lin, X., M. Trainer, and S. C. Liu (1988), On the nonlinearity of the tropospheric ozone production, *J. Geophys. Res. Atmos.*, 93(D12), 15879-15888, doi: 10.1029/JD093iD12p15879.
- Liu, J., M. Bergin, H. Guo, L. King, N. Kotra, E. Edgerton, and R. J. Weber (2013), Size-resolved measurements of brown carbon in water and methanol extracts and estimates of their contribution to ambient fine-particle light absorption, *Atmos. Chem. Phys.*, 13(24), 12389-12404, doi: 10.5194/acp-13-12389-2013.
- Liu, J., et al. (2014), Brown carbon in the continental troposphere, *Geophys. Res. Lett.*, 41(6), 2191-2195, doi: 10.1002/2013GL058976.
- Liu, J., et al. (2015), Brown carbon aerosol in the North American continental troposphere: sources, abundance, and radiative forcing, *Atmos. Chem. Phys.*, 15(14), 7841-7858, doi: 10.5194/acp-15-7841-2015.
- Liu, S. C., M. Trainer, F. C. Fehsenfeld, D. D. Parrish, E. J. Williams, D. W. Fahey, G. Hübler, and P. C. Murphy (1987), Ozone production in the rural troposphere and the implications for regional and global ozone distributions, *J. Geophys. Res. Atmos.*, 92(D4), 4191-4207, doi: 10.1029/JD092iD04p04191.
- Liu, X., et al. (2016), Agricultural fires in the southeastern U.S. during SEAC⁴RS: Emissions of trace gases and particles and evolution of ozone, reactive nitrogen, and organic aerosol, *J. Geophys. Res. Atmos.*, doi: 10.1002/2016JD025040.
- Liu, Z., et al. (2010), Evidence of Reactive Aromatics As a Major Source of Peroxy Acetyl Nitrate over China, *Environ. Sci. Technol.*, 44(18), 7017-7022, doi: 10.1021/es1007966.
- Liu, Z., et al. (2012), Summertime photochemistry during CAREBeijing-2007: RO_x budgets and O₃ formation, *Atmos. Chem. Phys.*, 12(16), 7737-7752, doi: 10.5194/acp-12-7737-2012.
- Lobert, J. M., D. H. Scharffe, W. M. Hao, T. A. Kuhlbusch, R. Seuwen, P. Warneck, and P. J. Crutzen (1991), Experimental evaluation of biomass burning emissions: Nitrogen and carbon containing compounds, in *Global Biomass Burning: Atmospheric, Climatic, and Biospheric Implications*, edited by J. S. Levine, pp. 289-304, MIT Press, Cambridge, MA.
- Lobert, J. M., W. C. Keene, J. A. Logan, and R. Yevich (1999), Global chlorine emissions from biomass burning: Reactive Chlorine Emissions Inventory, *J. Geophys. Res.*, 104(D7), 8373, doi: 10.1029/1998jd100077.

- Marion, T., P. E. Perros, R. Losno, and E. Steiner (2001), Ozone Production Efficiency in Savanna and Forested Areas during the EXPRESSO Experiment, *J. Atmos. Chem.*, 38(1), 3-30, doi: 10.1023/A:1026585603100.
- Marlon, J. R., et al. (2012), Long-term perspective on wildfires in the western USA, *Proc. Natl. Acad. Sci. USA*, 109(9), E535-E543.
- Mason, S. A., R. J. Field, R. J. Yokelson, M. A. Kochivar, M. R. Tinsley, D. E. Ward, and W. M. Hao (2001), Complex effects arising in smoke plume simulations due to inclusion of direct emissions of oxygenated organic species from biomass combustion, *J. Geophys. Res. Atmos.*, 106(D12), 12527-12539, doi: 10.1029/2001JD900003.
- Mason, S. A., J. Trentmann, T. Winterrath, R. J. Yokelson, T. J. Christian, L. J. Carlson, T. R. Warner, L. C. Wolfe, and M. O. Andreae (2006), Intercomparison of Two Box Models of the Chemical Evolution in Biomass-Burning Smoke Plumes, *J. Atmos. Chem.*, 55(3), 273-297, doi: 10.1007/s10874-006-9039-5.
- May, A. A., E. J. T. Levin, C. J. Hennigan, I. Riipinen, T. Lee, J. L. Collett, J. L. Jimenez, S. M. Kreidenweis, and A. L. Robinson (2013), Gas-particle partitioning of primary organic aerosol emissions: 3. Biomass burning, *J. Geophys. Res. Atmos.*, 118(19), 11,327-311,338, doi: 10.1002/jgrd.50828.
- May, A. A., et al. (2014), Aerosol emissions from prescribed fires in the United States: A synthesis of laboratory and aircraft measurements, *J. Geophys. Res. Atmos.*, 119(20), 11,826-811,849, doi: 10.1002/2014JD021848.
- McCarty, J., C. Justice, and S. Korontzi (2007), Agricultural burning in the Southeastern United States detected by MODIS, *Remote Sens. Environ.*, 108(2), 151-162, doi: 10.1016/j.rse.2006.03.020.
- McCarty, J. L., S. Korontzi, C. O. Justice, and T. Loboda (2009), The spatial and temporal distribution of crop residue burning in the contiguous United States, *Sci. Total. Environ.*, 407(21), 5701-5712, doi: 10.1016/j.scitotenv.2009.07.009.
- McCarty, J. L. (2011), Remote Sensing-Based Estimates of Annual and Seasonal Emissions from Crop Residue Burning in the Contiguous United States, *J. Air Waste Manag. Assoc.*, 61(1), 22-34, doi: 10.3155/1047-3289.61.1.22.
- McKenzie, L. M., D. E. Ward, and W. M. Hoa (1996), Chlorine and bromine in the biomass of tropical and temperate ecosystems, in *Biomass Burning and Global Change*, edited by J. S. Levin, MIT Press, Cambridge, Mass.
- McMeeking, G. R., et al. (2009), Emissions of trace gases and aerosols during the open combustion of biomass in the laboratory, *J. Geophys. Res. Atmos.*, 114(D19), doi: 10.1029/2009JD011836.

- Melvin, M. A. (2012), 2012 national prescribed fire use survey report, *01-12*, Coalition of Prescribed Fire Councils, Inc.
- Millet, D. B., et al. (2010), Global atmospheric budget of acetaldehyde: 3-D model analysis and constraints from in-situ and satellite observations, *Atmos. Chem. Phys.*, *10*(7), 3405-3425, doi: 10.5194/acp-10-3405-2010.
- Müller, M., et al. (2016), In situ measurements and modeling of reactive trace gases in a small biomass burning plume, *Atmos. Chem. Phys.*, *16*(6), 3813-3824, doi: 10.5194/acp-16-3813-2016.
- Naeher, L. P., M. Brauer, M. Lipsett, J. T. Zelikoff, C. D. Simpson, J. Q. Koenig, and K. R. Smith (2007), Woodsmoke Health Effects: A Review, *Inhal. Toxicol.*, *19*(1), 67-106, doi: 10.1080/08958370600985875.
- Oanh, N. T. K., T. L. Bich, D. Tipayarom, B. R. Manadhar, P. Prapat, C. D. Simpson, and L. J. S. Liu (2011), Characterization of particulate matter emission from open burning of rice straw, *Atmos. Environ.*, *45*(2), 493-502, doi: 10.1016/j.atmosenv.2010.09.023.
- Olszyna, K. J., E. M. Bailey, R. Simonaitis, and J. F. Meagher (1994), O₃ and NO_y relationships at a rural site, *J. Geophys. Res. Atmos.*, *99*(D7), 14557-14563, doi: 10.1029/94JD00739.
- Onasch, T. B., A. Trimborn, E. C. Fortner, J. T. Jayne, G. L. Kok, L. R. Williams, P. Davidovits, and D. R. Worsnop (2012), Soot Particle Aerosol Mass Spectrometer: Development, Validation, and Initial Application, *Aerosol Sci. Tech.*, *46*(7), 804-817, doi: 10.1080/02786826.2012.663948.
- Orlando, J. J., and G. S. Tyndall (2012), Laboratory studies of organic peroxy radical chemistry: an overview with emphasis on recent issues of atmospheric significance, *Chem. Soc. Rev.*, *41*(19), 6294-6317, doi: 10.1039/C2CS35166H.
- Ortega, A. M., D. A. Day, M. J. Cubison, W. H. Brune, D. Bon, J. A. de Gouw, and J. L. Jimenez (2013), Secondary organic aerosol formation and primary organic aerosol oxidation from biomass-burning smoke in a flow reactor during FLAME-3, *Atmos. Chem. Phys.*, *13*(22), 11551-11571, doi: 10.5194/acp-13-11551-2013.
- Park, R. J., D. J. Jacob, and J. A. Logan (2007), Fire and biofuel contributions to annual mean aerosol mass concentrations in the United States, *Atmos. Environ.*, *41*(35), 7389-7400, doi: 10.1016/j.atmosenv.2007.05.061.
- Paulot, F., J. D. Crounse, H. G. Kjaergaard, J. H. Kroll, J. H. Seinfeld, and P. O. Wennberg (2009a), Isoprene photooxidation: new insights into the production of acids and organic nitrates, *Atmos. Chem. Phys.*, *9*(4), 1479-1501, doi: 10.5194/acp-9-1479-2009.

- Paulot, F., J. D. Crounse, H. G. Kjaergaard, A. Kurten, J. M. St Clair, J. H. Seinfeld, and P. O. Wennberg (2009b), Unexpected epoxide formation in the gas-phase photooxidation of isoprene, *Science*, 325(5941), 730-733, doi: 10.1126/science.1172910.
- Perring, A. E., S. E. Pusede, and R. C. Cohen (2013), An Observational Perspective on the Atmospheric Impacts of Alkyl and Multifunctional Nitrates on Ozone and Secondary Organic Aerosol, *Chem. Rev.*, 113(8), 5848-5870, doi: 10.1021/cr300520x.
- Peterson, D. A., E. J. Hyer, J. R. Campbell, M. D. Fromm, J. W. Hair, C. F. Butler, and M. A. Fenn (2014), The 2013 Rim Fire: Implications for Predicting Extreme Fire Spread, Pyroconvection, and Smoke Emissions, *Bull. Amer. Meteor. Soc.*, 96(2), 229-247, doi: 10.1175/BAMS-D-14-00060.1.
- Radke, L. F., D. A. Hegg, P. V. Hobbs, J. D. Nance, J. H. Lyons, K. K. Laursen, R. E. Weiss, P. J. Riggan, and D. E. Ward (1991), Particulate and trace gas emissions from large biomass fire in North America, in *Global Biomass Burning: Atmospheric, Climatic, and Biospheric Implications*, edited by J. S. Levine, pp. 209-224, MIT Press, Cambridge, MA.
- Randerson, J. T., Y. Chen, G. R. van der Werf, B. M. Rogers, and D. C. Morton (2012), Global burned area and biomass burning emissions from small fires, *J. Geophys. Res.*, 117(G4), doi: 10.1029/2012jg002128.
- Reid, J. S., R. Koppmann, T. F. Eck, and D. P. Eleuterio (2005), A review of biomass burning emissions part II: intensive physical properties of biomass burning particles, *Atmos. Chem. Phys.*, 5(3), 799-825, doi: 10.5194/acp-5-799-2005.
- Reid, S. B., T. H. Funk, D. C. Sullivan, P. S. Stiefer, H. L. Arkinson, S. G. Brown, and L. R. Chinkin (2004), Research and development of emission inventories for planned burning activities for the Central State Regional Air Planning Association, paper presented at 13th International Emission Inventory Conference, Clearwater, FL, June 8-10.
- Reinhardt, T. E., and D. E. Ward (1995), Factors Affecting Methyl Chloride Emissions from Forest Biomass Combustion, *Environ. Sci. Technol.*, 29(3), 825-832, doi: 10.1021/es00003a034.
- Rogge, W. F., L. M. Hildemann, M. A. Mazurek, G. R. Cass, and B. R. T. Simoneit (1991), Sources of fine organic aerosol. 1. Charbroilers and meat cooking operations, *Environ. Sci. Technol.*, 25(6), 1112-1125, doi: 10.1021/es00018a015.
- Rudolph, J., A. Khedim, R. Koppmann, and B. Bonsang (1995), Field study of the emissions of methyl chloride and other halocarbons from biomass burning in Western Africa, *J. Atmos. Chem.*, 22(1), 67-80, doi: 10.1007/BF00708182.

- Ryerson, T. B., L. G. Huey, K. Knapp, J. A. Neuman, D. D. Parrish, D. T. Sueper, and F. C. Fehsenfeld (1999), Design and initial characterization of an inlet for gas-phase NO_y measurements from aircraft, *J. Geophys. Res. Atmos.*, *104*(D5), 5483-5492, doi: 10.1029/1998JD100087.
- Ryerson, T. B., E. J. Williams, and F. C. Fehsenfeld (2000), An efficient photolysis system for fast-response NO₂ measurements, *J. Geophys. Res. Atmos.*, *105*(D21), 26447-26461, doi: 10.1029/2000JD900389.
- Sachse, G. W., G. F. Hill, L. O. Wade, and M. G. Perry (1987), Fast-response, high-precision carbon monoxide sensor using a tunable diode laser absorption technique, *J. Geophys. Res. Atmos.*, *92*(D2), 2071-2081, doi: 10.1029/JD092iD02p02071.
- Saleh, R., C. J. Hennigan, G. R. McMeeking, W. K. Chuang, E. S. Robinson, H. Coe, N. M. Donahue, and A. L. Robinson (2013), Absorptivity of brown carbon in fresh and photo-chemically aged biomass-burning emissions, *Atmos. Chem. Phys.*, *13*(15), 7683-7693, doi: 10.5194/acp-13-7683-2013.
- Sander, S. P., et al. (2011), *Chemical Kinetics and Photochemical Data for Use in Atmospheric Studies, Evaluation No. 17*, JPL Publication 10-6, Jet Propulsion Laboratory, Pasadena, CA.
- Santín, C., S. H. Doerr, C. M. Preston, and G. González-Rodríguez (2015), Pyrogenic organic matter production from wildfires: a missing sink in the global carbon cycle, *Glob. Change Biol.*, *21*(4), 1621-1633, doi: 10.1111/gcb.12800.
- Savage, M., and T. W. Swetnam (1990), Early 19th-Century Fire Decline Following Sheep Pasturing in a Navajo Ponderosa Pine Forest, *Ecology*, *71*(6), 2374-2378, doi: 10.2307/1938649.
- Schnaiter, M., et al. (2005), Measurement of Wavelength-Resolved Light Absorption by Aerosols Utilizing a UV-VIS Extinction Cell, *Aerosol Sci. Tech.*, *39*(3), 249-260, doi: 10.1080/027868290925958.
- Schwarz, J. P., B. H. Samset, A. E. Perring, J. R. Spackman, R. S. Gao, P. Stier, M. Schulz, F. L. Moore, E. A. Ray, and D. W. Fahey (2013), Global-scale seasonally resolved black carbon vertical profiles over the Pacific, *Geophys. Res. Lett.*, *40*(20), 5542-5547, doi: 10.1002/2013GL057775.
- Seiler, W., and P. Crutzen (1980), Estimates of gross and net fluxes of carbon between the biosphere and the atmosphere from biomass burning, *Clim. Chang.*, *2*(3), 207-247, doi: 10.1007/BF00137988.
- Shetter, R. E., and M. Müller (1999), Photolysis frequency measurements using actinic flux spectroradiometry during the PEM-Tropics mission: Instrumentation description and some results, *J. Geophys. Res. Atmos.*, *104*(D5), 5647-5661, doi: 10.1029/98JD01381.

- Shirai, T., et al. (2003), Emission estimates of selected volatile organic compounds from tropical savanna burning in northern Australia, *J. Geophys. Res. Atmos.*, *108*(D3), doi: 10.1029/2001JD000841.
- Simmonds, P. G., et al. (2006), Global trends, seasonal cycles, and European emissions of dichloromethane, trichloroethene, and tetrachloroethene from the AGAGE observations at Mace Head, Ireland, and Cape Grim, Tasmania, *J. Geophys. Res. Atmos.*, *111*(D18), doi: 10.1029/2006JD007082.
- Simpson, I. J., et al. (2011), Boreal forest fire emissions in fresh Canadian smoke plumes: C₁-C₁₀ volatile organic compounds (VOCs), CO₂, CO, NO₂, NO, HCN and CH₃CN, *Atmos. Chem. Phys.*, *11*(13), 6445-6463, doi: 10.5194/acp-11-6445-2011.
- Singh, H. B., M. Kanakidou, P. J. Crutzen, and D. J. Jacob (1995), High concentrations and photochemical fate of oxygenated hydrocarbons in the global troposphere, *Nature*, *378*(6552), 50-54.
- Singh, H. B., et al. (2010), Pollution influences on atmospheric composition and chemistry at high northern latitudes: Boreal and California forest fire emissions, *Atmos. Environ.*, *44*(36), 4553-4564, doi: 10.1016/j.atmosenv.2010.08.026.
- Singh, H. B., C. Cai, A. Kaduwela, A. Weinheimer, and A. Wisthaler (2012), Interactions of fire emissions and urban pollution over California: Ozone formation and air quality simulations, *Atmos. Environ.*, *56*, 45-51, doi: 10.1016/j.atmosenv.2012.03.046.
- Slusher, D. L., L. G. Huey, D. J. Tanner, F. M. Flocke, and J. M. Roberts (2004), A thermal dissociation-chemical ionization mass spectrometry (TD-CIMS) technique for the simultaneous measurement of peroxyacyl nitrates and dinitrogen pentoxide, *J. Geophys. Res. Atmos.*, *109*(D19), doi: 10.1029/2004JD004670.
- Smith, R., M. Adams, S. Maier, R. Craig, A. Kristina, and I. Maling (2007), Estimating the area of stubble burning from the number of active fires detected by satellite, *Remote Sens. Environ.*, *109*(1), 95-106, doi: 10.1016/j.rse.2006.12.011.
- St. Clair, J. M., K. M. Spencer, M. R. Beaver, J. D. Crounse, F. Paulot, and P. O. Wennberg (2014), Quantification of hydroxyacetone and glycolaldehyde using chemical ionization mass spectrometry, *Atmos. Chem. Phys.*, *14*(8), 4251-4262, doi: 10.5194/acp-14-4251-2014.
- Stevens, J. T., H. D. Safford, and A. M. Latimer (2014), Wildfire-contingent effects of fuel treatments can promote ecological resilience in seasonally dry conifer forests, *Can. J. Forest Res.*, *44*(8), 843-854, doi: 10.1139/cjfr-2013-0460.
- Stockwell, C. E., R. J. Yokelson, S. M. Kreidenweis, A. L. Robinson, P. J. DeMott, R. C. Sullivan, J. Reardon, K. C. Ryan, D. W. T. Griffith, and L. Stevens (2014), Trace gas emissions from combustion of peat, crop residue, domestic biofuels, grasses,

- and other fuels: configuration and Fourier transform infrared (FTIR) component of the fourth Fire Lab at Missoula Experiment (FLAME-4), *Atmos. Chem. Phys.*, *14*(18), 9727-9754, doi: 10.5194/acp-14-9727-2014.
- Stockwell, C. E., P. R. Veres, J. Williams, and R. J. Yokelson (2015), Characterization of biomass burning emissions from cooking fires, peat, crop residue, and other fuels with high-resolution proton-transfer-reaction time-of-flight mass spectrometry, *Atmos. Chem. Phys.*, *15*(2), 845-865, doi: 10.5194/acp-15-845-2015.
- Surratt, J. D., A. W. H. Chan, N. C. Eddingsaas, M. Chan, C. L. Loza, A. J. Kwan, S. P. Hersey, R. C. Flagan, P. O. Wennberg, and J. H. Seinfeld (2010), Reactive intermediates revealed in secondary organic aerosol formation from isoprene, *Proc. Natl. Acad. Sci. USA*, *107*(15), 6640-6645.
- Susott, R. A., G. J. Olbu, S. P. Baker, D. E. Ward, J. B. Kauffman, and R. W. Shea (1996), Carbon, hydrogen, nitrogen, and thermogravimetric analysis of tropical ecosystem biomass, in *Biomass Burning and Global Change*, edited by J. S. Levine, pp. 249-259, MIT Press, Cambridge.
- Takegawa, N., et al. (2003), Photochemical production of O₃ in biomass burning plumes in the boundary layer over northern Australia, *Geophys. Res. Lett.*, *30*(10), doi: 10.1029/2003GL017017.
- Teng, A. P., J. D. Crounse, L. Lee, J. M. St. Clair, R. C. Cohen, and P. O. Wennberg (2015), Hydroxy nitrate production in the OH-initiated oxidation of alkenes, *Atmos. Chem. Phys.*, *15*(8), 4297-4316, doi: 10.5194/acp-15-4297-2015.
- Toon, O. B., et al. (2016), Planning, implementation and scientific goals of the Studies of Emissions and Atmospheric Composition, Clouds and Climate Coupling by Regional Surveys (SEAC⁴RS) field mission, *J. Geophys. Res. Atmos.*, doi: 10.1002/2015JD024297.
- Trainer, M., et al. (1993), Correlation of ozone with NO_y in photochemically aged air, *J. Geophys. Res. Atmos.*, *98*(D2), 2917-2925, doi: 10.1029/92JD01910.
- Trentmann, J., and M. O. Andreae (2003), Chemical processes in a young biomass-burning plume, *J. Geophys. Res.*, *108*(D22), doi: 10.1029/2003jd003732.
- Trentmann, J., B. Fröh, O. Boucher, T. Trautmann, and M. O. Andreae (2003), Three-dimensional solar radiation effects on the actinic flux field in a biomass-burning plume, *J. Geophys. Res. Atmos.*, *108*(D17), doi: 10.1029/2003JD003422.
- Trentmann, J., R. J. Yokelson, P. V. Hobbs, T. Winterrath, T. J. Christian, M. O. Andreae, and S. A. Mason (2005), An analysis of the chemical processes in the smoke plume from a savanna fire, *J. Geophys. Res.*, *110*(D12), doi: 10.1029/2004jd005628.

- Tsujimoto, Y., Y. Yamamoto, K. Hayashi, A. I. Zakaria, Y. Inusah, T. Hatta, M. Fosu, and J.-I. Sakagami (2013), Topographic distribution of the soil total carbon content and sulfur deficiency for rice cultivation in a floodplain ecosystem of the Northern region of Ghana, *Field Crop Res.*, *152*, 74-82, doi: 10.1016/j.fcr.2012.11.007.
- Turetsky, M. R., E. S. Kane, J. W. Harden, R. D. Ottmar, K. L. Manies, E. Hoy, and E. S. Kasischke (2011), Recent acceleration of biomass burning and carbon losses in Alaskan forests and peatlands, *Nature Geosci.*, *4*(1), 27-31, doi: 10.1038/ngeo1027.
- Urbanski, S. P. (2013), Combustion efficiency and emission factors for wildfire-season fires in mixed conifer forests of the northern Rocky Mountains, US, *Atmos. Chem. Phys.*, *13*(14), 7241-7262, doi: 10.5194/acp-13-7241-2013.
- Vakkari, V., et al. (2014), Rapid changes in biomass burning aerosols by atmospheric oxidation, *Geophys. Res. Lett.*, *41*(7), 2644-2651, doi: 10.1002/2014GL059396.
- van der Werf, G. R., J. T. Randerson, L. Giglio, G. J. Collatz, M. Mu, P. S. Kasibhatla, D. C. Morton, R. S. DeFries, Y. Jin, and T. T. van Leeuwen (2010), Global fire emissions and the contribution of deforestation, savanna, forest, agricultural, and peat fires (1997–2009), *Atmos. Chem. Phys.*, *10*(23), 11707-11735, doi: 10.5194/acp-10-11707-2010.
- van Leeuwen, T. T., et al. (2014), Biomass burning fuel consumption rates: a field measurement database, *Biogeosciences*, *11*(24), 7305-7329, doi: 10.5194/bg-11-7305-2014.
- Vay, S. A., et al. (2011), Patterns of CO₂ and radiocarbon across high northern latitudes during International Polar Year 2008, *J. Geophys. Res. Atmos.*, *116*(D14), doi: 10.1029/2011JD015643.
- Verma, V., T. Fang, H. Guo, L. King, J. T. Bates, R. E. Peltier, E. Edgerton, A. G. Russell, and R. J. Weber (2014), Reactive oxygen species associated with water-soluble PM_{2.5} in the southeastern United States: spatiotemporal trends and source apportionment, *Atmos. Chem. Phys.*, *14*(23), 12915-12930, doi: 10.5194/acp-14-12915-2014.
- Virkkula, A., N. C. Ahlquist, D. S. Covert, W. P. Arnott, P. J. Sheridan, P. K. Quinn, and D. J. Coffman (2005), Modification, Calibration and a Field Test of an Instrument for Measuring Light Absorption by Particles, *Aerosol Sci. Tech.*, *39*(1), 68-83, doi: 10.1080/027868290901963.
- Virkkula, A. (2010), Correction of the Calibration of the 3-wavelength Particle Soot Absorption Photometer (3 λ PSAP), *Aerosol Sci. Tech.*, *44*(8), 706-712, doi: 10.1080/02786826.2010.482110.

- Wang, Y., Y. Choi, T. Zeng, D. Davis, M. Buhr, L. Gregory Huey, and W. Neff (2007), Assessing the photochemical impact of snow NO_x emissions over Antarctica during ANTICI 2003, *Atmos. Environ.*, *41*(19), 3944-3958, doi: 10.1016/j.atmosenv.2007.01.056.
- Washenfelter, R. A., et al. (2015), Biomass burning dominates brown carbon absorption in the rural southeastern United States, *Geophys. Res. Lett.*, *42*(2), 653-664, doi: 10.1002/2014gl062444.
- Weibring, P., D. Richter, A. Fried, J. G. Walega, and C. Dyroff (2006), Ultra-high-precision mid-IR spectrometer II: system description and spectroscopic performance, *Appl. Phys. B*, *85*(2-3), 207-218, doi: 10.1007/s00340-006-2300-4.
- Weibring, P., D. Richter, J. G. Walega, and A. Fried (2007), First demonstration of a high performance difference frequency spectrometer on airborne platforms, *Opt. Express*, *15*(21), 13476-13495, doi: 10.1364/OE.15.013476.
- Westerling, A. L., H. G. Hidalgo, D. R. Cayan, and T. W. Swetnam (2006), Warming and Earlier Spring Increase Western U.S. Forest Wildfire Activity, *Science*, *313*(5789), 940-943, doi: 10.1126/science.1128834.
- Wilhelm Scherer, H. (2009), Sulfur in soils, *J. Plant Nutr. Soil Sci.*, *172*(3), 326-335, doi: 10.1002/jpln.200900037.
- Wisthaler, A., A. Hansel, R. R. Dickerson, and P. J. Crutzen (2002), Organic trace gas measurements by PTR-MS during INDOEX 1999, *J. Geophys. Res. Atmos.*, *107*(D19), doi: 10.1029/2001JD000576.
- Xiong, F., et al. (2015), Observation of isoprene hydroxynitrates in the southeastern United States and implications for the fate of NO_x, *Atmos. Chem. Phys.*, *15*(19), 11257-11272, doi: 10.5194/acp-15-11257-2015.
- Yang, A., N. A. H. Janssen, B. Brunekreef, F. R. Cassee, G. Hoek, and U. Gehring (2016), Children's respiratory health and oxidative potential of PM_{2.5}: the PIAMA birth cohort study, *Occup. Environ. Med.*
- Yates, E. L., et al. (2016), Airborne measurements and emission estimates of greenhouse gases and other trace constituents from the 2013 California Yosemite Rim wildfire, *Atmos. Environ.*, *127*, 293-302, doi: 10.1016/j.atmosenv.2015.12.038.
- Yevich, R., and J. A. Logan (2003), An assessment of biofuel use and burning of agricultural waste in the developing world, *Global Biogeochem. Cy.*, *17*(4), doi: 10.1029/2002gb001952.
- Yokelson, R. J., D. W. T. Griffith, and D. E. Ward (1996), Open-path Fourier transform infrared studies of large-scale laboratory biomass fires, *J. Geophys. Res.*, *101*(D15), 21067, doi: 10.1029/96jd01800.

- Yokelson, R. J., R. Susott, D. E. Ward, J. Reardon, and D. W. T. Griffith (1997), Emissions from smoldering combustion of biomass measured by open-path Fourier transform infrared spectroscopy, *J. Geophys. Res.*, *102*(D15), 18865, doi: 10.1029/97jd00852.
- Yokelson, R. J., J. G. Goode, D. E. Ward, R. A. Susott, R. E. Babbitt, D. D. Wade, I. Bertschi, D. W. T. Griffith, and W. M. Hao (1999), Emissions of formaldehyde, acetic acid, methanol, and other trace gases from biomass fires in North Carolina measured by airborne Fourier transform infrared spectroscopy, *J. Geophys. Res.*, *104*(D23), 30109, doi: 10.1029/1999jd900817.
- Yokelson, R. J., I. T. Bertschi, T. J. Christian, P. V. Hobbs, D. E. Ward, and W. M. Hao (2003), Trace gas measurements in nascent, aged, and cloud-processed smoke from African savanna fires by airborne Fourier transform infrared spectroscopy (AFTIR), *J. Geophys. Res. Atmos.*, *108*(D13), doi: 10.1029/2002JD002322.
- Yokelson, R. J., T. Karl, P. Artaxo, D. R. Blake, T. J. Christian, D. W. T. Griffith, A. Guenther, and W. M. Hao (2007), The Tropical Forest and Fire Emissions Experiment: overview and airborne fire emission factor measurements, *Atmos. Chem. Phys.*, *7*(19), 5175-5196, doi: 10.5194/acp-7-5175-2007.
- Yokelson, R. J., T. J. Christian, T. G. Karl, and A. Guenther (2008), The tropical forest and fire emissions experiment: laboratory fire measurements and synthesis of campaign data, *Atmos. Chem. Phys.*, *8*(13), 3509-3527, doi: 10.5194/acp-8-3509-2008.
- Yokelson, R. J., et al. (2009), Emissions from biomass burning in the Yucatan, *Atmos. Chem. Phys.*, *9*(15), 5785-5812, doi: 10.5194/acp-9-5785-2009.
- Yokelson, R. J., I. R. Burling, S. P. Urbanski, E. L. Atlas, K. Adachi, P. R. Buseck, C. Wiedinmyer, S. K. Akagi, D. W. Toohey, and C. E. Wold (2011), Trace gas and particle emissions from open biomass burning in Mexico, *Atmos. Chem. Phys.*, *11*(14), 6787-6808, doi: 10.5194/acp-11-6787-2011.
- Yokelson, R. J., et al. (2013), Coupling field and laboratory measurements to estimate the emission factors of identified and unidentified trace gases for prescribed fires, *Atmos. Chem. Phys.*, *13*(1), 89-116, doi: 10.5194/acp-13-89-2013.
- Zhang, L., R. Vet, J. M. O'Brien, C. Mihele, Z. Liang, and A. Wiebe (2009), Dry deposition of individual nitrogen species at eight Canadian rural sites, *J. Geophys. Res. Atmos.*, *114*(D2), doi: 10.1029/2008JD010640.
- Zhang, Y., Y. Wang, B. A. Gray, D. Gu, L. Mauldin, C. Cantrell, and A. Bandy (2014), Surface and free tropospheric sources of methanesulfonic acid over the tropical Pacific Ocean, *Geophys. Res. Lett.*, *41*(14), 5239-5245, doi: 10.1002/2014GL060934.

- Zhang, Y., et al. (2016), Large Vertical Gradient of Reactive Nitrogen Oxides in the Boundary Layer: Modeling Analysis of DISCOVER-AQ 2011 Observations, *J. Geophys. Res. Atmos.*, doi: 10.1002/2015JD024203.
- Zhang, Y. L., et al. (2015), Fossil vs. non-fossil sources of fine carbonaceous aerosols in four Chinese cities during the extreme winter haze episode of 2013, *Atmos. Chem. Phys.*, 15(3), 1299-1312, doi: 10.5194/acp-15-1299-2015.
- Zhao, R., A. K. Y. Lee, L. Huang, X. Li, F. Yang, and J. P. D. Abbatt (2015), Photochemical processing of aqueous atmospheric brown carbon, *Atmos. Chem. Phys.*, 15(11), 6087-6100, doi: 10.5194/acp-15-6087-2015.
- Zhong, M., and M. Jang (2014), Dynamic light absorption of biomass-burning organic carbon photochemically aged under natural sunlight, *Atmos. Chem. Phys.*, 14(3), 1517-1525, doi: 10.5194/acp-14-1517-2014.